ARCHIVES OF ACOUSTICS
4, 3 (1979)

PROBABILITY DENSITY DISTRIBUTION OF INSTANTANEOUS VALUES OF A SPEECH SIGNAL IN POLISH

STEFAN P. BRACHMAŃSKI, WOJCIECH MAJEWSKI

Institute of Telecommunication and Acoustics, Wrocław Technical University
(50-317 Wrocław)

In the present paper the results of investigating the probability density distribution of instantaneous values of a Polish speech signal are presented. The aim was to obtain data providing an additional criterion for the generation of artificial test signals. The signals are used in objective methods of measuring the quality of Polish speech transmission. The probability density distribution of instantaneous values of a speech signal in Polish was compared with the distributions in English, German, and Russian. The minimum duration of an acoustic signal, sufficient to obtain stationary characteristics of the probability density distribution of instantaneous values of a Polish speech signal, was determined. The distributions obtained were approximated by means of exponential functions.

1. Introduction

Speech is the most common means of transmitting information among people. The quality of the transmission depends on objective physical parameters of the devices used in transmitting speech signals and on subjective factors connected with the transmitter and the receiver of the information transmitted. All measurements of the quality of speech signal transmission should consider subjective factors. Either subjective methods of measurement or the evalution of objective methods should be performed with consideration of subjective factors.

Subjective measurements are laborious, expensive and require a large group of people. They cannot thus be generally and widely used [10]. There is an increasing demand for working objective methods of measuring the quality of speech signal transmission which would provide results similar to the subjective opinion of the users of telecommunication devices.

Most of the methods used or suggested so far are based on a comparison of the parameters of a test signal at the input of the transmission channel

with the parameters at the output. As a test signal we usually employ a deterministic signal [7, 8, 13, 14], a Gaussian random signal [3] or a speech signal representing a set of speech sounds, syllables or sentences [10, 13]. In the first two cases, the test signal should approximate the basic characteristics of a speech signal. In the third case, however, the test signal contains the characteristics of a standard speech signal if it is a sample of elements occurring in natural speech. The test signals usually provide consistency of the signal spectrum with the power density of the natural speech spectrum [7, 8, 10, 14].

The results of the investigations in paper [6] show that if

$$f_1(t) \leftrightarrow |F_1(\omega)| \tag{1}$$

and

$$f_2(t) = y(t)\ f_1(t) \leftrightarrow |F_2(\omega)|, \tag{2}$$

where $f_1(t)$ denotes a primary acoustic signal, $|F_1(\omega)|$ is the amplitude spectrum of the signal $f_1(t)$, $f_2(t)$ denotes a secondary acoustic signal, $|F_2(\omega)|$ is the amplitude spectrum of the signal $f_2(t)$, $y(t)$ denotes a function introducing nonlinear distortions of the signal $f_1(t)$, $\leftrightarrow$ denotes the mark of correspondence, then in spite of the fact that

$$\big||F_1(\omega)| - |F_2(\omega)|\big| < \delta, \tag{3}$$

where δ is the least spectral difference perceptible by means of the measuring method used, one reacts to the effect of nonlinear distortions caused by the function $y(t)$ because these distortions cause important changes in the probability density distribution of instantaneous values of the signal. Thus it seems advisable to include in a test signal not only spectral parameters, but also other additional statistical features of a speech signal that are important in signal perception. This concerns mainly the probability density distribution of instantaneous values of a natural speech signal.

Experimental investigations [1, 3] have shown that a speech signal with the statistical features mentioned above may be considered as a stationary ergodic random process $\{X(t)\}$, provided the signal fragment lasts at least several tens of seconds. It follows from the ergodic characteristics that the statistical features of a speech signal and, in particular, the probability density of instantaneous values of a speech signal may be computed by finding the mean value in time of the n-th sample $x_n(t)$ of a random process $\{X(t)\}$. The probability density $p(x)$ of instantaneous values of a random signal is the derivative of the distribution function of the random variable $x(t)$ [2], which may be expressed as

$$p(x) = \frac{dF(x)}{dx} = \frac{P[x \leqslant x(t) < x + dx]}{dx}, \tag{4}$$

where $F(x) = P[x(t) < x]$ is the distribution function of the random variable $x(t)$.

Practically, in analogue methods of signal analysis, the probability density of instantaneous values of a speech signal may be estimated [2] from the formula

$$p(x) = \frac{T_x}{T\Delta x}, \tag{5}$$

where Δx is the finite width of the time interval including x, T_x — the time interval where the signal $x_n(t)$ is within the section with a width equal to Δx, and T — the duration of the analysis $x_n(t)$. In digital methods of signal analysis, $p(x)$ may be estimated from the formula

$$p(x) = \frac{N_x}{N\Delta x}, \tag{6}$$

where N_x is the number of samples in the interval of width Δx and N is the total number of samples.

2. Method of investigation

Measurement of the probability density of instantaneous values of a speech signal in Polish is based on phonetic data obtained from a reading by 11 readers (10 male voices and 1 female voice) of the same newspaper text, at a constant sound intensity level. Long reading at the same level is very tiring, so to avoid changes in sound level intensity caused by readers fatigue, the test signal was recorded in five-minute series. The total time of signal duration for one reader was ten minutes.

A block diagram of the system for measuring the probability density of instantaneous values of a speech signal is shown in Fig. 1. The recordings were

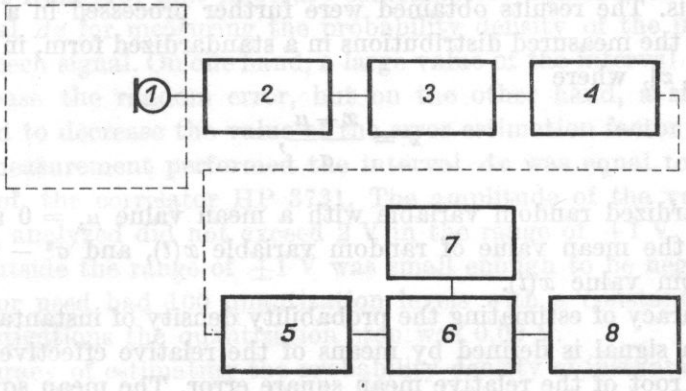

Fig. 1. A block diagram of the system for the measurement of the probability density of instantaneous values of a speech signal

1 — microphone, 2 — amplifier, 3 — bandpass filter (100-6000 Hz, 24 dB/oct.), 4 — tape recorder (v = 38.1 cm/s), 5 — tape recorder (v = 9.05 cm/s), 6 — correlator, 7 — clock, 8 — digital computer

made in an audio monitoring studio at the Institute of Telecommunication and Acoustics of Wrocław Technical University. To record the signal test, a non-directional condenser microphone (Neumann type UM 57) was used with a professional tape-recorder MS 181. The frequency response of the microphone was linear within ± 2 dB from 30 to 15 000 Hz, while the frequency response of the recording system did not exceed ± 1 dB in the frequency band 20-15 000 Hz. The microphone was placed in the nearfield of the speaker. The signal/noise ratio of the whole system was 50 dB.

The speech signal recorded was processed into discrete units by means of a Hewlett-Packard type HP 3721 correlator. The correlator HP 3721 has a constant sampling time of 333 μs [15]. According to the sampling theorem [2], this permits the presentation in digital form of all the information in the analogue signal below an upper limiting frequency of about 1500 Hz. The frequency analysis of the medium spectrum of speech in Polish shows that natural speech contains frequency components over 1500 Hz, but above 6000 Hz they are small enough to be neglected [11]. To perform the analysis of a speech signal in Polish within the range 100-6000 Hz, the frequency of the signal components was diminished four times by decreasing the speed of the magnetic tape by a factor of four. This procedure caused the system dynamic range to decrease by about 2 dB and the frequency response of the readout track did not exceed ± 1 dB in the range 20-10 000 Hz.

The duration of the analysis of speech signal was estimated by means of a clock connected to the correlator. The clock switched the correlator on at the movement of inputting the speech signal. From this moment on the clock measured the time of the signal speech analysis and, having achieved the assigned value of the analysis time, caused cessation of the processing of the signal in the correlator. The result of this processing by the correlator was the total number of samples at a given quantization level, at a given time of speech signal analysis. The results obtained were further processed in a digital computer to give the measured distributions in a standardized form, in a coordinate system $[p(z), z]$, where

$$z = \frac{x - \mu}{\sigma}, \tag{7}$$

z is a standardized random variable with a mean value $\mu_z = 0$ and variance $\sigma_z^2 = 1$, μ — the mean value of random variable $x(t)$, and σ^2 — the variance of the random value $x(t)$.

The accuracy of estimating the probability density of instantaneous values of the speech signal is defined by means of the relative effective error which is the square root of the relative mean square error. The mean square error of the probability density estimation of instantaneous values of a signal is defined [1] as the sum of the variance $D^2[\hat{p}(x)]$ and squared error estimation factor $b^2[\hat{p}(x)]$.

The variance $D^2[\hat{p}(x)]$ of the estimate of the probability density of instantaneous values of a speech signal describes the random part and is defined by the formula

$$D^2[\hat{p}(x)] = \frac{p(x)}{2BT\Delta x}, \tag{8}$$

where

$$p(x) = \lim_{\substack{T\to\infty \\ \Delta x\to 0}} \hat{p}(x)$$

is the probability density of instantaneous values of the speech signal, $\hat{p}(x)$ — the weighted estimate of the function $p(x)$, T — the duration of the speech signal analysis, B — the frequency band width of the speech signal and Δx — a finite interval including x.

The error estimation factor $b[\hat{p}(x)]$ for the instantaneous value of a speech signal describes the systematic part of the error and is defined by the approximate relation

$$b[\hat{p}(x)] \approx \frac{1}{24}\Delta x^2 \ddot{p}(x), \tag{9}$$

where $\ddot{p}(x)$ is the second derivative of the function $p(x)$ with respect to the argument x.

A relative effective error ε of the estimate of the probability density of instantaneous values of the speech signal may be calculated from

$$\varepsilon \approx \left\{\frac{1}{2BT\Delta x p(x)} + \frac{\Delta x^4}{576}\left[\frac{\ddot{p}(x)}{p(x)}\right]^2\right\}^{1/2}. \tag{10}$$

It follows from (10) that there are contradictory demands as to the width of the interval Δx for measuring the probability density of the instantaneous value of a speech signal. On one hand, a large value of the interval Δx is necessary to decrease the random error, but on the other hand, a smaller width Δx is required to decrease the value of the error estimation factor [2].

In the measurement performed the interval Δx was equal to the quantization step of the correlator HP 3731. The amplitude of the voltage of the speech signal analyzed did not exceed 2 V in the range of ± 1 V. The number of samples outside the range of ± 1 V was small enough to be neglected. Since the corrrelator used had 100 quantization levels with a constant step, in the present investigations the quantization step was 0.02 V.

The accuracy of estimating the probability density of instantaneous values of a speech signal was defined by means of the relative effective error. Examples of its values for the case most dependent on the time T of duration of the speech signal analysis are given in Table 1.

Table 1. The relative error $\varepsilon[\%]$ for various durations T of speech signal analysis

T [min]	$p(x)$					
	0.005	0.01	0.05	0.1	0.5	1.0
1	6.56	4.64	2.08	1.47	0.82	1.85
5	3.08	2.20	0.97	0.69	0.51	1.50
10	2.15	1.50	0.68	0.48	0.48	1.60

3. Results of the experiment

To estimate the minimum duration of the speech signal analysis which is sufficient to obtain a stationary distribution of the probability density of instantaneous values of a speech signal in Polish, distribution measurements for various durations of speech signal analysis were performed. The duration of the analysis started with 1 minute and was then gradually lengthened by 1 minute increments to reach eventually 10 minutes.

The probability density distributions of instantaneous values of a speech signal lasting 1, 5 and 10 minutes are presented in Fig. 2. In this figure the distributions measured for four speakers (three male voices and one female voice) are presented. They are the ones most dependent on the signal duration. In other cases the dependence was only slight, so the analysis was made for durations shorter than 1 minute. It turned out that increasing the duration of the speech signal analysis over 40 seconds caused only slight changes in the probability density distribution of instantaneous values of a speech signal in Polish.

The agreement of the distributions for one speaker and various durations was checked by means of the Smirnov test [4]. It has been shown that at a confidence level of $\alpha = 0.05$ the hypothesis of the agreement of the probability density distributions of instantaneous values of a speech signal in Polish, with test signals lasting at least 60 seconds, cannot be rejected. From these results one may assume that at a given quantization step, those distributions do not change for an analysis lasting at least 60 seconds. Thus, measurement of these distributions should not last less than 60 seconds.

Comparison of the probability density distributions of instantaneous values of a speech signal in Polish for different speakers was performed by means of the Smirnov test. It has been shown that at a confidence level of $\alpha = 0.05$ the population of speakers was homogeneous and the hypothesis of the agreement of the distributions cannot be rejected. Thus the results obtained may help to estimate the mean probability density distribution of instantaneous values of a speech signal in Polish. This distribution is presented in Fig. 3.

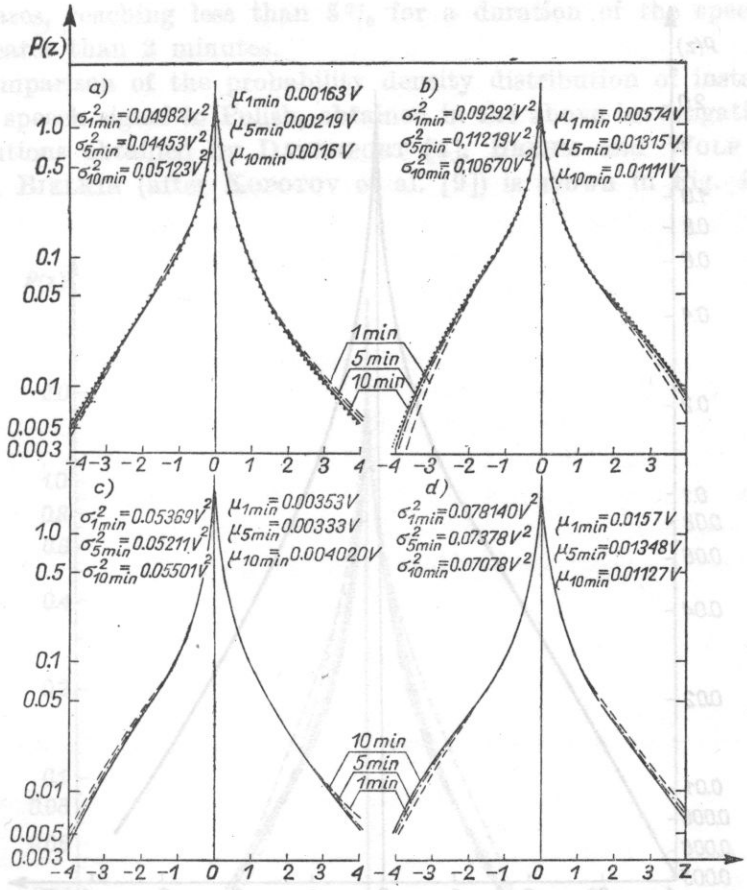

Fig. 2. The probability density distribution of instantaneous values of a Polish speech signal for four speakers and three durations of speech signal analysis
a, b, c – male voices, *d* – female voice

The probability density distribution of instantaneous values of a speech signal in Polish, obtained as a result of the present investigations, may be approximated by

$$p(z) = ae^{-b|z|} + ce^{-d|z|}. \tag{11}$$

Values of the coefficients a, b, c and d were found using the least squares method [2, 11]. The formula approximating the empirical probability density distribution of instantaneous values of a speech signal in Polish was obtained in the form

$$p(z) = \frac{0.049}{\sigma_1} e^{-0.194|z|/\sigma_1} + \frac{0.346}{\sigma_2} e^{-1.4|z|/\sigma_2}, \tag{12}$$

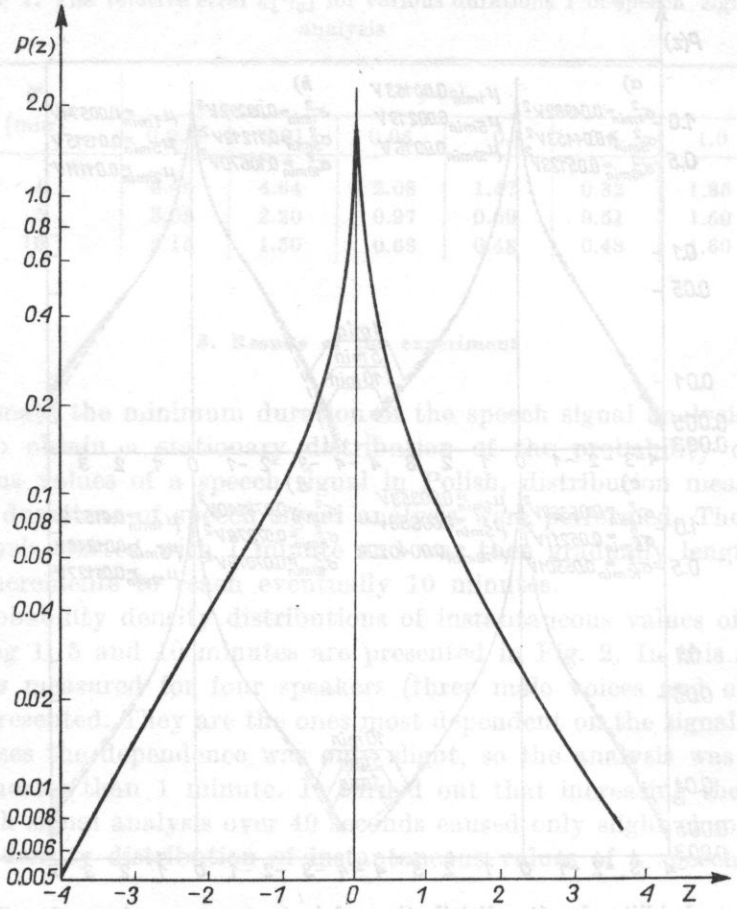

Fig. 3. Mean probability density distributions of instantaneous values of a speech signal in Polish

where $\sigma_1^2 = 0.66\sigma^2$ and $\sigma_2^2 = 0.34\sigma^2$, σ^2 being the variance of the empirical probability density distribution of instantaneous values of a speech signal in Polish.

4. Conclusion

The results obtained show that at a given quantization step the stationary probability density distributions of instantaneous values of a speech signal in Polish are obtained for an analysis duration T of at least 60 seconds. The relative effective error for an analysis time $T = 60$ seconds, and for the method described, does not exceed 7 % for the least favourable case — largest absolute amplitude values. With longer duration of the analysis the relative effective

error decreases, reaching less than 5% for a duration of the speech signal analysis greater than 2 minutes.

The comparison of the probability density distribution of instantaneous values of a speech signal in Polish, obtained in the above investigations, with the distributions obtained by DAVENPORT [4], BREHM and WOLF [3], and SHITOV and BIELKIN (after KOPOTOV et al. [9]) is shown in Fig. 4.

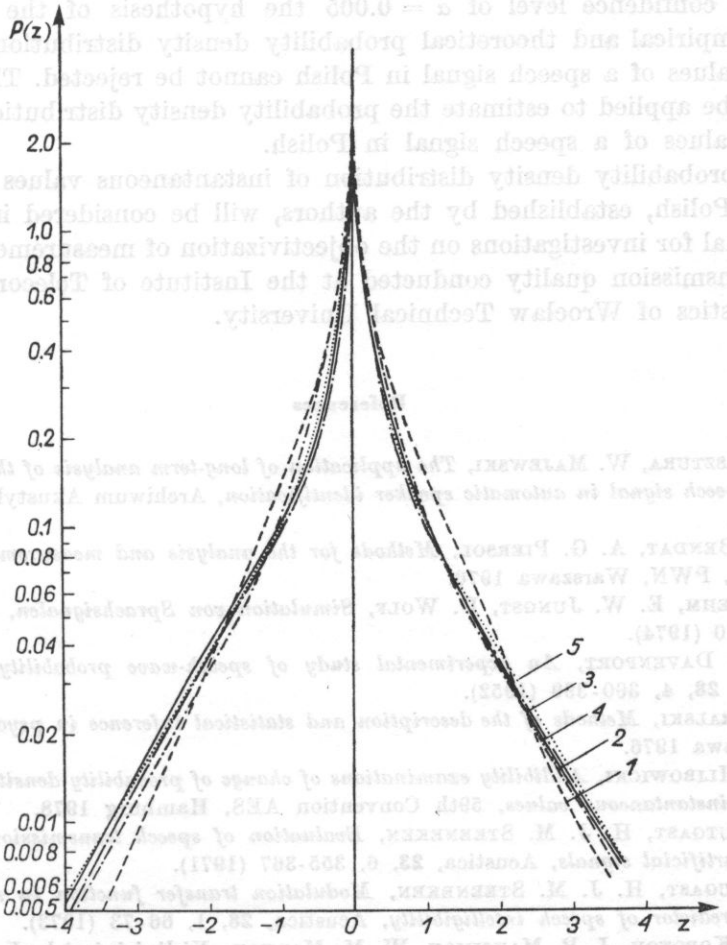

Fig. 4. The probability density distribution of instantaneous values of a speech signal

1 – after Davenport, 2 – after Brehm and Wolf, 3 – after Shitov and Bielkin, 4 – after Brachmański and Majewski, 5 – from relation (12)

To verify the hypothesis of the equivalence of the probability density distribution of instantaneous values of a speech signal in Polish with the distributions for English [4], German [3] and Russian [9], the $\varkappa^2$ consistency test

was applied. The $\varkappa^2$ consistency test showed that at a confidence level $\alpha = 0.005$ the hypothesis of the consistency of the probability density distributions of instantaneous values of a speech signal in Polish, compared with the distributions in German and Russian, cannot be rejected.

To verify the empirical consistency of probability density distribution of instantaneous values of a speech signal in Polish with the theoretical distribution calculated from (12), the $\varkappa^2$ consistency test was applied. It was shown that at a confidence level of $\alpha = 0.005$ the hypothesis of the consistency of both empirical and theoretical probability density distributions of instantaneous values of a speech signal in Polish cannot be rejected. Thus, formula (12) may be applied to estimate the probability density distribution of instantaneous values of a speech signal in Polish.

The probability density distribution of instantaneous values of a speech signal in Polish, established by the authors, will be considered in generating a test signal for investigations on the objectivization of measurement of speech signal transmission quality conducted at the Institute of Telecommunication and Acoustics of Wrocław Technical University.

References

[1] Cz. BASZTURA, W. MAJEWSKI, *The application of long-term analysis of the zero-crossing of a speech signal in automatic speaker identification*, Archiwum Akustyki, **13**, 1, 3-15 (1978).

[2] J. S. BENDAT, A. G. PIERSOL, *Methods for the analysis and measurement of random signals*, PWN, Warszawa 1976.

[3] M. BREHM, E. W. JUNGST, D. WOLF, *Simulation von Sprachsignalen*, AEU, **28**, 11, 445-450 (1974).

[4] W. B. DAVENPORT, *An experimental study of speech-wave probability distributions* JASA, **28**, 4, 390-399 (1952).

[5] A. GÓRALSKI, *Methods of the description and statistical inference in psychology*, PWN, Warszawa 1976.

[6] S. R. HLIBOWICKI, *Audibility examinations of change of probability density of acoustical signal instantaneous values*, 59th Convention AES, Hamburg 1978.

[7] T. HOUTGAST, H. J. M. STEENEKEN, *Evaluation of speech transmission channels by using artificial signals*, Acustica, **23**, 6, 355-367 (1971).

[8] T. HOUGAST, H. J. M. STEENEKEN, *Modulation transfer function in room acoustics as a predictor of speech intelligibility*, Acustica, **28**, 1, 66-73 (1973).

[9] P. G. KOPOTOV, J. P. MAKSIMOV, W. M. MARKOV, *Nielinieinie iskazhenia riechevovo signala*, Elektrosviaz, **8**, 29-34 (1976).

[10] W. MAJEWSKI, Cz. BASZTURA, S. P. BRACHMAŃSKI et al., *Objectivization of measurements methods of articulation intelligibility*, Report No. I/28/R-199/77, Wrocław 1977.

[11] L. Z. RUMSZYCKI, *Mathematical elaboration of the results of experiments*, WNT, Warszawa 1973.

[12] J. ZALEWSKI, W. MAJEWSKI, *Polish speech spectrum obtained from superposed samples and its comparison with spectra of other languages*, Proc. of 7th International Congress on Acoustics, Budapest 1971.

[13] *Acoustics – recommended methods for measuring the intelligibility of speech*, Draft ISO/DP 4870, 1975.
[14] Green Book of CCITE, *Wire transmission*, III-1, WKiŁ, Warszawa 1976.
[15] *Service Manual Model 3721 Correlator*, Hewlett-Packard 1971.

Received on April 13, 1978

ARCHIVES OF ACOUSTICS
4, 3 (1979)

RELATION OF EAR PROTECTOR ATTENUATION TO NOISE SPECTRA AND METHODS FOR ITS DETERMINATION

DANUTA TRYNKOWSKA, RYSZARD MICHALSKI

Central Institute of Occupational Safety (00-349 Warszawa)

454 spectra of industrial noise the sound level of which exceeded 90 dB (A), i.e. the maximum permissible values as established by the Polish Standard PN-70/B-02151 were analyzed. The real-ear attenuation for seven ear protectors was investigated and attenuation values for each of 454 noise spectra were calculated. An analysis of the attenuation of ear protectors as a function of the noise spectrum index Δ_{CA} was made and the regression curves for $S_A = f(\Delta_{CA})$ were determined. Several methods for the determination of attenuation were given and a comparative analysis of the results was made. It follows from the analysis that the best method for determination of the attenuation uses the mean spectrum.

1. Introduction

As established by Polish Standards PN-70/B-02151 [10] and PN-77/N-01310 [12] and by the recommendations of ISO/R 1999-1971 (*E*) [7], the weighted noise level expressed in dB (A) is the criterion for the estimation of the harmful effect of noise on the human organism. Thus, when considering the ear protector performance, one should use the levels reaching the ears when protectors are used, as measured in these units. Knowledge of the quantity defined as attenuation in Polish Standard PN-76/N-01309 [11] has practical significance for the estimation of the performance and choice of ear protectors. Ear protector attenuation is the quantity determining the sound level reduction at the tympanum due to the use of ear protector. As established by the recommendation ISO/R 1999-1971 (*E*) and the above mentioned Polish Standard, the attenuation S_A is expressed in dB (A) and calculated from the formula

$$S_A = L_A - 10 \log \sum_f \text{antilog} \frac{L_f - S_f + K_{A,f}}{10} \quad \text{dB(A)}, \tag{1}$$

where L_A – sound level in dB(A) occurring at the work place, L_f – band pressure level (in dB) in an octave band of centre frequency f, S_f – mean real-ear

attenuation of ear protectors (in dB) at the frequency f, $K_{A,f}$ – coordinates of correction curve A for the sound level meter (in dB) at a frequency f (f = 63, 125, 250, 500, 1000, 2000, 4000, 8000 Hz).

It follows from formula (1) that the value of the ear protector attenuation depends on the spectral distribution of the noise considered and for one type of ear protector can vary over a range of a dozen dB(A) or so, depending on the spectral distribution of the noise [4, 8, 15-19]. Calculation of the attenuation S_A from formula (1) also requires the determination from measurements of: eight values of the band pressure level L_f in octave bands, eight values of the real-ear attenuation S_f of the ear protectors, and the performance of rather complicated calculations. Thus for several years investigators have looked for a simpler way of characterizing the noise spectra than that of giving the values of the band pressure level in eight octave or (24) 1/3-octave bands and for a rapid method – as little dependent on the noise spectrum as possible – for the determination of ear protector attenuation or the sound level L_s of the noise in dB(A) reaching the ears when using ear protector. Research in this direction was initiated by BOTSFORD [2-4].

Taking into consideration the difference between the correction curves A and C used in acoustic meters, Botsford postulated a thesis that the difference between the weighted sound levels $L_C - L_A = \Delta_{CA}$, subsequently called the *noise spectrum index*, determines the noise spectral distribution. He analyzed about 1000 spectra, including 580 spectra of industrial noise, and stated that the relation suggested is valid for two thirds of real noise sources.

On the basis of Botsford's verified theory, WAUGH [18] divided industrial noise into five categories depending on the value of the Δ_{CA}-index (Table 1).

Table 1. Division of noise spectra into categories

Category	1	2	3	4	5
Δ_{AC} [dB]	$\leqslant 0$	0.1-2.0	2.1-4.0	4.1-9.0	> 9

For comparison, he standardized noise spectra so that sound level was the same for each spectrum, e.g. L_A = 90 dB(A). It is achieved by subtracting from the band pressure level in each octave band the number of decibels by which the sound level of noise considered exceeds the chosen value of L_A.

Standardization of the noise spectrum does not change the value of the attenuation S_A for ear protectors under the assumption (consistent with the results of investigations previously obtained [13]) that the real-ear attenuation of ear protectors does not depend on the sound pressure level.

Waugh investigated 619 spectra of individual noise sources and determined a mean spectrum for each category. Comparing values of the attenuation S_A for 30 types of ear protectors, calculated from formula (1), on the basis of the

above-mentioned mean spectra and 619 specific noise spectra, Waugh found that the attenuation S_A, determined from the mean noise spectrum for a given category, is different from the mean attenuation determined on this basis of all spectra which belong to the given category by about 1 dB(A). Thus in practice for the selection of ear protectors it is enough to estimate the attenuation on the basis of the mean spectrum for the category comprising the noise spectrum considered.

Botsford assumed that there is a quantity characteristic of ear protectors which does not depend on the spectral distribution of the noise [3, 4]. As a result of an investigation on the six mean noise spectra he found that the difference $L_C - L_S$ = SLC is the desired quantity, where L_S is the sound level of noise in dB(A) corrected by the ear protector. The quantity SLC (short for *Sound Level Conversion*) permits determination of the sound level reaching an ear protected by an ear protector when the sound level L_C – of the noise is known. Changing the noise spectrum index Δ_{CA} from 0 to 20 dB, Botsford obtained a change in the value of SLC for different types of ear protectors over a range of only several decibels, whereas their attenuation S_A varied over more than 20 decibels.

The quantity SLC is related to the attenuation S_A and noise spectrum indices Δ_{CA} by the following relation:

$$\text{SLC} = S_A + \Delta_{CA}. \tag{2}$$

Substituting into formula (2) the mean value of SLC for a given type of ear protector instead of SLC and the value of Δ_{CA}, Botsford obtained values of attenuation S_A which differed at most by 0 ± 3 dB(A) from the values determined in an exact manner from formula (1).

On the basis of the values of attenuation S_A determined for the six spectra of Botsford [4], Johnson and Nixon [8] obtained equations for the regression curves of the attenuation S_A as a function of noise spectrum index Δ_{CA} for different types of ear protectors, i.e. determining the coefficients b aid m in the equation

$$S_A = b + m\Delta_{CA} \tag{3}$$

by the method of least squares. By comparison of the values of attenuation S_A determinated by the linear regression method (formula (3)), the exact method (formula (1)) and SLC method (formula (2)), Johnson and Nixon found that the method they used gave attenuation values closest to those obtained by the exact method. Although slightly less exact, Botsford's method was, however, far simpler.

The present paper includes part of results of investigations [16] aimed the determination of ear protector attenuation for noise spectra occurring in domestic industry and at the creation of a method for rapid selection of the domestically available ear protectors most suitable for the noise involved. In the present

paper, the discussion is limited to the investigation of real-ear attenuation of ear protectors, analysis of industrial noise spectra and the investigation of the relation of ear protector attenuation to the spectral distribution of the noise.

2. Characteristics of real-ear attenuation of ear protector

The real-ear attenuation S_f of ear protectors was determined by an audiometric method using the audibility threshold shift of a group of ten people, complying with the requirements of Polish Standard PN-76/01309 [11, 16]. The values of the realear attenuation S_f, found for seven selected types of ear protectors and the appropriate standard deviations s, are shown in Table 2.

Table 2. Real-ear attenuation S_f of ear protectors and standard deviation s [dB]

Type of ear protectors	Quantity	Frequency [Hz]							
		63	125	250	500	1000	2000	4000	8000
TD-1A	S_f	6.3	4.4	0.0	14.6	25.8	23.2	26.3	22.4
	s	4.9	3.7	5.0	3.9	4.8	6.3	5.1	6.5
TD-5	S_f	8.0	6.6	7.3	16.2	27.2	22.1	29.4	25.1
	s	4.2	3.0	3.3	3.0	2.9	4.6	4.4	4.6
Saturn II	S_f	10.7	10.3	13.2	12.4	13.8	21.5	29.7	29.2
	s	8.6	8.2	7.0	6.8	7.5	10.0	7.9	11.1
E-A-R	S_f	18.8	18.2	21.0	19.9	23.0	30.9	42.2	35.0
	s	3.8	3.9	4.9	5.5	6.4	5.8	7.9	7.2
Ear defender	S_f	16.5	13.7	15.1	13.6	17.3	25.6	27.7	26.5
	s	9.5	7.9	8.1	7.8	6.8	7.5	6.2	7.7
3M Brand No 8773	S_f	21.4	17.3	18.9	18.8	19.1	23.9	25.9	31.8
	s	3.6	2.9	4.3	4.8	2.3	7.0	7.9	6.7
Contraphon wool	S_f	6.2	6.5	8.5	8.6	11.5	21.2	27.1	28.5
	s	3.3	3.3	4.5	3.3	3.6	5.3	6.2	5.0

Ear muffs TD-1A and TD-5 and ear plugs Saturn II are the latest types of domestically produced ear protectors, contraphon wool is imported from the GDR. The other types are only sporadically used domestically.

It can be concluded from Table 2 that the ear muffs TD-5 are characterized by a higher real-ear attenuation for low and medium tones, compared with ear muffs TD-1A, whereas amongst ear plugs, E-A-R have the best and contraphon wool the worst properties.

3. Analysis of noise spectra in domestic industry

For the investigation of spectral distributions of noise occurring in the Polish industry, 454 records were selected from about 900 spectra of quasi stationary noises and analyzed. The sound level of the selected noises exceeded 90 dB(A) — the maximum acceptable value, as established by the Polish Standards PN-70/B-02151 and PN-77/N-01310, p. 01 [10, 12].

These spectra were gathered from measurements made by the Technological Acoustic Department of the Central Institute of Occupational Safety, Sanitary and Epidemiological Board in Warsaw, and the Research and Design Office of the Textile Industry in Łódź. These results comprised values of the octave band pressure level over a range of central frequencies of 63-8000 Hz.

Having the values of pressure levels, L_f, in octave bands at mean frequencies $f = 63, 125, 250, 500, 1000, 2000, 4000, 8000$ Hz for the noise considered, the sound levels of the noise L_A and L_C were determined from the relations

$$L_A = 10 \log \sum_f 10^{0.1(L_f + K_{A,f})}, \tag{4}$$

$$L_C = 10 \log \sum_f 10^{0.1(L_f + K_{C,f})}, \tag{5}$$

and also the difference

$$\Delta_{AC} = L_C - L_A, \tag{6}$$

where $K_{A,f}$ and $K_{C,f}$ are the coordinates of correction curves A and C of a sound level meter, with values given in Table 3. For the above calculations

Table 3. The coordinates of the correction curves A and C

f [Hz]	63	125	250	500	1000	2000	4000	8000
$K_{A,f}$ [dB]	−26.2	−16.1	−8.6	−3.2	0	1.2	1.0	−1.1
$K_{C,f}$ [dB]	−0.8	−0.2	0	0	0	−0.2	−0.8	−3.0

a special analytical programme for a Hewlett Packard 9810 A minicomputer was designed, which was included as a subprogramme in the analytical programme for calculating the attenuation S_A, the reduced attenuation S_{As}, and the SLC of the types of ear protectors investigated.

The noise spectra investigated were divided into five categories, depending on the values of noise spectrum index $\Delta_{CA} = L_C - L_A$ in accordance with Table 1, and a mean noise spectrum was determined for each category. The octave band pressure level values for mean noise spectra standardized to the value $L_A = 90$ dB(A) are given in Table 4.

Table 4. The mean noise spectra for domestic industry standardized to 90 dB(A)

Category	Octave band centre frequencies [Hz]								
	63	125	250	500	1000	2000	4000	8000	Δ_{CA} [dB]
1	67.8	69.8	71.8	76.1	80.8	84.0	84.9	82.8	−1.1
2	75.5	78.5	80.9	84.3	85.8	84.0	80.0	75.1	0.8
3	82.1	84.6	85.9	87.6	85.6	82.4	77.0	70.9	2.9
4	88.6	88.5	89.5	88.0	85.3	81.1	75.3	68.1	5.2
5	99.1	97.4	91.2	88.4	83.5	78.1	71.3	62.1	11.6

4. Determination of the attenuation S_A and reduced attenuation $S_{A,S}$ for ear protectors

The attenuation of ear protectors investigated was determined for two cases:

1. When using as a starting point the mean real-ear attenuation S_f of ear protectors – the attenuation thus determined aws denoted by S_A.

It follows from statistical considerations that in such a case the ear protectors will diminish the noise sound level by at least S_A dB(A) for about 50% of the users.

2. When using as a starting point the reduced real-ear attenuation $S_{f,s}$, equal to the mean value of the real-ear attenuation $S_{f,s}$ reduced by standard deviation s ($S_{f,s} = S_f - s$) – the attenuation calculated in this way was named "reduced" and denoted by $S_{A,S}$. Accounting for standard deviation, diminution of the sound level by at least $S_{A,s}$ dB(A) is achieved by ear protectors for about 85% of the users.

The attenuation S_A and reduced attenuation $S_{A,s}$ for a set of noise spectra, occurring in domestic industry, and the mean values of $\bar{S}_A$ and $\bar{S}_{A,s}$ for each spectrum category were determined [16]. Calculated values of S_A and $S_{A,s}$ for each type ear protector were plotted on the coordinate systems Δ_{CA}, S_A and Δ_{CA}, $S_{A,s}$. A graphic representation of the calculations for E-A-R plugs is presented in Fig. 1, as an example. Mean values of $\bar{S}_A$ and $\bar{S}_{A,s}$ are given in Table 5.

As can be seen in Fig. 1 and Table 5, with increasing value of the noise spectrum index Δ_{CA}, i.e. when passing from noises whose spectra contain strong

Table 5. The mean attenuation $\bar{S}_A$ and mean reduced attenuation $\bar{S}_{A,s}$ of ear protectors [dB(A)]

Type of ear protectors	Quantity	The noise spectrum category				
		1	2	3	4	5
TD-1A	$\bar{S}_A$	21.2	16.2	12.0	8.9	5.8
	$\bar{S}_{A,s}$	15.7	11.3	7.1	4.1	1.1
TD-5	$\bar{S}_A$	23.6	20.3	17.2	14.5	11.2
	$\bar{S}_{A,s}$	19.4	16.7	13.9	11.3	8.0
Saturn II	$\bar{S}_A$	20.5	16.3	14.8	14.1	13.0
	$\bar{S}_{A,s}$	12.1	8.6	7.4	6.6	5.2
E-A-R	$\bar{S}_A$	29.3	25.0	23.1	22.2	21.0
	$\bar{S}_{A,s}$	23.1	19.0	17.3	16.6	15.8
Ear defender	$\bar{S}_A$	22.7	18.9	17.1	16.2	15.3
	$\bar{S}_{A,s}$	15.5	11.6	9.7	8.6	7.6
3 M Brand No. 8773	$\bar{S}_A$	23.9	21.3	20.2	19.7	19.1
	$\bar{S}_{A,s}$	18.0	16.7	16.0	15.6	15.1
Contraphon wool	$\bar{S}_A$	18.2	13.6	11.7	10.6	9.3
	$\bar{S}_{A,s}$	14.1	9.9	8.0	6.9	5.6

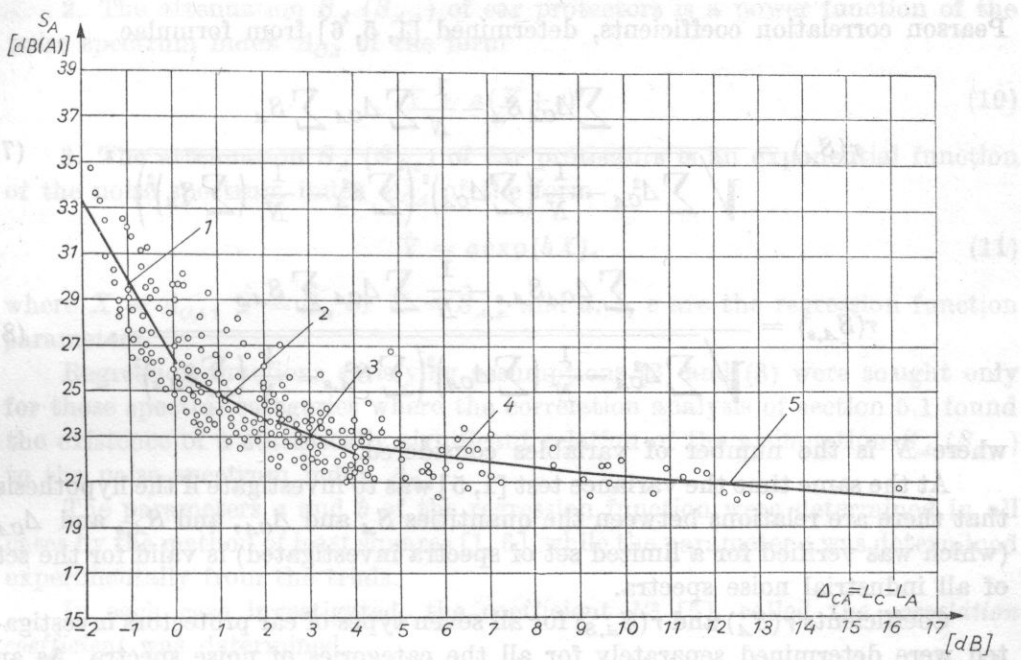

Fig. 1. Attenuation S_A of E-A-R plugs; linear regression curves and their equations $1 - S_A = 26.4 - 3.5\ \Delta_{CA}$; $2 - S_A = 26.0 - 1.1\ \Delta_{CA}$; $3 - S_A = 25.6 - 0.8\ \Delta_{CA}$; $4 - S_A = 23.4 - 0.2\ \Delta_{CA}$; $5 - S_A = 22.6 - 0.1\ \Delta_{CA}$

high frequency components to noises with strong low frequency components, the attenuation S_A and the reduced attenuation $S_{A,S}$ of all types of ear protectors decrease. The most rapid variation in the attenuation S_A and the reduced attenuation $S_{A,s}$ occurs with categories of noise spectra 1-3 for all types of ear protectors. The ear plugs are characterized by a lower relation of the attenuation S_A and the reduced attenuation $S_{A,S}$ to the noise spectral distribution, compared to the ear muffs. The relative variation in values of the attenuation S_A and the reduced attenuation $S_{A,s}$ is 5-11 dB(A) for the ear plugs and 11-20 dB(A) for the ear muffs.

5. Analysis of the results

The spacing of the analytic points on the curves relating S_A and $S_{A,s}$ to the value of the noise spectrum index Δ_{CA} suggests the existence of a correlation between these variables and functional relations $S_A = f(\Delta_{CA})$ and $S_{A,s} = f(\Delta_{CA})$. The correlation was investigated and regression relations determined.

5.1. Investigation of the correlation. The existence of correlation between the quantities S_A and Δ_{CA}, and $S_{A,s}$ and Δ_{CA} was investigated using the

Pearson correlation coefficients, determined [1, 5, 6] from formulae

$$r(S_A) = \frac{\sum \Delta_{CA} S_A - \frac{1}{N} \sum \Delta_{CA} \sum S_A}{\sqrt{\sum \Delta_{CA}^2 - \frac{1}{N} \left(\sum \Delta_{CA}\right)^2 \left(\sum S_A^2 - \frac{1}{N} \left(\sum S_A\right)^2\right)}}, \tag{7}$$

$$r(S_{A,s}) = \frac{\sum \Delta_{CA} S_{A,s} - \frac{1}{N} \sum \Delta_{CA} \sum S_{A,s}}{\sqrt{\sum \Delta_{CA}^2 - \frac{1}{N} \left(\sum \Delta_{CA}\right)^2 \left(\sum S_{A,s}^2 - \frac{1}{N} \left(\sum S_{A,s}\right)^2\right)}}, \tag{8}$$

where N is the number of variables considered.

At the same time the variance test [1, 5] was to investigate if the hypothesis that there are relations between the quantities S_A and Δ_{CA}, and $S_{A,s}$ and Δ_{CA} (which was verified for a limited set of spectra investigated) is valid for the set of all industrial noise spectra.

Coefficients $r(S_A)$ and $r(S_{A,S})$ for all seven types of ear protectors investigated were determined separately for all the categories of noise spectra. As an example, values of the coefficients $r(S_A)$ and $r(S_{A,s})$ for E-A-R plugs are given in Table 6. It was found that in general the attenuation S_A and the reduced

Table 6. The correlation coefficients $r(S_A)$ and $r(S_{A,s})$ for E-A-R plugs

Noise category	1	2	3	4	5
$r(S_A)$	−0.726	−0.425	−0.467	−0.284	−0.502
$r(S_{A,s})$	−0.681	−0.391	−0.424	−0.200	−0.390

attenuation $S_{A,s}$, of the ear protectors considered, depend strongly on the value of Δ_{CA} for spectral categories 1, 2 and 3 (a strong negative relationship), whereas it is almost independent of the noise spectral distribution for noises in categories 4 and 5.

5.2. Investigation of the regression. The analysis carried out in section 5.1 showed the existence of the distinct relation of attenuation S_A and reduced attenuation $S_{A,s}$ to the noise spectrum index Δ_{CA}, and thus to the noise spectrum. In order to determine the form of this dependence, regression analyses were made with the following assumptions:

1. The attenuation S_A ($S_{A,S}$) of ear protectors is a linear function of the noise spectrum index Δ_{CA} for each category of noise spectra:

$$\hat{Y} = aX + b. \tag{9}$$

2. The attenuation S_A ($S_{A,s}$) of ear protectors is a power function of the noise spectrum index Δ_{CA} of the form

$$\hat{Y} = a(X+c)^b. \tag{10}$$

3. The attenuation S_A ($S_{A,s}$) of ear protectors is an exponential function of the noise spectrum index Δ_{CA} of the form

$$\hat{Y} = a\exp(bX), \tag{11}$$

where $X = \Delta_{CA}$, $\hat{Y} = \hat{S}_A$ or $\hat{Y} = \hat{S}_{A,s}$ and a, b, c are the regression function parameters.

Regression functions satisfying assumptions (2) and (3) were sought only for those spectral categories where the correlation analysis of section 5.1 found the existence of a statistically significant relation of the attenuation S_A ($S_{A,s}$) to the noise spectrum index Δ_{CA}.

The parameters a and b of the regression function were determined in all cases by the method of least squares [1, 6], while the parameter c was determined experimentally from the trials.

In each case investigated, the coefficient R^2 [5], called the *correlation coefficient* was determined,

$$R^2 = \frac{\sum Y^2 - \frac{1}{N}\left(\sum Y\right)^2 - \sum (Y-\hat{Y})^2}{\sum Y^2 - \frac{1}{N}\left(\sum Y\right)^2}, \tag{12}$$

where Y is a variable (in the present case $Y = S_A$ or $Y = S_{A,s}$), N – the number of variables considered, $\hat{Y}$ – the value determined from the regression equation for a given X (here $X = \Delta_{CA}$).

The coefficient R^2 can take values from 0 to 1, and the larger R^2, the better the regression function Y describes the dependence considered [1, 5].

5.2.1. Linear regression of the ear protector attenuation in different categories of noise spectra. The equations for curves describing the dependence the attenuation S_A and reduced attenuation $S_{A,s}$ on the noise spectrum index Δ_{CA} were determined by a linear regression analysis. The linear regression dependences are statistically significant at the level $\alpha = 0.05$. A significant linear dependence of attenuation S_A and reduced attenuation $S_{A,s}$ on Δ_{CA}, i.e. on the noise spectral distribution, occurs for all ear protectors investigated in spectral categories 1, 2 and 3, in category 4 for the following types of protectors: TD-1A, Saturn II, E-A-R, contraphon wool, and in category 5 for the plugs Saturn II and E-A-R only.

Fig. 1 shows regression curves of the attenuation S_A in particular noise spectral categories for E-A-R plugs.

5.2.2. Curvilinear regression of the ear protector attenuation. On the sample of 3*M* Brand No. 8773 plugs it was found that the mean values $\bar{S}_A$ ($\bar{S}_{A,s}$) and $\bar{\Delta}_{CA}$ in particular categories had practically the same regression equations as all the individual values S_A ($S_{A,s}$) and Δ_{CA} over the ranges of these quantities considered. Thus, when looking for a general regression function that would not only be valid within one category, the mean values $\bar{S}_A$, $\bar{S}_{A,s}$ and $\bar{\Delta}_{CA}$ for the different categories were used. Using the method of least squares and with the experimental determination for the case of the square regression (formula (10)) of such a value of the parameter c that the coefficient R^2 would reach the maximum possible value, curvilinear regression equations were obtained as presented in Tables 7 and 8.

Table 7. Equations of curvilinear regression of the attenuation S_A of ear protectors ($\hat{S}_A$ in dB(A) and Δ_{CA} in dB)

Type of ear protectors	Equation of curvilinear regression	Regression coefficient		Regression in spectral categories
		curvilinear R^2	linear R^2	
TD-1A	$\hat{S}_A = 75.5\,(\Delta_{CA}+5)^{-0.902}$ $\hat{S}_A = 18.5 \exp(-0.135\,\Delta_{CA})$	0.994 0.994	0.981	1 – 4
TD-5	$\hat{S}_A = 21.9 \exp(-0.075\,\Delta_{CA})$	0.994	0.979	1 – 4
Saturn II	$\hat{S}_A = 23.5\,(\Delta_{CA}+3)^{-0.236}$ $\hat{S}_A = 17.7 \exp(-0.033\,\Delta_{CA})$ $\hat{S}_A = 20.5\,(\Delta_{CA}+2)^{-0.187}$	0.943 0.761 0.974	0.706	1 – 5
E-A-R	$\hat{S}_A = 32.5\,(\Delta_{CA}+3)^{-0.175}$ $\hat{S}_A = 31\,(\Delta_{CA}+2.5)^{-0.157}$	0.952 0.967	0.734	1 – 5
Ear defender	$\hat{S}_A = 28.2\,(\Delta_{CA}+3)^{-0.284}$	0.994	0.936	1 – 3
3M BRAND No 8773	$\hat{S}_A = 22.7 \exp(-0.044\,\Delta_{CA})$	0.928	0.917	1 – 3
Contraphon	$\hat{S}_A = 22.9\,(\Delta_{CA}+3)^{-0.356}$	0.975	0.742	1 – 5

For comparison, the values of the coefficient R^2 for the linear regression are also given in these tables. It was found that curvilinear regression equations describe the observed dependencies of the attenuation $\hat{S}_A$ ($\hat{S}_{A,s}$) on the noise spectrum index Δ_{CA} better than the linear regression equations (R^2 for curvilinear regressions is greater than R^2 for linear regressions), and the square law regression proved better than the exponential for all cases except the ear muffs TD-1A and TD-5.

In Fig. 2 points corresponding to the values of $\bar{S}_A$ and $\bar{\Delta}_{CA}$ for E-A-R plugs for particular categories are plotted, and the regression curves obtained drawn together with the regression linear curves within particular spectral categories.

Table 8. Equations of curvilinear regression of the reduced attenuation $S_{A,s}$ of ear protectors ($\hat{S}_{A,s}$ in dB(A) and Δ_{CA} in dB)

Type of ear protectors	Equations of curvilinear regression	Regression coefficient		Regression in spectral categories
		curvilinear R^2	linear R^2	
TD-1A	$\hat{S}_{A,S} = 20144954.7\ (\Delta_{CA}+20)^{-4.748}$	0.996	0.97	1 – 4
	$\hat{S}_{A,S} = 13.4 \exp(-0.214\ \Delta_{CA})$	0.999		
TD-5	$\hat{S}_{A,S} = 18.1 \exp(-0.085\ \Delta_{AC})$	0.999	0.988	1 – 4
Saturn II	$\hat{S}_{A,S} = 16.5\ (\Delta_{CA}+3)^{-0.44}$	0.987	0.78	1 – 5
	$\hat{S}_{A,S} = 9.8 \exp(-0.064\ \Delta_{CA})$	0.883		
E-A-R	$\hat{S}_{A,S} = 28.6\ (\Delta_{CA}+3)^{-0.288}$	0.986	0.917	1 – 3
	$\hat{S}_{A,S} = 25.7\ (\Delta_{CA}+3)^{-0.198}$	0.922	0.677	1 – 5
Ear defender	$\hat{S}_{A,S} = 21.4(\Delta_{CA}+3)^{-0.434}$	0.991	0.865	1 – 4
3M BRAND No 8773	$\hat{S}_{A,S} = 19.1\ (\Delta_{CA}+3)^{-0.094}$	0.971	0.791	1 – 5
	$\hat{S}_{A,S} = 17.1 \exp(-0.013\ \Delta_{CA})$	0.811		
Contraphon	$\hat{S}_{A,S} = 20.6\ (\Delta_{CA}+3)^{-0.519}$	0.992	0.857	1 – 4

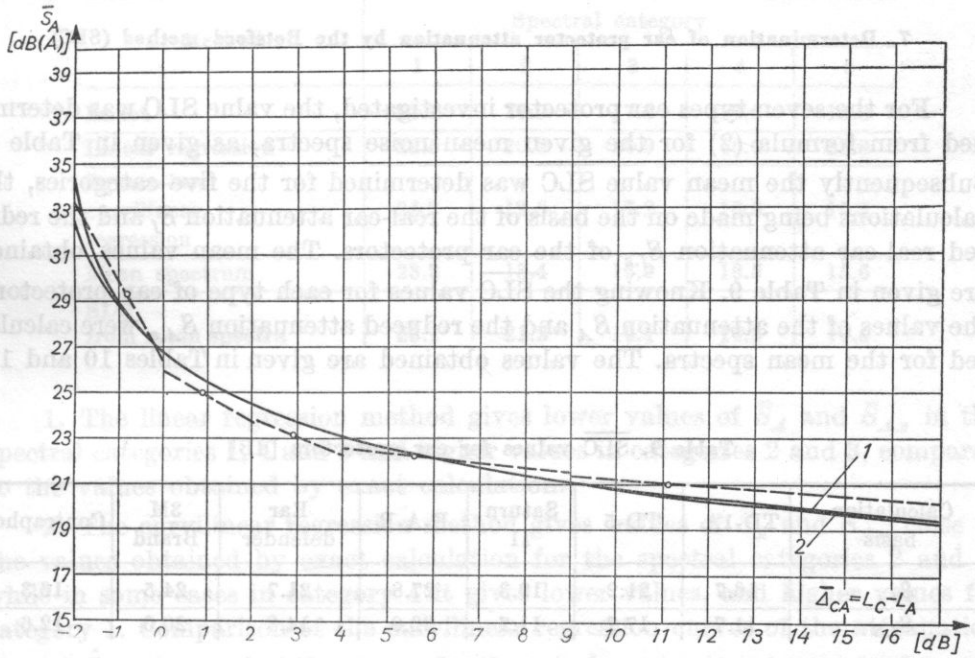

Fig. 2. Regression curves of the attenuation $\bar{S}_A$ of inserts E-A-R plugs (Optac) and their equations

$1 - S_A = 32.5\ (\Delta_{CA}+3)^{-0,175}$; $2 - S_A = 30.953(\Delta_{CA}+2.5)^{-0.157}$

Analyzing the linear and curvilinear regression curves separately for each type of ear protector, it was found that curvilinear regression curves with a high coefficient R^2 are the optimal regression curves for the sets of values of S_A ($S_{A,s}$) and Δ_{CA} considered.

6. Determination of ear protector attenuation on the basis of mean noise spectra

For the seven types of ear protector investigated the attenuation S_A and the reduced attenuation $S_{A,s}$ were determined by the exact method for five mean noise spectra, as shown in Table 4. The values obtained for each type of ear protector were plotted on diagram analogous to Fig. 1. The curves were plotted through the points thus obtained and extrapolated beyond the extremal points. On the basis of the curves thus determined for the attenuation S_A and the reduced attenuation $S_{A,s}$ relative to the points corresponding to the attenuation values of the ear protectors for the 454 noise spectra investigated, it was considered that these curves represent well the dependence of the mean attenuation of the ear protectors on the noise spectrum index Δ_{CA}. Instead of investigating the attenuations S_A and $S_{A,s}$ for a large range of spectra, it is sufficient to determine the curves for $S_A = f(\Delta_{CA})$ and $S_{A,s} = f(\Delta_{CA})$ on the basis of only five values: those obtained for the mean spectra in particular categories.

7. Determination of ear protector attenuation by the Botsford method (SLC)

For the seven types ear protector investigated, the value SLC was determined from formula (2) for the given mean noise spectra, as given in Table 4. Subsequently the mean value $\overline{\text{SLC}}$ was determined for the five categories, the calculations being made on the basis of the real-ear attenuation S_f and the reduced real-ear attenuation $S_{f,s}$ of the ear protectors. The mean values obtained are given in Table 9. Knowing the $\overline{\text{SLC}}$ values for each type of ear protectors, the values of the attenuation S_A and the reduced attenuation $S_{A,s}$ were calculated for the mean spectra. The values obtained are given in Tables 10 and 11.

Table 9. $\overline{\text{SLC}}$ values for ear protectors [dB]

Calculation basis	TD-1A	TD-5	Saturn II	E-A-R	Ear defender	3M Brand	Contraphon
S_f	16.7	21.2	19.3	27.8	21.7	24.5	16.3
$S_{f,S}$	11.7	17.7	11.7	22.0	14.3	20.0	12.6

8. Comparison of the different methods of determining ear protector attenuation

As an example, the values of the mean attenuation $\overline{S}_A$ and the reduced attenuation $\overline{S}_{A,s}$ of the E-A-R plugs obtained by different methods are shown together in Tables 10 and 11. Similar comparisons were made for all ear protectors investigated. The analysis led to the following conclusions:

Table 10. Mean attenuation $\bar{S}_A$ of the E-A-R plugs obtained by different methods (in dB(A))

Method	Spectral category				
	1	2	3	4	5
Exact	29.3	25.0	23.1	22.2	21.0
Linear regression	27.0	26.0	24.7	23.2	19.8
Square-law curvilinear regression	30.5	26.5	23.8	22.1	20.2
Mean spectrum	29.4	24.4	22.7	22.1	20.8
$\overline{\text{SLC}}$ from mean spectra	28.9	27.0	24.9	22.3	16.2

Table 11. Mean reduced attenuation $\bar{S}_{A,s}$ of the E-A-R plugs obtained by different methods (in dB(A))

Method	Spectral category				
	1	2	3	4	5
Exact	23.1	19.0	17.3	16.6	15.8
Linear regression	22.5	20.0	16.9	16.6	15.8
Square-law curvilinear regression	24.7	19.5	17.2	16.6	15.8
Mean spectrum	23.2	18.4	16.9	16.5	15.6
$\overline{\text{SLC}}$ from mean spectra	23.1	21.2	19.1	16.8	10.4

1. The linear regression method gives lower values of $\bar{S}_A$ and $\bar{S}_{A,s}$ in the spectral categories 1, 4 and 5 and higher values in categories 2 and 3, compared to the values obtained by exact calculation.

2. The curvilinear regression method gives values of $\bar{S}_A$ and $\bar{S}_{A,s}$ close to the values obtained by exact calculation for the spectral categories 2 and 3, while in some cases in category 4 it gives lower values, and higher values for category 1. Comparison of the curvilinear regression curves of the attenuation $\hat{S}_A$ and $\hat{S}_{A,s}$ shows that the curves for the set of sepctra in category 1 ($\Delta_{CA} \leqslant 0$) represent well the nature of the dependence of the attenuation on the difference Δ_{CA}, with the square-law curve giving better representation of the dependence than the exponential one.

3. The mean spectrum method gives values of $\bar{S}_A$ and $\bar{S}_{A,s}$ slightly lower in categories 2, 3, 4 and 5 and slightly higher in category 1, compared to the values of $\bar{S}_A$ and $\bar{S}_{A,s}$ obtained by exact calculation.

4. The Botsford method (SLC) for mean noise spectra always gives lower values of $\bar{S}_A$ and $\bar{S}_{A,s}$ in category 5, often gives higher values in categories 2, 3 and 4, while in category 1 it gives values equal to or lower than the values of $\bar{S}_A$ and $\bar{S}_{A,s}$ obtained by exact calculation, within the range of 0.1-6.7 dB(A).

5. In view of its precision and the simplicity of rapid determination of ear protector performance and their matching to noises with different spectral distributions, the mean spectrum method appears to be the most suitable.

6. The mean attenuation curves $\bar{S}_A = f(\Delta_{CA})$ and $S_{A,s} = f(\Delta_{CA})$ are characteristic of a given type of ear protector and the mean values of the reduced attenuation $S_{A,s}$ for each of the five noise spectral categories should be given as the data characterizing the protective properties of the ear protectors.

References

[1] H. M. Blalock, *Social statistics* (in Polish), PWN, Warszawa 1975, p. 305-354.

[2] J. H. Botsford, *Simple method for identifying acceptable noise exposures*, JASA, 424, 810-819 (1967).

[3] J. H. Botsford, *Using sound levels to gauge human response to noise*, Sound and Vibration, **3**, 10, 16-28 (1969).

[4] J. H. Botsford, *How to estimate* dB (A) *reduction of ear protectors*, Sound and Vibration, **7**, 11, 32-33 (1973).

[5] R. Elandt, *Mathematical statistics in agricultural experimental research* (in Polish), PWN, Warszawa 1964, p. 370.

[6] J. Greń, *Models and tasks of mathematical statistics* (in Polish), PWN, Warszawa 1970, p. 97-103.

[7] ISO Recommendation *R*/1999-1971 (*E*) Acoustics, *Assessment of occupational noise exposure for hearing conservation purposes.*

[8] D. L. Johnson, C. W. Nixon, *Simplified methods for estimating hearing protector performance*, Sound and Vibration, **8**, 6, 20-27 (1974).

[9] A. Lüpke, *Die Auswahl von Gehörschützern nach ihrer Schalldämmung*, Kampf der Lärm, **22**, 5, 128-131 (1975).

[10] Polish Standard No. PN-70/*B*-02151, *Building acoustics. Noise control in buildings.*

[11] Polish Standard No. PN-76/*N*-01309, *Ear protectors. Method of determination of attenuation and* dB (A) *reduction.*

[12] Polish Standard No. PN-77/*N*-01310 p. 01, *Methods of the measurement and evaluation of noise at work places. Stable noise level in continuous exposition.*

[13] D. Trynkowska, *Measurement method of sound attenuation provided by earmuffs* (in Polish), Prace CIOP, XXII, **73**, 63-82 (1972).

[14] D. Trynkowska, *Measurement method of noise attenuation provided by ear-plugs* (in Polish), Prace CIOP, XXIII, **78**, 245-250 (1973).

[15] D. Trynkowska, I. Franaszczuk, *Investigations of attenuation and factors deciding about the comfort of using ear protectors designed for textile-workers* (in Polish), Prace CIOP, XXVI, **83**, 51-74 (1976).

[16] D. Trynkowska, R. Michalski, *The determination of classification bases for individual ear protectors on the basis of their acoustic properties* (in Polish), work Report 04. U. 07. 02., CIOP (1978).

[17] VDI 2560, *Persönlicher Schallschutz*, Project, 1974.
[18] R. WAUGH, dB(A) *attenuation of ear protectors*, JASA, **53**, 2 440-447 (1973).
[19] R. WAUGH, *Investigation of sound level conversion as a means of rating ear protector performance*, American Industrial Hygiene Association Journal, **37**, 4, 239-245 (1976).

Received on August 26, 1978

ARCHIVES OF ACOUSTICS
4, 3 (1979)

SOUND RADIATION PRODUCED BY A SHIP PROPELLER

EUGENIUSZ KOZACZKA

Naval College (81-919 Gdynia)

The theory of the generation of acoustic radiation by a ship propeller working in a stream with a non-uniform stationary distribution is briefly discussed in this paper. Relations permitting calculation of acoustic pressure values produced by a ship propeller working under given conditions are also derived. The acoustic method for determining the coefficients characterizing the load variation of ship propeller blades working in a non-uniform liquid stream with stationary characteristics is also discussed. This method can also be used for estimation of the velocity field non-uniformity for the flow of the medium in which the propeller works. Experimental measurements were carried out and calculations made, based on the equations derived, and the values were compared. Numerical computations were made, based on purpose-designed programmes. Spectral analysis was carried out numerically using an FFT algorithm.

Basic notation

a — effective radius of the ship propeller ($a = 0.8\, r_M$) [m]
b — ship propeller width [m]
c — sound velocity in water [m/s]
D — ship propeller diameter [m]
$f = F/2\pi a$ — force density distribution on the circumference of the propeller circle [N/m]
f_N — normal component of the force density f [N/m]
F — action of the ship propeller on the medium [N]
$G(R|r, \omega)$ — Green's function
H/D — propeller pitch
i — imaginary number ($i = \sqrt{-1}$)
$J_q(x)$ — Bessel function of the first kind of order q
k — wave number [1/m]
K_M — torque coefficient
K_T — thrust coefficient
M — torque applied to the propeller [Nm]
m — number of harmonic of the sound pressure
n — propeller speed [rps]
L — sound pressure level [dB]
p — sound pressure [N/m^2]
p_N — thrust-related sound pressure

p_S — torque-related sound pressure [N/m^2]
p_m — sound pressure of m-th harmonic [N/m^2]
r_M — ship propeller radius [m]
R — distance between the propeller centre and the observation point [m]
S/S_0 — area coefficient
T — propeller thrust [N]
z — number of the propeller blades
a_m — coefficient related to the load distribution along the chord
β_l — coefficient for the ship propeller load distribution
$\delta(x)$ — Dirac function
φ, ψ, θ — coordinates
λ — wavelength — $\lambda = 2\pi/k$ [m]
ϱ — density of the medium [kg/m^3]
ω — angular velocity [rad/s]

1. Introduction

The theory of sound generation by rotary sources working in a gaseous medium has a comparatively large literature. Investigations in this field deal mainly with the problems related to the methods for noise level diminution in bladed machines. In particular, these papers describe the phenomena of the sound generation by an aircraft propeller, helicopter rotors, compressors, turbines, and also fans. Less attention has been paid, however, to sound generation by a ship propeller.

In the literature on the subject this problem, for the range of steady-state conditions, i.e. a steady load on a rotary system, has been solved by methods used in mathematical physics. The method of separation of the variables (Fourier method) has been used most frequently. These problems have also often been solved using integral transforms (the Hankel-Fourier transformation). In the present paper the phenomenon of sound radiation by a source of the propeller type will be solved by the Green function method, which is the most effective for solution of stationary cases in infinite region.

Reviewing the literature on the theory of the sound generation by rotary blade systems, mention should be made of the first paper, now classical, of GUTIN [12] describing the phenomenon of sound radiation by an aircraft propeller. The results given in this paper are valid even today, e.g. in the case of an aircraft propeller working in a uniform air stream [21].

LIGHTHILL's paper [17] in which the author presented the so-called *acoustic analogy approach*, now totally accepted, was another essential step in the development of the theory of sound generation by aerodynamic sources.

In his paper Lighthill did not specify precisely the form of the excitement source itself, assuming that it was *a priori* known. The idea of the acoustical analogy method lies in a representation of the phenomenon of sound generation by complicated physical processes, as a so-called *equivalent source* [3].

Further development of the theory of sound generation, as related to acoustical analogy, has been directed to the determination of the acoustic effects related to the action of a solid on the flow of a liquid. The first paper on this subject was published by CURLE [2].

Paper [6] is important from the viewpoint of the relation between the acoustical analogy and the action of the solid boundaries in the liquid stream flow. Further development of the theory of sound generation by aerodynamic sources is related to the investigation of the structure of noise produced by fans and compressors [7, 8, 18, 19], aircraft propellers, and helicopter rotors [13, 20, 22, 26, 27]. GOLDSTEIN presented a description of the phenomenon of sound generation by sources of the propeller type, with a relatively general approach. In his papers on aeroacoustics [9-11] he presented a theory of sound generation by aerodynamic sources and suggested its practical applications.

Mention should also be made of the papers of DOKUCHAEV [4, 5] which are related to a description of sound generation by concentrated forces moving on the circumference and helix.

As regards those papers whose content is strictly related to sound radiation by a ship propeller, only a few works have been published. The most interesting are those of TSAKONAS et al. [24, 25]. It should be mentioned here that the model of the phenomenon of sound generation by a ship propeller which was used in the above-mentioned papers is based on the analysis in BRESLIN's paper [1].

It follows from this review that only a few papers have been devoted to the description of phenomena involved in sound radiation by a ship propeller.

In the present investigation a model of the sound generation by blade systems was used where the action of the blades was replaced with the effect of concentrated forces rotating on the circumference of a circle.

2. Description of sound radiation by a ship propeller working in a uniform velocity field of water flow

Let us consider the problem of sound radiation by a ship propeller working in the "sub-cavitation" range. When the phenomenon of cavitation does not occur, sound radiation is mainly related to the action of the propeller blades on the medium around them. The radiation has almost purely a dipole distribution. In the following discussion we shall assume that the ship propeller has z blades and rotates with angular velocity ω.

The problem of sound generation by a ship propeller will be solved by a method which uses the properties of Green's function. The Green function for infinite region is determined from the solution of the heterogeneous Helmholtz equation of the form

$$(\nabla^2 + k^2) G(\boldsymbol{R} | \boldsymbol{r}, \omega) = -\delta(\boldsymbol{R} - \boldsymbol{r}) \tag{1}$$

with the SOMMERFELD condition [11, 23]

$$\lim_{|\boldsymbol{R}|\to\infty} |\boldsymbol{R}| \left[\frac{\partial G(\boldsymbol{R}|\boldsymbol{r}, \omega)}{\partial |\boldsymbol{R}|} + ikG(\boldsymbol{R}|\boldsymbol{r}, \omega) \right] = 0, \tag{2}$$

where $\boldsymbol{R}$ is the vector connecting the origin of coordinates with the observation point, $\boldsymbol{r}$ — the vector connecting the origin of coordinates with a point source, ω — the angular velocity, $\delta(x)$ — the Dirac function, ∇^2 — the Laplace operator, and k — the wave number.

We have

$$\nabla^2 = \operatorname{div}\operatorname{grad} = \frac{1}{R^2}\frac{\partial}{\partial R}\left(R^2 \frac{\partial}{\partial R}\right) + \frac{1}{R^2 \sin\theta}\frac{\partial}{\partial \theta}\left(\sin\theta \frac{\partial}{\partial \theta}\right) + \frac{1}{R^2 \sin^2\theta}\frac{\partial^2}{\partial \psi^2},$$

$$\delta(\boldsymbol{R}-\boldsymbol{r}) = \frac{\delta(R-r)\delta(\psi-\varphi)\delta\theta}{R^2 \sin\theta}.$$

The solution of equation (1) with condition (2) has the following form:

$$G(\boldsymbol{R}|\boldsymbol{r}, \omega) = \frac{e^{-ik|\boldsymbol{R}-\boldsymbol{r}|}}{4\pi|\boldsymbol{R}-\boldsymbol{r}|}. \tag{3}$$

Knowing the form of the Green function, one can determine the acoustic pressure produced by a moving body, with a preset force density distribution acting on the surrounding medium, using [11, 16] the relation

$$p(R, \psi, \theta, t) = \iint_S f_i G_i(\boldsymbol{R}|\boldsymbol{r}, \omega) dS(\boldsymbol{x}), \tag{4}$$

where $G_i(\boldsymbol{R}|\boldsymbol{r}, \omega)$ is the partial derivative with respect to the i-th coordinate, and f_i is the i-th component of the force density distribution.

The force density distribution per unit area blade is determined from the equation

$$f_i = \frac{f_i^{(1)}}{|n_3^{(1)}|} + \frac{f_i^{(2)}}{|n_3^{(2)}|}, \tag{5}$$

where n_3 is a unit vector normal to the ship propeller blade surface, $i = \{x_3, \varphi\}$.

Figure 1 shows the action of the forces on the ship propeller blade.

Since in practice the analytical form of the expression describing ship propeller blade area is usually not known, the force generated by a ship propeller on the medium should be determined experimentally by measuring the thrust and the torque. Hence for the determination of acoustic effects produced by a ship propeller it is enough to present the force density distribution on the circumference of a circle with a radius, called the *effective radius* [13]. The force density distribution can be expressed by the formula

$$f = \frac{F_1}{2\pi r} \sum_{m=-\infty}^{\infty} a_m e^{im(\omega t-\varphi)} \delta(r-a), \tag{6}$$

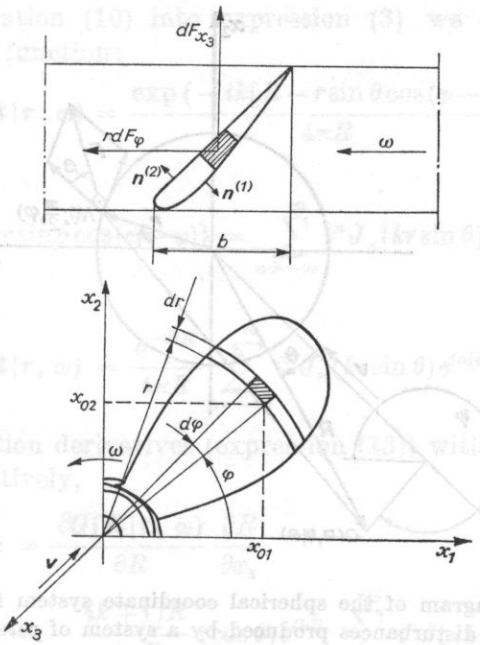

Fig. 1. The action of ship propeller blades on the surrounding medium

where a is the effective ship propeller radius ($a \simeq 0.8\, r_M$), r_M – the ship propeller radius, F_1 – the force of a ship propeller acting on the medium, α_m – the coefficient accounting for the finite width of the ship propeller blades.

If a ship propeller has z blades, equation (6) takes the form

$$f = \frac{F}{2\pi R} \sum_{m=-\infty}^{\infty} \alpha_m e^{imz(\omega t-\varphi)}\, \delta(r-a), \tag{7}$$

where z is the number of blades.

Expression (7) describes the force density distribution over unit circumference of a circle of radius $r = a$ for a propeller load which is constant as a function of the rotation angle.

The force density distribution can be represented as the vector sum of components related to the ship propeller thrust (normal to the surface of the propeller circle) and the torque (tangential to the circumference of the effective propeller circle). Figure 2 shows the acoustic pressure produced by a rotating system of concentrated forces, representing the action of the blades on the liquid medium.

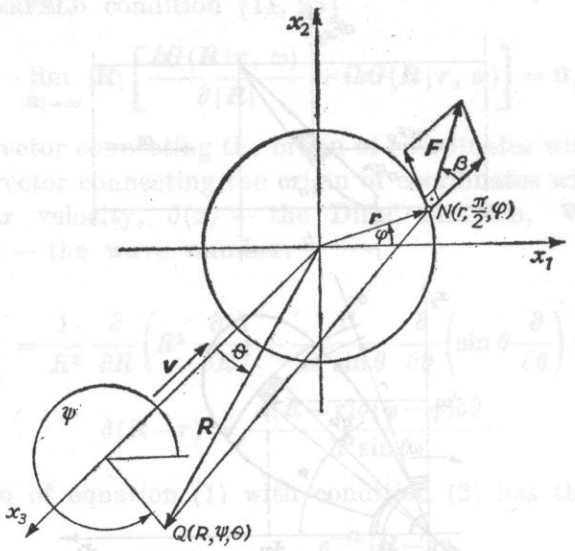

Fig. 2. A schematic diagram of the spherical coordinate system for determination of the distribution of acoustic disturbances produced by a system of rotating concentrated forces

The components of the force density distribution are represented by the following relations:

$$f_{x_3} = \frac{|F|}{2\pi R}\cos\beta \sum_{m=-\infty}^{\infty} a_m e^{im\varkappa(\omega t-\varphi)}\delta(r-a), \tag{8}$$

$$f_{\varphi} = \frac{|F|}{2\pi R}\sin\beta \sum_{m=-\infty}^{\infty} a_m e^{im\varkappa(\omega t-\varphi)}\delta(r-a). \tag{9}$$

It will be assumed further on that the acoustics pressure is calculated for distances R satisfying the relation $R \gg r$.

The coordinates of the observation point are

$$Q(R,\psi,\theta) = \{R\cos\psi\sin\theta, R\sin\psi\sin\theta, R\cos\theta\},$$

whereas the force action point coordinates are given by

$$N\left(r,\varphi,\frac{\pi}{2}\right) = \{r\cos\varphi, r\sin\varphi, 0\}.$$

The distance of the force action point from the observation point is

$$|\boldsymbol{R}-\boldsymbol{r}| = [R^2+r^2-2Rr\sin\theta\cos(\varphi-\psi)]^{1/2} \approx R-r\sin\theta\cos(\varphi-\psi). \tag{10}$$

Substituting relation (10) into expression (3) we obtain the following form for the Green function:

$$G(\boldsymbol{R}|\boldsymbol{r}, \omega) = \frac{\exp\{-ik[R - r\sin\theta\cos(\varphi - \psi)\}}{4\pi R}. \tag{11}$$

Since (see [23])

$$\exp\{ikr\sin\theta\cos(\varphi - \psi)\} = \sum_{n=-\infty}^{\infty} i^n J_n(kr\sin\theta)\, e^{in(\varphi-\psi)},$$

we have

$$G(\boldsymbol{R}|r, \omega) = \frac{e^{-ikR}}{4\pi R} \sum_{n=-\infty}^{\infty} i^n J_n(kr\sin\theta)\, e^{in(\varphi-\psi)}. \tag{13}$$

The Green function derivatives (expression (13)) with respect to variables x_3 and ψ are, respectively,

$$G_{x_3}(\boldsymbol{R}|\boldsymbol{r}, \omega) = \frac{\partial G(\boldsymbol{R}|\boldsymbol{r}, \omega)}{\partial R}\frac{\partial R}{\partial x_3}$$

$$= -\frac{ik + 1/R}{4\pi R}(\cos\theta)\, e^{ikR} \sum_{n=-\infty}^{\infty} i^n J_n(kr\sin\theta)\, e^{in(\varphi-\psi)}, \tag{14}$$

$$G_{\psi}(\boldsymbol{R}|\boldsymbol{r}, \omega) = \frac{1}{r}\frac{\partial G(\boldsymbol{Rr}, \omega)}{\partial \psi}$$

$$= -\frac{e^{-ikR}}{4\pi R} \sum_{n=-\infty}^{\infty} n i^n J_n(kr\sin\theta)\, e^{in(\varphi-\psi)}. \tag{15}$$

A ship propeller with z blades produces an acoustic pressure given by the following relation:

$$p(R, \psi, \theta, t)$$

$$= -\iint_S \frac{|\boldsymbol{F}|}{2\pi r} \sum_{m=-\infty}^{\infty} \sum_{n=-\infty}^{\infty} a_m \frac{e^{-imzkR}}{4\pi R}\left[-\left(imzk + \frac{1}{R}\right)\cos\beta\cos\theta + \frac{in}{r}\sin\beta\right] \times$$

$$\times i^n J_n(mzkr\sin\theta)\exp\{i[mz\omega t - (mz - n)\varphi - n\psi]\}\,\delta(r - a)\, r\,dr\,d\varphi. \tag{16}$$

Expression (16) describes the acoustic pressure distribution around a system of z concentrated forces, rotating at an angular velocity ω. The resultant force of the ship propeller action on the surrounding medium is constant. After integration of expression (16) we obtain the following relation:

$$p(R, \psi, \theta, t) = -\frac{|\boldsymbol{F}|}{4\pi R} \sum_{m=-\infty}^{\infty} a_m \left[-\left(imzk + \frac{1}{R}\right)\cos\beta\cos\theta + \frac{imz}{a}\sin\beta\right] \times$$

$$\times i^{mz} J_{mz}(mzka\sin\theta)\exp\left\{imz\left[\omega\left(t - \frac{R}{c}\right) - \psi\right]\right\}. \tag{17}$$

The acoustic pressure described by relation (17) can be given by the sum

$$p(R, \psi, \theta, t) = p_{x_3}(R, \psi, \theta, t) + p_{\psi}(R, \psi, \theta, t), \tag{18}$$

where

$$p_{x_3}(R, \psi, \theta, t) = \frac{|F|}{4\pi R} \sum_{m=-\infty}^{\infty} a_m \left[imzk + \frac{1}{R} \right] [\cos\beta \cos\theta] \times$$

$$\times i^{mz} J_{mz}(mzk \sin\theta) \exp\left\{ imz \left[\omega\left(t - \frac{R}{c}\right) - \psi \right] \right\}, \tag{19}$$

and

$$p_{\psi}(R, \psi, \theta, t) = -\frac{|F|}{4\pi R} \sum_{m=-\infty}^{\infty} a_m \frac{mz}{a} (\sin\beta) \times$$

$$\times i^{mz} J_{mz}(mzka \sin\theta) \exp\left\{ imz \left[\omega\left(t - \frac{R}{c}\right) - \psi \right] \right\}. \tag{20}$$

The possibility of a spatial division of the total acoustic pressure into the sum of pressures produced by forces normal and tangential to the propeller circle has an essential practical significance.

Expression (19) describes the acoustic pressure distribution produced by the axial force. The force can be represented by a continuous distribution of acoustic dipoles on the circumference of a circle with radius equal to the effective ship propeller radius. The dipole axes are parallel to the propeller rotation axis. The directional characteristic of the sound radiation by such a source is defined as the product of $\cos\theta$ and a Bessel function of the first kind of the mz-th order $[J_{mz}(x \sin)]$. The value of the acoustic pressure depends on the magnitude od the axial force, and thus on the ship propeller thrust. Figure 3a shows schematically the directional characteristic of the thrust-produced radiation.

Expression (20) describes the acoustic pressure distribution produced by a force tangential to a circle of radius a. An acoustic field is created by acoustic dipoles whose axes are tangential to the plane of the propeller circle. The directional characteristic of radiation has its maximum value on the plane of the propeller circle. The value of the acoustic pressure is related to the magnitude of the axial force, i.e. it is proportional to the torque applied to the ship propeller. Figure 3b shows schematically the characteristic of the radiation produced by a force tangential to the propeller circle.

Using the properties of complex series to express it in the trigonometric form resulting from the relation

$$\sum_{k=-\infty}^{\infty} W_k = W_0 + \sum_{k=1}^{\infty} (W_{-k} + W_k), \quad i^n = e^{in\pi/2}, \tag{21}$$

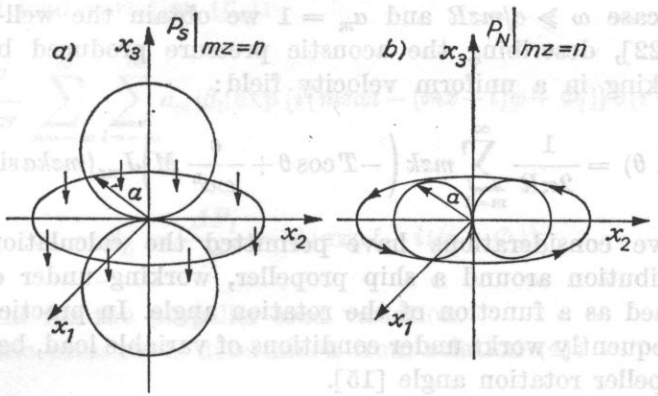

Fig. 3. Directional characteristics of the radiation of acoustic disturbances by a ship propeller, *a* – thrust produced radiation, *b* – torque produced radiation

and neglecting the term with index 0 which represents the constant behaviour, for expression (17) we get

$$p(R, \psi, \theta, t) = \frac{|F|}{2\pi R}\left\{\sum_{m=1}^{\infty} a_m\left(-mzk\cos\beta\cos\theta + \frac{mz}{a}\sin\beta\right)\sin\xi - \right.$$

$$\left. - \frac{\cos\beta\cos\theta}{R}\cos\xi\right\} J_{mz}(mzk\sin\theta), \quad (22)$$

where

$$\xi = mz\left[\omega\left(t - \frac{R}{c}\right) - \left(\psi - \frac{\pi}{2}\right)\right].$$

Using the relation between the axial force and the ship propeller thrust and between the tangential force and the torque, which can be written as

$$F_{x_3} = -|F|\cos\beta = -T, \quad (23)$$

$$F_{\varphi} = |F|\sin\beta = \frac{M}{a}, \quad (24)$$

and substituting them into relation (22), we obtain an expression for the acoustic pressure distribution in space in relation to the thrust and the torque:

$$p(R, \psi, \theta, t) = \frac{1}{2\pi R}\sum_{m=1}^{\infty} a_m\left\{\left(-mzkT\cos\theta + \frac{mz}{a^2}M\right)\sin\xi - \right.$$

$$\left. - \frac{T\cos\theta}{R}\cos\xi\right\} J_{mz}(mzka\sin\theta). \quad (25)$$

For the case $\omega \gg c/mzR$ and $a_m = 1$ we obtain the well-known Gutin formula [21, 22], describing the acoustic pressure produced by an aircraft propeller working in a uniform velocity field:

$$p(R, \theta) = \frac{1}{2\pi R} \sum_{m=1}^{\infty} mzk \left(-T \cos\theta + \frac{c}{\omega a^2} M \right) J_{mz}(mzka \sin\theta). \tag{26}$$

The above considerations have permitted the calculation of acoustic pressure distribution around a ship propeller, working under constant load, to be performed as a function of the rotation angle. In practice, a ship propeller most frequently works under conditions of variable load, being dependent upon the propeller rotation angle [15].

3. Sound radiation by a ship propeller working under conditions of variable load

Let us now consider the problem of sound radiation by a ship propeller whose load changes with variation in the rotation angle. This is a typical case where the velocity field distribution of water stream varies over the plane of the propeller circle. The case of the stream velocity variation as a function of the ship propeller rotation angle will be discussed here, with the distribution being invariable in time (stationary case).

In practice a ship propeller nearly always works under conditions of variable load. If a variable velocity field distribution occurs in the water, the ship propeller blades work at different attack angles depending on the angle of rotation. This causes variation in the thrust and torque. Figure 4 shows an

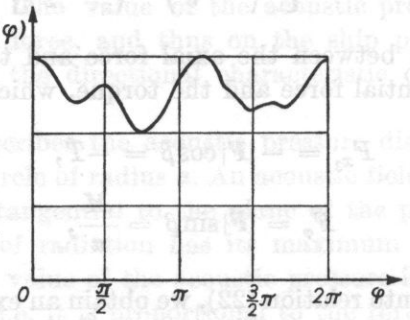

Fig. 4. An example of the ship propeller load distribution variation dependence on the rotation angle

example of a variable ship propeller load which is dependent upon the rotation angle.

The force density distribution on the ship propeller blades can be given a double complex Fourier series, taking into account the effects of finite blade

width (a_m) and load variation (β_L):

$$f = \frac{F}{2\pi r} \sum_{m=-\infty}^{\infty} \sum_{l=-\infty}^{\infty} a_m |\beta_l| \exp\{i[mz\omega t - (mz+l)\varphi + \Phi_l]\}\, \delta(r-a), \tag{27}$$

where

$$\beta_L = \frac{\Delta F_l}{F} = |\beta_l| \exp\{-i(l\varphi - \Phi_l)\}$$

is the coefficient for the propeller load variation.

The acoustic pressure is determined from relation (4):

$$p(R, \psi, \theta, t)$$

$$= -\int_0^{r_M} \int_0^{2\pi} \frac{|F|}{2\pi r} \sum_{m=-\infty}^{\infty} \sum_{l=-\infty}^{\infty} \sum_{n=-\infty}^{\infty} \frac{a_m |\beta_l|}{4\pi R} \left[-\left(imzk + \frac{1}{R} \right) \cos\beta \cos\theta + \frac{in}{r} \sin\beta \right] \times$$

$$\times i^n J_n(mzkr \sin\theta) \exp\left\{ i \left[mz\omega \left(t - \frac{R}{c} \right) - (mz+l-n)\varphi - n\varphi + \Phi_l \right] \right\} \delta(r-a)\, r\, d\varphi\, dr. \tag{28}$$

After integrating expression (28) we obtain

$$p(R, \psi, \theta, t)$$

$$= \frac{|F|}{4\pi R} \sum_{m=-\infty}^{\infty} a_m \sum_{l=-\infty}^{\infty} |\beta_l| \left[-\left(imzk + \frac{1}{R} \right) \cos\beta \cos\theta + \frac{mz+l}{a} \sin\beta \right] \times$$

$$\times J_{mz+l}(mzka \sin\theta) \exp\left\{ i \left[mz\omega \left(t - \frac{R}{c} \right) - (mz+l) \left(\varphi - \frac{\pi}{2} \right) + \Phi_l \right] \right\}. \tag{29}$$

Using equation (21) and representing the double complex series in the form of a double trigonometric series, we obtain

$$p(R, \psi, \theta, t) = \frac{|F|}{2\pi R} \sum_{m=1}^{\infty} a_m \left\{ \sum_{l=0}^{\infty} |\beta_l| \left(\left[-mzk \cos\beta \cos\theta + \frac{mz-l}{a} \sin\beta \right] \times \right. \right.$$

$$\left. \times \sin\xi - \frac{\cos\beta \cos\theta}{R} \cos\xi_1 \right) J_{mz-l}(mzka \sin\theta) + \sum_{l=0}^{\infty} |\beta_l| \times$$

$$\left. \times \left[-mzk \cos\beta \cos\theta + \frac{mz+l}{a} \sin\beta \right] \left(\sin\xi_2 - \frac{\cos\beta \cos\theta}{R} \cos\xi_2 \right) J_{mz+l}(mzka \sin\theta), \right. \tag{30}$$

where

$$\xi_1 = mz\omega\left(t-\frac{R}{c}\right)-(mz-l)\left(\psi-\frac{\pi}{2}\right)+\Phi_l,$$

$$\xi_2 = mz\omega\left(t-\frac{R}{c}\right)-(mz+l)\left(\psi-\frac{\pi}{2}\right)+\Phi_l.$$

From the cylindrical properties of Bessel functions it is known that

$$J_{mz-l}(x) \gg J_{mz+l}(x), \tag{31}$$

where m and l are natural numbers.

On the basis of relations (31), (23) and (24), expression (30) can take the following form:

$$p(R,\psi,\theta,t) = \frac{1}{2\pi R}\sum_{m=1}^{\infty}\sum_{l=0}^{\infty}\alpha_m|\beta_l|\times$$

$$\times\left\{\left[-mzkT\cos\theta+\frac{mz-l}{a^2}M\right]\sin\xi_1-\frac{T\cos\theta}{R}\cos\xi_1\right\}J_{mz-l}(mzka\sin\theta). \tag{32}$$

For $\omega \ll c/mzR$, expression (32) becomes the following:

$$p(R,\psi,\theta,t) = \frac{1}{2\pi R}\sum_{m=1}^{\infty}\sum_{l=0}^{\infty}\alpha_m|\beta_l|\times$$

$$\times\left[\frac{mz-l}{a^2}M\sin\xi_1-\frac{T\cos\theta}{R}\cos\xi_1\right]J_{mz-l}(mzka\sin\theta). \tag{33}$$

Expression (33) describes the acoustic pressure distribution near a ship propeller in the case of a propeller rotating with a small angular velocity. This relation can be used for the analytical determination of the acoustic pressure in order to verify the data obtained from experiment carried out in an anechoic basin, for example.

For determination of the acoustic pressure at long distances from the source, one can use the relation

$$p(R,\psi,\theta,t) = \frac{1}{2\pi R}\sum_{m=1}^{\infty}\sum_{l=0}^{\infty}\alpha_m|\beta_l|\times$$

$$\times\left(-mzkT\cos\theta+\frac{mz-l}{a^2}M\right)J_{mz-l}(mzka\sin\theta), \tag{34}$$

where $\omega \gg c/mzR$.

Expression (32) describes the spatial acoustic pressure distribution produced by the rotation of a ship propeller with z blades, acting on the surrounding medium with a thrust of a mean strength T and a torque with a mean value M.

The ship propeller load variation is described by the coefficients β_L. The formula permits the determination of the acoustic pressure distribution if the thrust, the torque and the coefficients α_m and β_l are known. Figure 5 shows the method of determining the acoustic pressure under the assumption that $\varphi = \omega t$. Figure 6 shows the acoustic pressure amplitude variation as a function of distance.

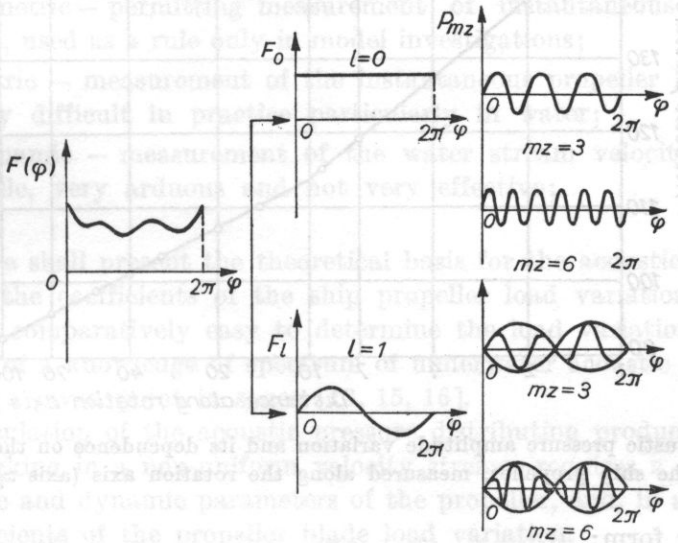

Fig. 5. Determination of the acoustic pressure components related to the ship propeller load variation as a function of the rotation angle (26)

These results were obtained from calculations using present propeller parameters. Experimental research most frequently measures the effective value of the acoustic pressure. The effective value of the m-th harmonic was determined from the following formula:

$$p_{msk}(R, \psi, \theta) = \frac{|a_m|}{2\sqrt{2}\pi R} \times$$

$$\times \left\{ \sum_{l=0}^{\infty} \left[|\beta_l| \frac{-mzk\cos\theta + M(mz-l)/a^2}{\cos\varphi_1} \right]^2 \right\}^{1/2} J_{mz-l}(mzka\sin\theta), \qquad (35)$$

where

$$\varphi_1 = \operatorname{arc\,tg}\left[\frac{T\cos\theta}{R(mzkT\cos\theta - (mz-l)/a^2)\,M} \right].$$

Using the relations between the thrust and the torque and the thrust coefficient and torque coefficient respectively [15, 16], expression (35) takes

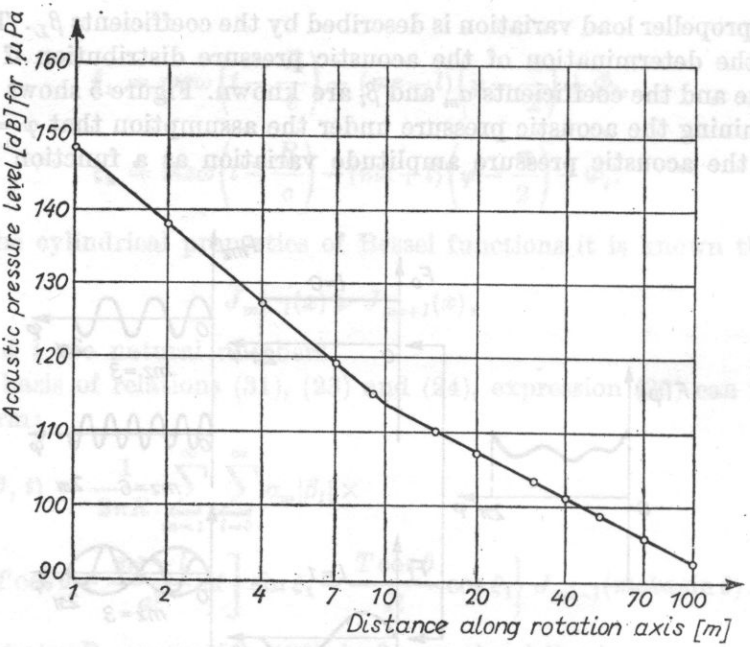

Fig. 6. The acoustic pressure amplitude variation and its dependence on the distance from the ship propeller, measured along the rotation axis (axis x_3)

the following form:

$$p_{msk}(R, \psi, \theta) = \frac{\sqrt{2}\varrho |a_m| \omega^2 r_m^4}{\pi^3 R} \times$$

$$\times \left\{ \sum_{l=0}^{\infty} \left[|\beta_l| \frac{-mzkK_T \cos\theta + 2.5(mz-l)K_M/a}{\varphi_1} \right]^2 \right\}^{1/2} J_{mz-l}(mzka\sin\theta). \quad (36)$$

Relations (35) and (36) are also valid for a thrust force equal to zero (e.g. for a propeller with ssymmetrical blade profiles working at a zero angle of attack), since the resultant force in the direction φ is different from zero. In this case the value of the acoustic pressure will, obviously, be considerably smaller than that for a propeller producing a given thrust force value.

4. Acoustic method for the determination of the coefficients of the ship propeller blade load variation

In practice the velocity field distribution of water stream flowing onto a ship propeller is, generally, unknown. Thus the variation of the velocity circulation on the blades, which depends on the propeller rotation angle, is unknown. It has been shown previously [14] that the theory of sound generation by a propeller type system, neglecting the instantaneous load variation, gives

values for the acoustic pressure lower than those experimentally obtained. One of the conditions for the determination of real values of the acoustic pressure produced by a ship propeller under given working conditions, is a knowledge of coefficients of the ship propeller load variation [9, 11, 13, 15, 27].

The measurements of this variation can be made by one of the following methods:

dynamometric – permitting measurement of instantaneous thrust and torque values, used as a rule only in model investigations;

tensometric – measurement of the instantaneous propeller blade strains, comparatively difficult in practice particularly in water;

hydrodynamic – measurement of the water stream velocity within the propeller circle, very arduous and not very effective;

acoustic.

Below we shall present the theoretical basis for the acoustical method of determining the coefficients of the ship propeller load variation. Using this method it is comparatively easy to determine the load variation coefficients on the basis of a knowledge of spectrum of underwater acoustic disturbances, measured at a given point in space [13, 15, 16].

The calculation of the acoustic pressure distribution produced by a ship propeller working in a non-uniform velocity stream, requires a knowledge of the geometric and dynamic parameters of the propeller, and, in addition, that of the coefficients of the propeller blade load variation.

Let us consider the case of a variation in the velocity field which is stationary in time and random within the propeller circle (stationary space-time random field).

Green's function along the x_3 axis, related to the density distribution of acoustic dipoles whose axes are normal to the plane in the propeller circle (see the coordinate system in Fig. 7) has [15, 16] the form

$$G_{x_3}(\boldsymbol{R}|\boldsymbol{r},\ \omega) = -\frac{e^{-imzkR}}{4\pi R^2}\left[imzk\bar{x}_3 + \frac{\bar{x}_3}{R}\right], \tag{37}$$

where $R = [r^2 + \bar{x}_3^2]^{1/2}$, and $k = \omega/c$ is the wave number.

The acoustic pressure along the x_3 axis can be determined [16] from the relation

$$p(R, x_3, t) = -\int_S\int \frac{f_{x_3} e^{-imzkR}}{4\pi R^2}\left[imzk\bar{x}_3 + \frac{\bar{x}_3}{R}\right] dS(\boldsymbol{x}), \tag{38}$$

which after integration takes the form

$$p(R_a, x_3, t) = T\sum_{m=-\infty}^{\infty} \frac{a_m|\beta_{mz}|}{4\pi R_a^2}\left[imzk\bar{x}_3 + \frac{\bar{x}_3}{R_a}\right]\exp\left\{imz\omega\left(t - \frac{R_a}{c}\right)\right\}, \tag{39}$$

where $R_a = [a^2 + \bar{x}_3^2]^{1/2}$.

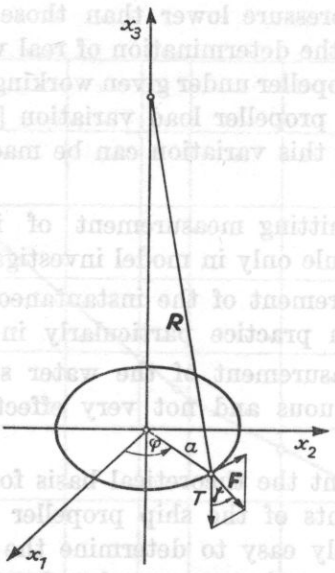

Fig. 7. The coordinate system used in the present investigations

Using the properties of the complex variable function and making further transformations of expression (39) we obtain the formula for the pressure of the m-th harmonic on the rotation axis at a distance $\bar{x}_3$ from the propeller centre,

$$p(R_a, x_3, t) = 2T \sum_{m=1}^{\infty} \frac{\alpha_m |\beta_{mz}|}{4\pi R_a^2} \left[-mzk\bar{x}_3 \sin\xi + \frac{\bar{x}_3}{R_a} \cos\xi \right], \tag{40}$$

where

$$\xi = mz\omega\left(t - \frac{R_a}{c}\right) + \Phi_{mz}.$$

The moduli of load variation coefficients in relation to the effective value of the m-th harmonic of the acoustic pressure are obtained from expression (40) in the following form:

$$|\beta_{mz}| = \frac{2\sqrt{2}R_a^2 p_{msk}}{T|\alpha_m|} \left[(mzk\bar{x}_3)^2 + \left(\frac{\bar{x}_3}{R_a}\right)^2 \right]^{-1/2}. \tag{41}$$

This formula permits calculation of coefficients of the ship propeller load variation. The effective acoustic pressure values of the m-th harmonic are determined from measurements which are most frequently performed in the following way:

the acoustic pressure variation is recorded in real time,

a narrow band analysis of the acoustic pressure variation is made using an analogue or digital method.

Values of the m-th harmonic of the acoustic pressure are determined from the spectrum, using the relation

$$p_{msk} = p_{msk}(mnz) \tag{42}$$

where m is the order of the harmonic, n – the angular velocity of the ship propeller, p_{msk} – the effective acoustic pressure value of the m-th harmonic, and z – the number of ship propeller blades.

A measurement of the thrust force is made at the same time.

The load distribution along the chord is related to the coefficient a_m.

It has been assumed in this paper that the load distribution along the chord has a rectangular shape [16, 26]. In this connection, the coefficient a_m is determined from the relation

$$a_m = 2z \frac{\bar{a}(r)}{2\pi} \sin c \frac{zm\bar{a}(r)}{2\pi}, \tag{43}$$

where $\bar{a}(r)$ is the angle between the projections of the leading and trailing edges of the blade onto the propeller circle plane.

This type of distribution is an idealization of the problem, since the propeller blade load along the chord is not constant. In addition, this distribution changes, depending on the attack of the angle of the propeller blade. It is obviously difficult to give an estimate of the error, since it is mainly dependent on the ship propeller blade width and the angle of the attack of the blade. For very narrow blades, the estimated error is comparatively small. It increases with increasing blade width. The angle of attack of the ship propeller blade also has a significant effect on the load distribution. Thus the exact pressure distribution on the propeller blade should be calculated individually for a given type of propeller and its working parameters.

5. The experimental part

Experiments were made in an anechoic basin. Instantaneous acoustic pressure values were registered, using a digital 7502 type Brüel and Kjaer recorder. The sampling frequency was changed individually for each case. A schematic diagram of the system used in the spectral analysis is shown in Fig. 8, and the hydrodynamic propeller characteristics are shown in Fig. 9.

The spectral analysis was performed numerically using a fast Fourier transformation algorithm. During the preparation of the data for spectral analysis, a cosine taper was used over 1/10 of each end of data. In addition, the spectrum was smoothed using the frequency method [16].

The spectrum of underwater acoustic disturbances produced by a ship propeller at an angular velocity $n = 10$ rps is shown in Fig. 10 for $\Delta f = 0.49$ Hz.

Knowing the acoustic pressure values for given harmonics, interrelated by the relation $f = m \cdot n \cdot z$, the propeller blade load coefficients were determined from relation (41) using formula (43). A computer programme was specially written (*Cis* 1) [16], which permitted, on the basis of the spectrum of distur-

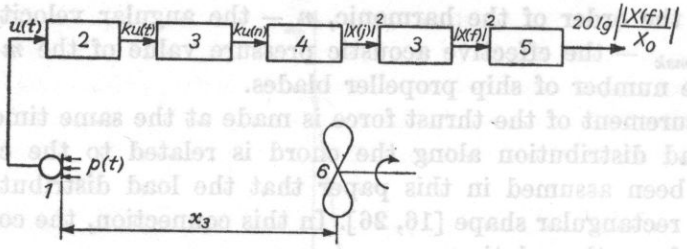

Fig. 8. A schematic diagram of the system used for spectral analysis

1 – a 8101-type Brüel and Kjaer measuring hydrophone, 2 – a 2606-type Brüel and Kjaer measuring amplifier, 3 – a 7502-type Brüel and Kjaer single pass recorder, 4 – EMC ODRA-1305, 5 – a level recorder, 6 – a ship propeller

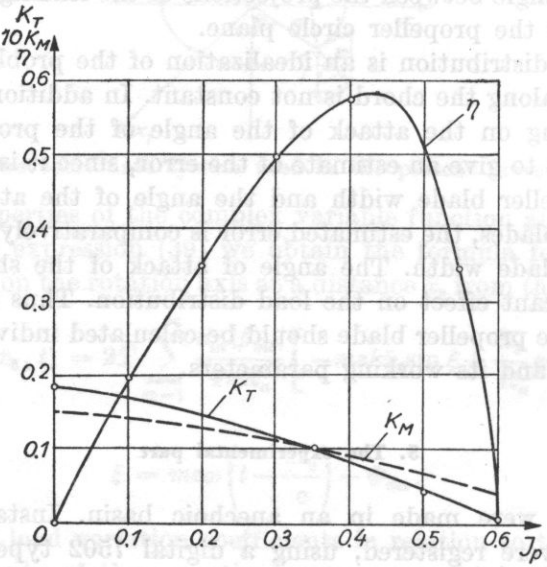

Fig. 9. Hydrodynamic characteristics of the ship propeller under investigation

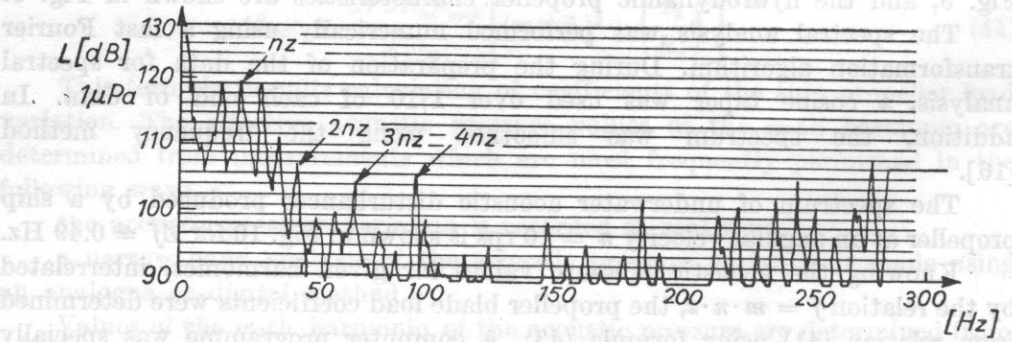

Fig. 10. The spectrum of underwater acoustic disturbances at a velocity $n = 10$ rps, $\bar{x}_3 = 8$ m

bances and working parameters of the propeller, a direct determination of the coefficients $\beta_{mz=l}$. Figure 11 shows examples of the values of these coefficients and their dependence on the value of mz.

Figure 12 shows the instantaneous acoustic pressure produced by a ship propeller at an angular velocity $n = 16.6$ rps. The acoustic pressure was record-

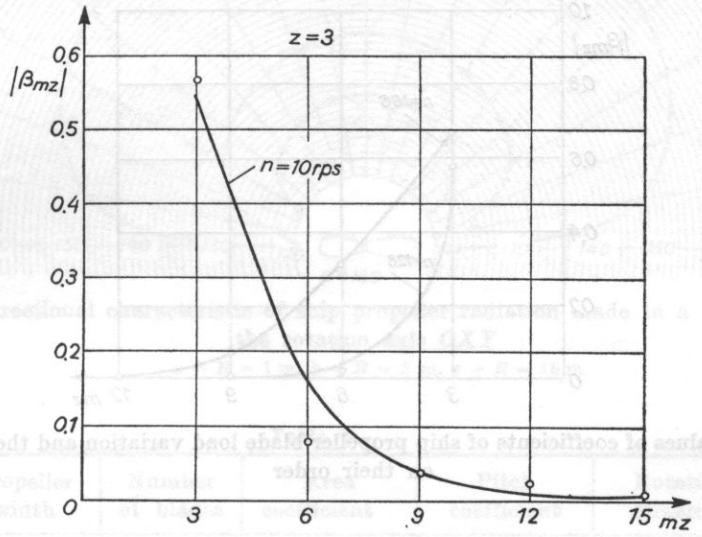

Fig. 11. The values of coefficients for the ship propeller blade load variation at $n = 10$ rps

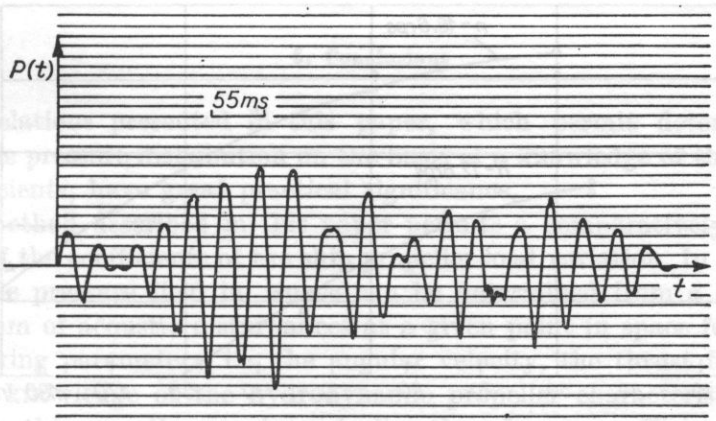

Fig. 12. Instantaneous acoustic pressure produced by a ship propeller at a distance $R = 8$ m at angular velocity $n = 16.6$ rps.

ed at a point on the propeller rotation axis, 8 metres from the propeller centre.

Figure 13 shows the coefficients of the ship propeller blade load variation for the above case.

From (36) the first four harmonics of the spectrum of underwater acoustic disturbances were calculated and compared with the values obtained from a direct measurement. The curves for these characteristics are shown in Fig. 14.

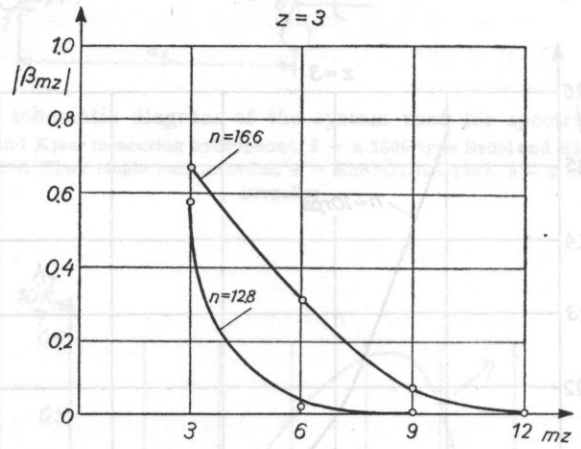

Fig. 13. The values of coefficients of ship propeller blade load variation and their dependence on their order

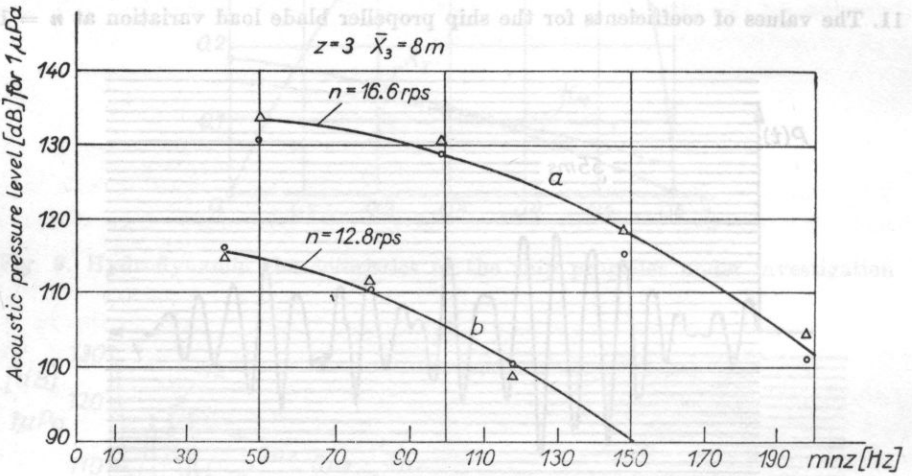

Fig. 14. Values of spectrum lines depending on their order
a – calculated from relation (36), *b* – from measurements

The directional characteristics of the sound radiated by a ship propeller were calculated for distances $R = 1$ m, 5 m, and 10 m from the propeller on the plane OXY (see Fig. 2), and are shown in Fig. 15.

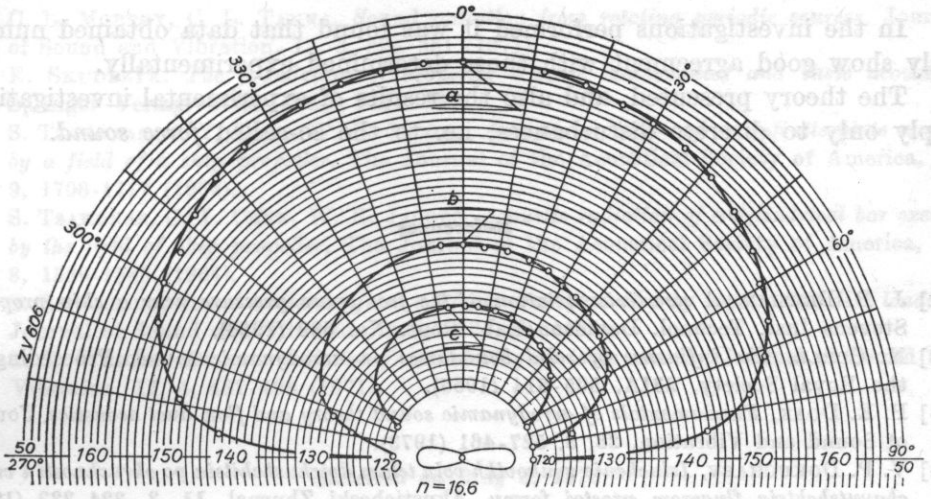

Fig. 15. A directional characteristic of ship propeller radiation made in a plane lying on the rotation axis OXY

$a - R = 1$ m, $b - R = 5$ m, $c - R = 10$ m

Table 1.

Propeller width	Number of blades	Area coefficient	Pitch coefficient	Rotation direction
D [m]	z	S/S_0	H/D	—
0.50	3	0.35	0.48	left

6. Conclusions

The relations presented in this paper, which permit determination of the acoustic pressure distribution on the basis of a knowledge of the load variation coefficients, have great practical significance.

The method described in this paper permits a comparatively easy determination of the coefficients of the ship propeller load variation. In consequence, the acoustic pressure field in space can be determined from a knowledge of the spectrum of acoustic disturbances at a given point in space for given propeller working parameters, i.e. the angular velocity, the thrust force and the torque. A knowledge of the hydrodynamic propeller characteristics can also be used. In this case the angular velocity, the advance coefficient, the thrust coefficient, and the torque coefficient must be known (see relation (36)).

From the viewpoint of the correctness of investigations an effort must be made to ensure that during the measurements the propeller works under steady-state conditions.

It is recommended that the methods of measurement are used that permit the spectra to be obtained with high frequency resolution (narrow band spectra).

In the investigations performed it was found that data obtained numerically show good agreement with those determined experimentally.

The theory presented, and also the results of experimental investigations, apply only to discrete disturbances, i.e. to the so-called *force sound.*

References

[1] J. P. BRESLIN, *A new interpretation of the free space pressure near a ship propeller,* Stevens Inst. Technol. Davidson Lab. Rept. No. 689 (1958).

[2] N. CURLE, *The influence of solid boundaries on aerodynamic sound,* Proceedings of the Royal Society, **231**A, 505-514 (1955).

[3] P. E. DOAK, *Fundamentals of aerodynamic sound theory and flow duct acoustics,* Journal of Sound and Vibration, **28**, 3, 527-461 (1973).

[4] V. P. DOKUCHAEV, *Izluchenie zvukovikh voln telam dvizhushchitsia po okruzhnosti i vrashchayutshchtsia flugerom prostoj formy,* Akusticheski Zhurnal, **11**, 3, 324-333 (1965).

[5] V. P. DOKUCHAEV, *Izluchenie zvukovikh voln telom dvizhushchitsia po vintovikh liniakh,* Akusticheski Zhurnal, **13**, 2, 192-198 (1967).

[6] J. E. FOWCES WILLIAMS, D. H. HAWKINGS, *Sound generated by turbulence and surfaces in arbitrary motion,* Philosophical Transactions of the Royal Society of London, **264**A, 321-342 (1969).

[7] J. E. FOWCES WILLIAMS, D. H. HAWKINGS, *Theory relating to the noise of rotating machinery,* Journal of Sound and Vibration, **10**, 1, 10-21 (1969).

[8] I. E. GARRICK, C. E. WATKINS, *A theoretical study of the effect of forward speed on the free-space sound pressure field around propellers,* NACA Rep. No. 1198 (1954).

[9] M. GOLDSTEIN, *Unified approach to aerodynamic sound generation in the presence of solid boundaries,* The Journal of the Acoustical Society of America, **56**, 2, 497-509 (1974).

[10] M. GOLDSTEIN, *Aeroacoustics,* NASA, Sp-346, Washington, D. C. 1 (1974).

[11] M. GOLDSTEIN, *Aeroacoustics,* McGraw Hill Book Company, New York 1976, 153-187.

[12] L. J. GUTIN, *O zvukovom pole vrashchyushchego vozdushnogo vinta,* Zhurnal Tekhnicheskoi Fizyki, **6**, 5, 899 909 (1936).

[13] F. K. KASPER, *Determination of rotor harmonic blade loads from acoustic measurements,* NASA, CR-2580, Washington, D. C. (1975).

[14] E. KOZACZKA, *Investigations of underwater acoustic disturbances produced by a ship propeller* Archives of Acoustics, **3**, 2, 121-139 (1978).

[15] E. KOZACZKA, *Sound radiation by a ship propeller working under conditions of stationary load variation* (in Polish), Naval College Scientific Reports, **3/58**, 45-62 (1978).

[16] E. KOZACZKA, *Investigations of underwater acoustic disturbances produced by a ship propeller* (in Polish), Naval College Scientific Reports, **59**A, 12-45 (1978).

[17] M. J. LIGHTHILL, *On sound generated aerodynamically, I — General theory,* Proceedings of the Royal Society, **211**A, 1, 27-50 (1968).

[18] M. V. LOWSON, *Reduction of compressor noise radiation,* The Journal of the Acoustical Society of America, **43**, 1, 37-50 (1968).

[19] M. V. LOWSON, *Theoretical analysis of compressor noise,* The Journal of the Acoustical Society of America, **47**, 1/2, 371-385 (1970).

[20] M. V. LOWSON, B. J. OLLERHEAD, *A theoretical study of helicopter rotor noise,* Journal of Sound and Vibration, **9**, 2, 197-222 (1969).

[21] I. J. MINNOVICH, A. D. PIERNIK, W. S. PETROVSKI, *Gidrodynamicheskie istochniki zvuka,* Sudostroenie, Leningrad 1972, 83-127.

[22] C. L. MORFEY, C. L. TANNA, *Sound radiation from rotating periodic sources*, Journal of Sound and Vibration, **15**, 3, 325-351 (1971).

[23] E. SKUDRZYK, *The foundation of acoustics — basic mathematics and basic acoustics*, Springer Verlag, Wien - New York 1971.

[24] S. TSAKONAS, C. Y. CHEN, W. R. JACOBS, *Acoustic radiation of an infinite plate excited by a field of a ship propeller*, The Journal of the Acoustical Society of America, **36**, 9, 1708-1717 (1964).

[25] S. TSAKONAS, C. Y. CHEN, W. R. JACOBS, *Acoustic radiation of a cylindrical bar excited by the field of ship propeller*, The Journal of the Acoustical Society of America, **36**, 8, 1569-1588 (1964).

[26] S. E. WRIGHT, *Sound radiation from a lifting rotor generated by asymmetric disk loading*, Journal of Sound and Vibration, **9**, 2, 223-240 (1969).

[27] S. E. WRIGHT, *Discrete radiation from rotating periodic sources*, Journal of Sound and Vibration, **17**, 4, 437-498 (1971).

Received on May 5, 1978

ARCHIVES OF ACOUSTICS
4, 3 (1979)

ULTRASONIC TRANSDUCERS USING RADIAL VIBRATIONS OF A PIEZOELECTRIC DISK

JERZY GOLANOWSKI, TADEUSZ GUDRA

Institute of Telecommunication and Acoustics of Wrocław Technical University
(50-370 Wrocław)

Suggestions concerning the use of radial vibrations of a piezoelectric disk in ultrasonic transducers working in the frequency range below 100 kHz are presented. Experimental data from investigations of two types of transducers are given, one using axial coupling of a piezoelectric disk with a metal rod vibrating in the longitudinal mode, the other using circumferential coupling of a piezoelectric disk and a metal plate. The amplitude and phase characteristics of admittance, the resonance curves, the temperature characteristics of impedance and the resonance displacement amplitudes are presented.

1. Introduction

Piezoelectric plates used for ultrasound generation most often work in the thickness mode. Radial vibrations of piezoelectric disks [8] have been used comparatively rarely to date. Use of these vibrations is of interest because of the possibility of ultrasound generation in air at frequencies of several tens of kHz. In addition, a piezoelectric disk vibrating in the radial mode has a low electrical imput impedance (typically a few ohms), which in turn is of interest from the viewpoint of matching to transistor supply systems.

It is possible to build vibrating structures with a piezoelectric disk vibrating in the radial mode as the active resonator. The disk can be coupled with such resonators as a cylinderplate or rod with the resonators being excited to flexural, radial or thickness vibrations with directional conversion or without it. Table 1 shows the manner of building the resonance coupled structures.

This paper presents experimental data of investigations of two types of coupled structures — denoted in Table 1 as transducers *c* and *f*. The transducer *c* is a resonance system with directional R-L conversion, where the piezoelectric disk is axially coupled with a rod vibrating in the longitudinal mode. The transducer *f* is a piezoelectric disk circumferentially coupled, without conversion,

Table 1. Manners of building the coupled resonance structures using the radial vibrations of a piezoelectric disk

	Rod			Plate			Cylinder		
	F	R	L	F	R	L	F	R	L
Disk	a	b	c	d	e	f	g	h	i

F – flexural, R – radial, L – longitudinal
a, b, ..., i – transducers

with a metal plate, creating a transducer vibrating in the longitudinal mode. For practical reasons it is advisable to build the simplest single or two-resonance structures, e.g. the transducers described in the sequel.

2. Transducer using axial coupling with conversion

Resonators with directional R-L conversion were designed by K. ITO and E. MORI [5, 6] who suggested R-L type converters in the form of uniform resonance structures requiring ultrasonic energy supply from outside. Such a solution is troublesome since it requires additional vibration sources. A considerably simpler design for an R-L type converter [2] is presented in Fig. 1.

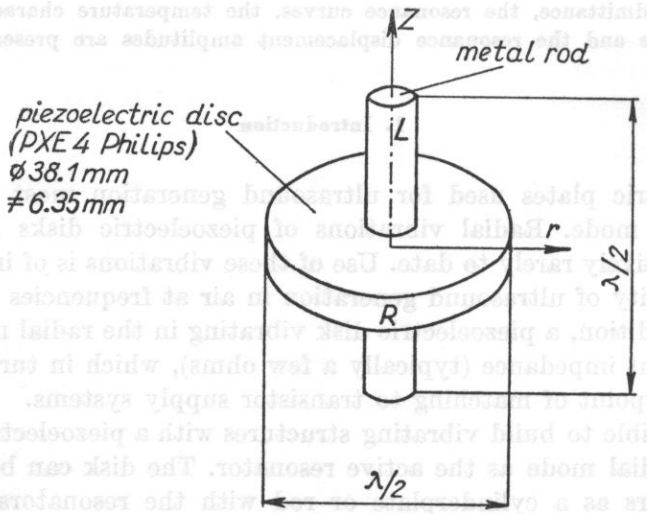

Fig. 1. A non-uniform R-L type converter

The converter is a non-uniform system made of a piezoelectric disk acting as a half-wave radial vibration resonator and a metal rod acting as a half-wave longitudinal vibration resonator, connected with a Hottinger Z-70 cyanoacrylate glue. The rod length is chosen so that its fundamental resonance frequency lies in the radial resonance range of the disk.

The piezoelectric disk and the rod are coupled together at the velocity node of radial vibration for the disk, and that of longitudinal vibration for the rod. With a suitable choice of dimensions, such a system permits comparatively large amplitudes of rod surface vibrations to be obtained. Energy transmission from the disk to the rod occurs due to a Poisson effect in the mechanically coupled common part of the converter. When the free vibration frequencies of individual resonators are different from each other, each of them vibrates as a free system, whereas when these frequencies are close to one another, there is an interaction of the two resonators [9].

One characteristic of such a converter is its electrical input admittance. An example of a graph of the admittance modulus is presented in Fig. 2.

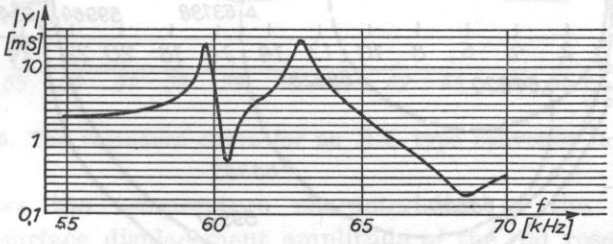

Fig. 2. The modulus of electrical admittance for a nonuniform R-L type converter

The maxima of this graph correspond to the free vibration frequencies of the converter. The gap between the frequencies depends on the dimensions of the part common to both resonators and is the longer the bigger the dimensions are [9]. The maximum values of the modulus of the electrical admittance of the converter depend on the resonator length and are equal for an aligned converter.

Fig. 3 shows the amplitude and phase characteristics of the electrical admittance of an R-L type converter without loading and with unilateral water loading. An example of the dependence of the modulus of electrical impedance, the argument, and the frequency of the minimum modulus of the impedance, on temperature is shown in Fig. 4. It is noteworthy that the modulus of the impedance changes only slightly in the given temperature range. This assures a stable matching of the supply generator over this temperature variation. The values of the modulus of electrical impedance on the curve apply to a converter working in air.

Fig. 5 presents the curve of the dependence of the surface displacement amplitude in a longitudinal vibration resonator on the frequency. Measurements were made using an MM004-type Brüel-Kjaer capacitance sensor. The characteristic has two maxima corresponding to the converter resonance frequencies. These maxima correspond to maximum values of the graph of modulus of the converter admittance against frequency.

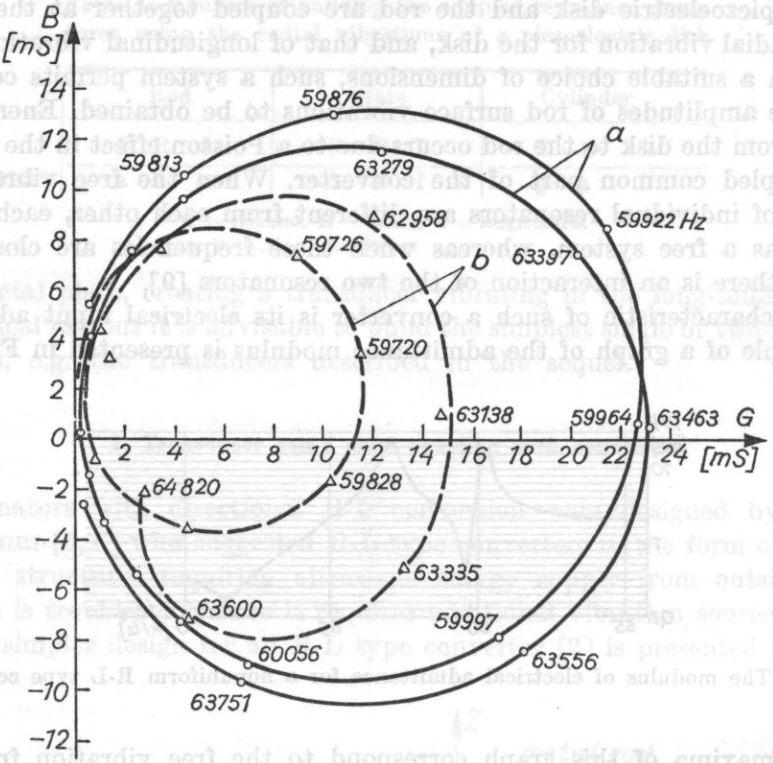

Fig. 3. The amplitude and phase characteristics of the electrical admittance of an R-L type converter
(a) unloaded converter, (b) unilaterally water loaded converter

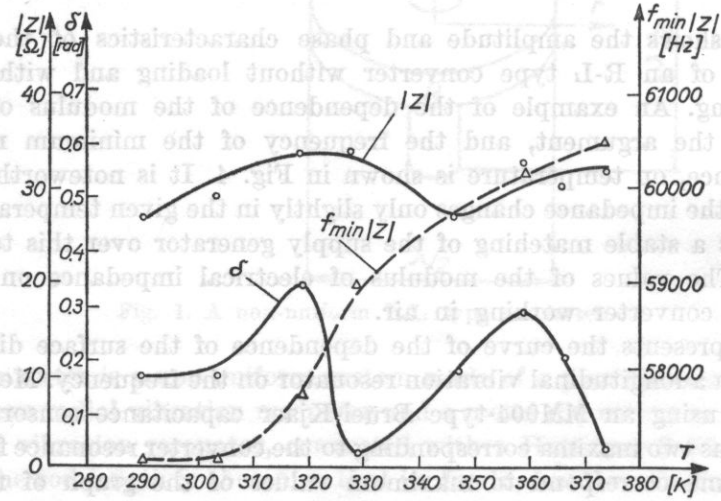

Fig. 4. The temperature characteristics of the impedance of an R-L type converter

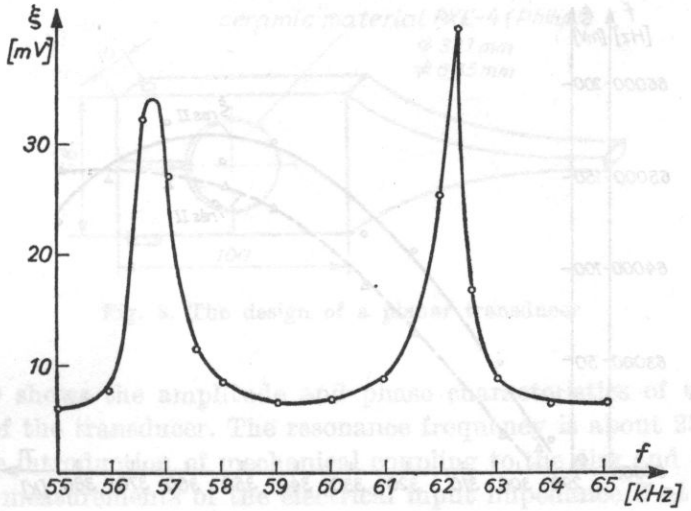

Fig. 5. The resonance curve for an R-L type converter in air

Fig. 6 shows the temperature characteristics of the resonance frequency and the surface displacement amplitude of the rod resonator for f_{resI}, and Fig. 7 shows similar characteristics for f_{resII}.

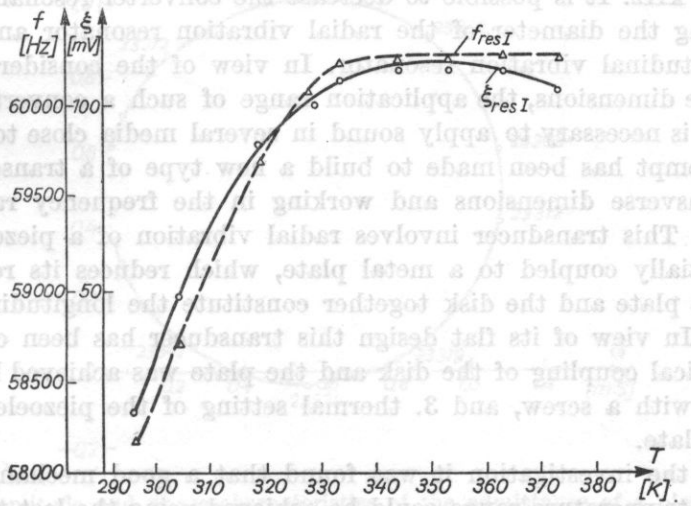

Fig. 6. The temperature characteristics of the resonance frequency and the surface displacement amplitude in the rod resonator for f_{resI}

It can be concluded from the characteristics shown that the displacement amplitude maxima occur at temperatures of 330-350 K, i.e. the optimal working temperature for the converter investigated occurs in this range.

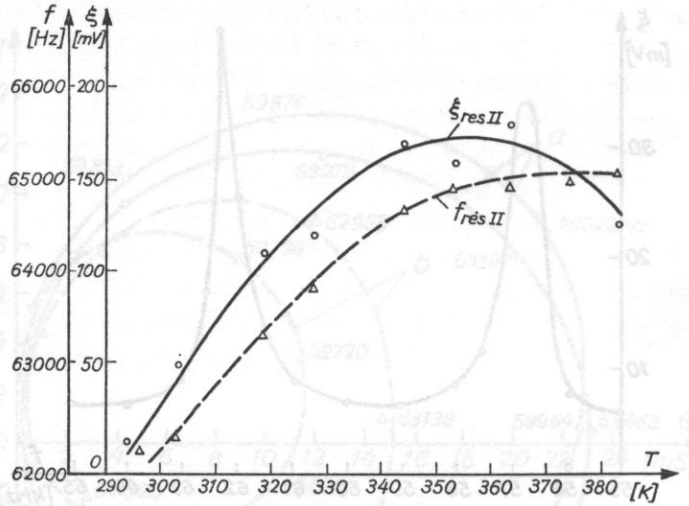

Fig. 7. The characteristics, as in Fig. 6, for f_{resII}

3. Transducer using circumferential coupling without conversion

The R-L converter described above operates in the range of frequencies at about 60 kHz. It is possible to decrease the converter resonance frequency by increasing the diameter of the radial vibration resonator and the length of the longitudinal vibration resonator. In view of the considerable increase of transverse dimensions, the application range of such a converter is limited, e.g. when it is necessary to apply sound in several media close to one another [1]. An attempt has been made to build a new type of a transducer having smaller transverse dimensions and working in the frequency range near to 20 kHz [4]. This transducer involves radial vibration of a piezoelectric disk circumferentially coupled to a metal plate, which reduces its resonance frequency. The plate and the disk together constitute the longitudinal vibration transducer. In view of its flat design this transducer has been called *planar*.

Mechanical coupling of the disk and the plate was achieved by: 1. gluing, 2. coupling with a screw, and 3. thermal setting of the piezoelectric disk in the metal plate.

During the investigation it was found that a good mechanical coupling over a wide temperature range could be achieved using the last two methods.

3.1. A planar transducer mechanically coupled with a screw. An example of a transducer design mechanically coupled with a screw is shown in Fig. 8. It is composed of a piezoelectric disk of Philips PXE-4 ceramic material and a duraluminium plate. A slot in the plate permits a screw-adjusted mechanical coupling of the disk and the plate.

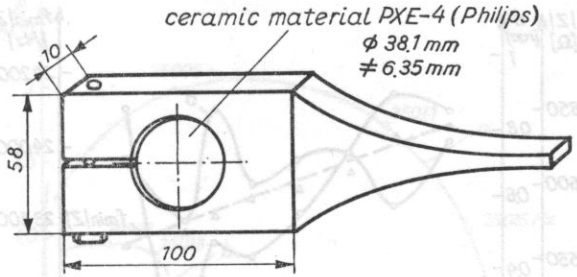

Fig. 8. The design of a planar transducer

Figure 9 shows the amplitude and phase characteristics of the electrical admittance of the transducer. The resonance frequency is about 23 kHz. With a view to the introduction of mechanical coupling to the disk and the plate [7] temperature measurements of the electrical input impedance Z at a frequency corresponding to the minimum of the modulus of impedance were made. The measurement results for a specimen transducer are shown in Fig. 10.

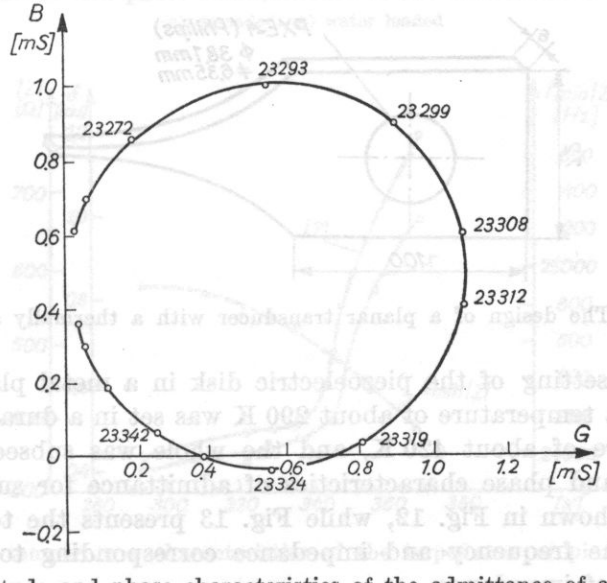

Fig. 9. The amplitude and phase characteristics of the admittance of a planar transducer in air

In the temperature range of 290-370 K the frequency $f_{\min|Z|}$ diminishes by about 300 Hz, whereas the modulus and the argument of the impedance change by about 500-750 and 0.5-0.9 radians, respectively.

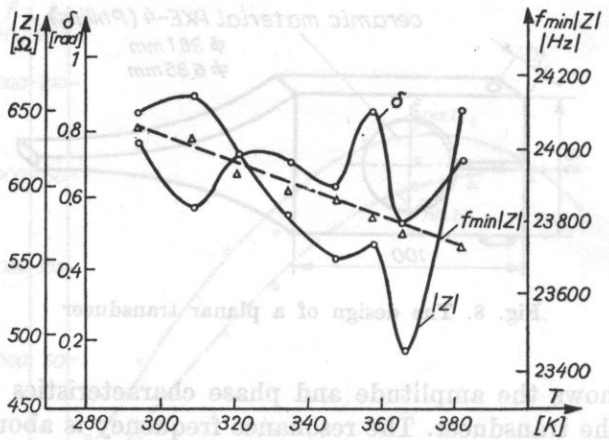

Fig. 10. The temperature characteristics of the impedance of planar transducer

3.2. A planar transducer mechanically coupled by the thermal method. Figure 11 shows the design of a planar transducer with a concentrator of resonant frequency of about 25 kHz, in which mechanical coupling was achiev-

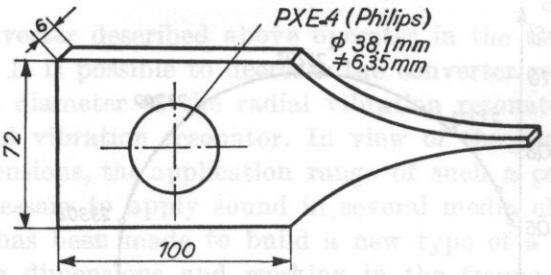

Fig. 11. The design of a planar transducer with a thermally set disk

ed by thermal setting of the piezoelectric disk in a metal plate. The piezoelectric disk at a temperature of about 290 K was set in a duraluminium plate at a temperature of about 420 K, and the whole was subsequently cooled. The amplitude and phase characterictics of admittance for such a design of transducer are shown in Fig. 12, while Fig. 13 presents the temperature dependencies of the frequency and impedance corresponding to the minimum of the modulus of impedance.

Both the graphs of the modulus of impedance and the argument of impedance are almost flat in the temperature range of 290-340 K, which implies a good mechanical coupling of the disk and the plate in this temperature range.

Figure 14 shows the curve for the dependence of the concentrator surface displacement amplitude on frequency. The measurement was made using an electrostatic MM-004 type Brüel and Kjaer sensor. Figure 15 shows the de-

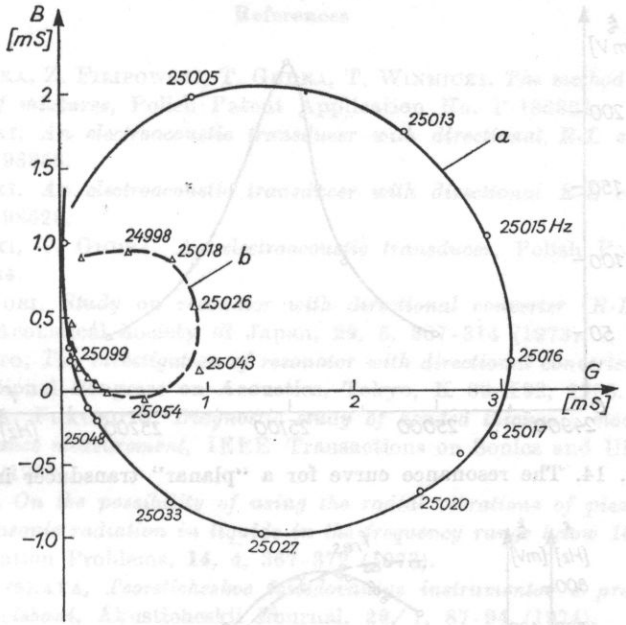

Fig. 12. The amplitude and phase characteristics of the admittance of planar transducer (*a*) unloaded, (*b*) water loaded

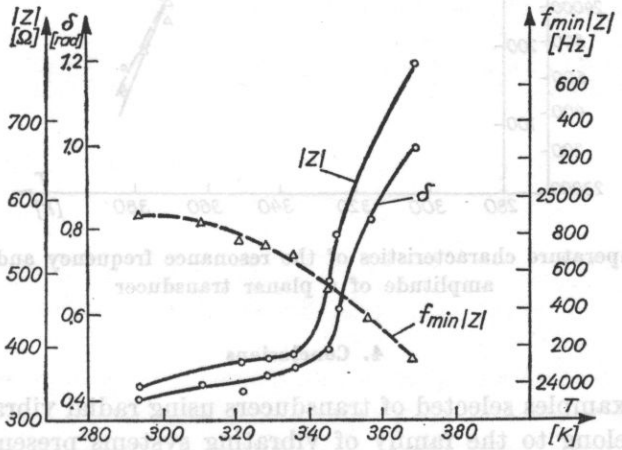

Fig. 13. The temperature characteristics of the impedance of planar transducer

pendence on temperature of the resonance frequency and the resonance displacement amplitude of the concentrator surface in air.

The quality factor for the transducer, as determined on the basis of the resonance curve, is about 600. The temperature dependence of the resonance displacement amplitude of the concentrator surface corresponds to the temperature dependence of impedance shown in Fig. 13.

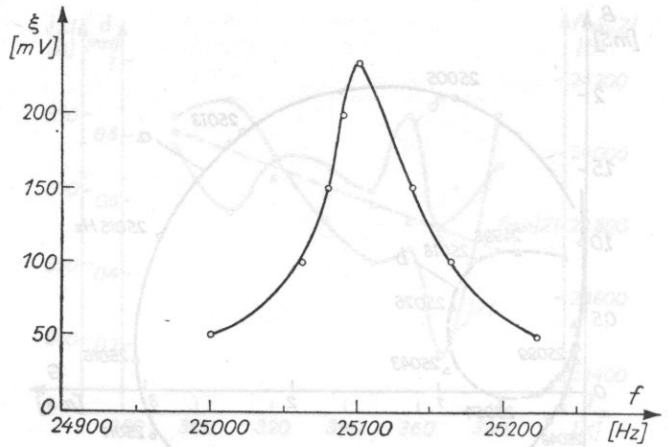

Fig. 14. The resonance curve for a "planar" transducer in air

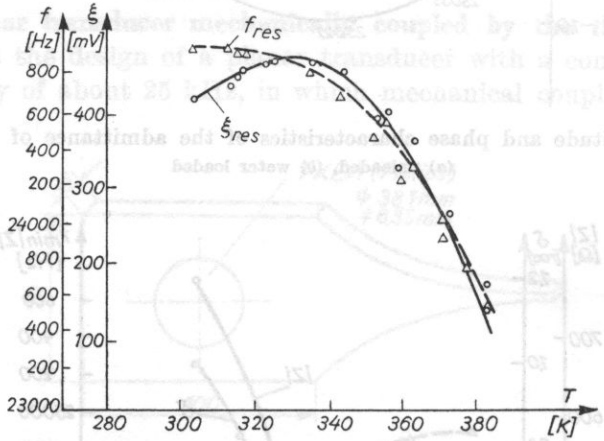

Fig. 15. The temperature characteristics of the resonance frequency and the displacement amplitude of a planar transducer

4. Conclusions

The two examples selected of transducers using radial vibration of a piezoelectric disk belong to the family of vibrating systems presented in Table 1. The transducers described are characterized by the transformation of radial vibrations to longitudinal ones. In the case of a planar transducer such a transformation occurs without directional conversion. In addition, this transducer has small transverse dimensions, and the advantage of both transducer types is their simple design and production technology.

Other designs resulting from Table 1 will be the object of further investigations, e.g. a transducer with directional R-L conversion where the longitudinal vibration resonator is a cylinder [3].

References

[1] G. BŁAŻEJEWSKA, Z. FILIPOWSKI, T. GUDRA, T. WINNICKI, *The method for the permeable separation of mixtures*, Polish Patent Application No. P-185881.

[2] J. GOLANOWSKI, *An electroacoustic transducer with directional R-L conversion*, Polish Patent No. 98858.

[3] J. GOLANOWSKI, *An electroacoustic transducer with directional R-L conversion*, Polish Patent No. 98529.

[4] J. GOLANOWSKI, T. GUDRA, *An electroacoustic transducer*, Polish Patent Application No. P-201984.

[5] K. ITO, E. MORI, *Study on resonator with directional converter (R-L type converter)*, Journal of Acoustical Society of Japan, **29**, 5, 307-314 (1973).

[6] E. MORI, K. ITO, *The investigation of resonator with directional converter*, Reports of the 6th International Congress on Acoustics, Tokyo, K 89-K92, 1968.

[7] T. NOGUCHI, A. FUKUMOTO, *Diagnostic study of bonded thickness mode transducers by input impedance measurement*, IEEE Transactions on Sonics and Ultrasonics, **SU-20**, 4, 365-370 (1973).

[8] W. PAJEWSKI, *On the possibility of using the radial vibrations of piezoelectric plates to generate ultrasonic radiation in liquids in the frequency range below 100 kHz*, Proceedings of Vibration Problems, **14**, 4, 367-372 (1973).

[9] G. F. POVOLOTSKAYA, *Teoreticheskoe issledovaniye instrumentov s preobrazovanem napravleniya kolebani*, Akusticheskii Zhurnal, **20**, 1, 87-94 (1974).

Received on April 13, 1978

ARCHIVES OF ACOUSTIC
4, 3 (1979)

INVESTIGATION OF THE ACOUSTIC FIELD DISTRIBUTION IN PIEZOELECTRIC TRANSDUCERS BY THE BRAGG DIFFRACTION METHOD

ZYGMUNT KLESZCZEWSKI

Institute of Physics of Silesian Technical University (44-100 Gliwice)

In the paper the possibility of using the light, diffracted by acoustic waves, for the investigation of the distribution of acoustic fields in solids is presented, and the results obtained are described. Quartz and $LiIO_3$ transducers with a fundamental frequency of 200-400 MHz were the sources of a longitudinal acoustic wave. The transducer length was several mm, and the transducer width was about 1 mm. Fused and crystalline quartzes were used as media. The acoustic field was probed with a narrow laser beam, and the angular distribution of the diffracted light intensity was measured. The experimental results obtained were compared with theoretical calculations.

1. Introduction

One of possible uses of the interaction of an acoustic wave and a laser beam is the determination of the intensity distribution in acoustic fields in solids.

In practical applications transducers of very small dimensions (2-5 mm^2) are very often used, particularly for frequencies above 100 MHz. The application of a laser beam to investigate such transducers is very useful because it can be narrowly collimated. At the same time, the knowledge of the acoustic beam geometry in such transducers is sometimes very important, particularly in acousto-optical devices. The investigation of the field distribution by the Bragg diffraction method is performed by the measurement of the diffracted light intensity distributions or, as mentioned above, by probing the field with a suitably narrow laser beam [2, 4, 6].

The objectives of this paper are a brief theoretical discussion of the problem and a description of the experimental results obtained.

2. Theoretical basis. Angular distribution of the diffracted light intensity

Let us assume that an acoustic wave with a frequency Ω and a wave vector $\boldsymbol{q}$ propagates in a medium (Fig. 1). Its passage causes a change in the electrical permeability of the medium,

$$\varepsilon = \varepsilon^{(0)} + \Delta\varepsilon(y)\sin(qz - \Omega t), \tag{1}$$

where $\varepsilon^{(0)}$ is the electrical permeability of the undisturbed medium, and $\Delta\varepsilon(y)$ – the electrical permeability variation amplitude.

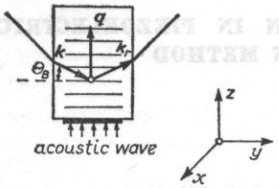

Fig. 1. The Bragg diffraction geometry
$\boldsymbol{k}$ – the incident light wave vector, $\boldsymbol{k}_r$ – the undulatory light vector after diffraction, $\boldsymbol{q}$ – the undulatory vector of the light wave

If a laser beam also travels in the medium, then for the geometry shown in Fig. 1 the electrical field intensity of the light wave may be expressed in the form

$$E_0 = V_0 \exp\{i(ky\sin\theta - kz\cos\theta - \omega t)\}, \tag{2}$$

where V_0, k, ω are the amplitude, wave vector and frequency of the incident light wave, respectively.

In the present case of light diffraction by acoustic waves of high frequency (above 200 MHz), only lines of the first order appear in the spectrum of the diffracted light. Thus, the electrical field of the diffracted light wave may be expressed in the form

$$\begin{aligned} E_1 = {} & V_1(y)\exp\{i[ky\sin\theta + (k\cos\theta + q)z - (\omega + \Omega)t]\} + \\ & + V_{-1}(y)\exp\{i[k\sin\theta + (k\cos\theta - q)z - (\omega + \Omega)t]\}, \end{aligned} \tag{3}$$

where $V_1(y)$ and $V_{-1}(y)$ are the amplitudes of the diffracted light wave for the first order lines.

Using the wave equation

$$\nabla^2 \boldsymbol{E} = \frac{1}{c^2}\frac{\partial^2}{\partial t^2}(\varepsilon \boldsymbol{E}) \tag{4}$$

and equations (1)-(3), one can show [8] that the diffracted light amplitude may be expressed by the formula

$$V_1 = e^{-i\beta y}\int_{y_1}^{y_2} \alpha V_0 e^{i\beta y'}\, dy', \tag{5}$$

where

$$\alpha = \frac{\Delta\varepsilon(y)k}{4\varepsilon\cos\theta}, \qquad \beta = \frac{q}{\cos\theta}(\sin\theta_B - \sin\theta),$$

and θ_B is the Bragg angle.

The integration limits are defined by the area of the interaction of the light and acoustic waves. An analogous equation can be obtained for the line of order -1.

A practical calculation of V_1 from equation (5) requires a knowledge of $\Delta\varepsilon(y)$. We shall consider the simplest cases of the relation $\Delta\varepsilon(y)$, assuming at the same time that the variation in the electrical permeability of the medium is proportional to the acoustic wave amplitude.

1. $a = a_0$ in the area $-L/2 \leqslant y \leqslant L/2$ (a flat transducer with a uniform amplitude distribution).

Then from formula (5) we have

$$\frac{V_1}{V_0} = a_0 L e^{iqy\Delta\theta} \frac{\sin(qL\Delta\theta/2)}{qL\Delta\theta/2}, \tag{6a}$$

$$\frac{I_1}{I_0} = \left|\frac{V_1}{V_0}\right|^2 = a_0^2 L^2 \frac{\sin^2(qL\Delta\theta/2)}{(qL\Delta\theta/2)^2}, \tag{6b}$$

where I_1/I_0 is the ratio of the diffracted and the incident light intensities.

Furthermore, if $\theta = \theta_B$ and the diffracted light intensity is small, the ratio I_1/I_0 is proportional to the acoustic beam intensity [8].

2. $a = a_0 e^{-y^2/R^2}$. We have

$$\frac{V_1}{V_0} = e^{-iqy\Delta\theta} \sqrt{\pi} a_0 R e^{-(q\Delta\theta R)^2/4}, \tag{7a}$$

while

$$\frac{I_1}{I_0} = \left|\frac{V_1}{V_0}\right|^2 = \pi a_0^2 R^2 e^{-(q\Delta\theta R)^2/2}. \tag{7b}$$

3. If

$$a = \begin{cases} a_0 & \text{for } -\frac{1}{2}(W+L) \leqslant y \leqslant -\frac{1}{2}(W-L) \\ & \text{and } \frac{1}{2}(W-L) \leqslant y \leqslant \frac{1}{2}(W+L), \\ 0 & \text{outside this area,} \end{cases}$$

then

$$\frac{V_1}{V_0} = -2a_0 L e^{iqL\Delta\theta} \frac{\sin(qL\Delta\theta/2)}{qL\Delta\theta/2} \cos\frac{qW\Delta\theta}{2}, \tag{8a}$$

$$\frac{I_1}{I_0} = 4a_0 L^2 \frac{\sin^2(qL\Delta\theta/2)}{(qL\Delta\theta/2)^2} \cos^2\frac{qW\Delta\theta}{2}. \tag{8b}$$

It follows from (6)-(8) that the ratio V_1/V_0 is the Fourier transform of the function a. From measurements of the angular distribution of the diffracted light intensity, we can draw conclusions about the vibration amplitude distribution on the transducer surface. It should be stressed, however, that the measurement of I_1/I_0 gives only the ratio $|V_1/V_0|$ and that the calculation of the inverse Fourier transform from the experimental curve is quite complicated. In the experimental part we shall show that, however, these measurements give much information about the transducer oscillations.

3. Acoustic field in flat and cylindrical transducers

In addition to the angular distributions discussed above, application of Bragg diffraction permits the acoustic field to be probed with a suitably narrow laser beam. From these measurements it is possible to determine directly the relative intensity of the acoustic field in a crystal, at the point of the interaction of the acoustic wave and light.

The acoustic field amplitude at any point of the field can be calculated, using the well-known [7] diffraction formula

$$S(x, y, z) = \frac{iq}{2\pi} \int\int_A S(x_0, y_0, 0) \frac{|z|}{r^2} e^{-iqr} dx_0 dy_0, \tag{9}$$

where $S(x_0, y_0, 0)$ is the vibration amplitude and (x_0, y_0) are the coordinates of a point in the plane of the transducer.

For an anisotropic medium the case is more complicated because the velocity of acoustic wave propagation is different in different crystallographic directions. This is accounted for numerically by the so-called *anisotropy parameter* expressed by the elastic constants of shape. A detailed discussion of the problem for an anisotropic medium can be found in paper [1].

Figure 2 shows the position of the transducer in the coordinate system assumed for the calculations. The transducer dimensions and the direction of the laser light propagation are also marked there. In the measurement

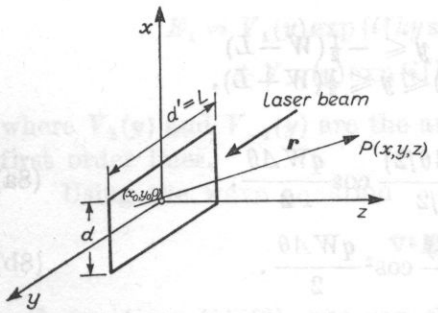

Fig. 2. Transducer dimensions and position in the coordinate system assumed for calculation

method, used for the results reported here, the laser beam interacted with the acoustic wave along the whole cross-section of the ultrasonic wave. Therefore, an additional integration along the direction Y should be carried out in expression (9) (Fig. 2). In consequence, taking into account the elastic anisotropy of the medium and the attenuation of the acoustic wave, for the acoustic field amplitude $S(x, z)$, related to the total path of the interaction of the light and

the acoustic wave, we get

$$S(x,z)=\frac{iqe^{-\alpha z}}{2\pi(1-2b)}\int_{-\infty}^{\infty}\int_{-d/2}^{d/2}\int_{-d'/2}^{d'/2}S(x_0,y_0,0)\times$$
$$\times\exp\left\{iq\left[z+\frac{(x-x_0)^2+(y-y_0)^2}{2z(1-2b)}\right]\right\}dydx_0dy_0, \quad (10)$$

where α is the attenuation coefficient for the acoustic wave and b — the anisotropy parameter.

Values of the anisotropy parameter for some crystallographic systems are given in paper [5]. For the present case of the acoustic wave propagation along the Z axis of crystals of the trigonal system we have

$$b=\frac{(C_{33}-C_{13}-2C_{44})(C_{33}+C_{13})}{2C_{33}(C_{33}-C_{44})}, \quad (11)$$

where C_{ij} are components of the tensor of elastic constants.

If a flat transducer with a uniform amplitude distribution is the source of the field, then

$$S(x_0,y_0,0)=\begin{cases}S_0 & \text{for } -\dfrac{d}{z}\leqslant x_0\leqslant\dfrac{d}{2} \text{ and } -\dfrac{d'}{z}\leqslant y_0\leqslant\dfrac{d'}{2},\\ 0 & \text{outside this area.}\end{cases} \quad (12)$$

Substituting (12) into (10), after an elementary integration we obtain

$$|S(x,z)|^2=S_0^2e^{-2\alpha z}\frac{d'^2}{\Lambda z(1-2b)}\left|\int_{-d/2}^{d/2}\exp\left\{-iq\frac{(x-x_0)^2}{2z(1-2b)}\right\}dx_0\right|^2, \quad (13)$$

where Λ is the acoustic wavelength.

The field intensity distribution according to (13) was calculated, using a digital computer. Figure 3 shows an example of the theoretical intensity distribution of an acoustic field at a frequency of 215 MHz in crystalline quartz for a propagation direction along the Z axis. It was assumed that $d'=5$ mm, $d=1$ mm, and that the parameter b — calculated from expression (11) — is in the present equal to -0.232.

If, however, a cylindrical transducer with a uniform amplitude distribution is the source of the field, then

$$S(x_0,y_0,0)=\begin{cases}S_0e^{iqx_0^2/2R} & \text{for } -\dfrac{d}{2}\leqslant x_0\leqslant\dfrac{d}{2} \text{ and } -\dfrac{d'}{2}\leqslant y_0\leqslant\dfrac{d'}{2},\\ 0 & \text{outside this area.}\end{cases} \quad (14)$$

Substituting (14) into (10) we obtain

$$|S(x,z)|^2=$$
$$S_0^2e^{-2\alpha z}\frac{d'^2}{\Lambda z(1-2b)}\left|\int_{-d/2}^{d/2}\exp\left\{\frac{iqxx_0}{z(1-2b)}+\frac{iqx_0^2}{2}\left[\frac{1}{R}-\frac{1}{z(1-2b)}\right]\right\}dx_0\right|^2. \quad (15)$$

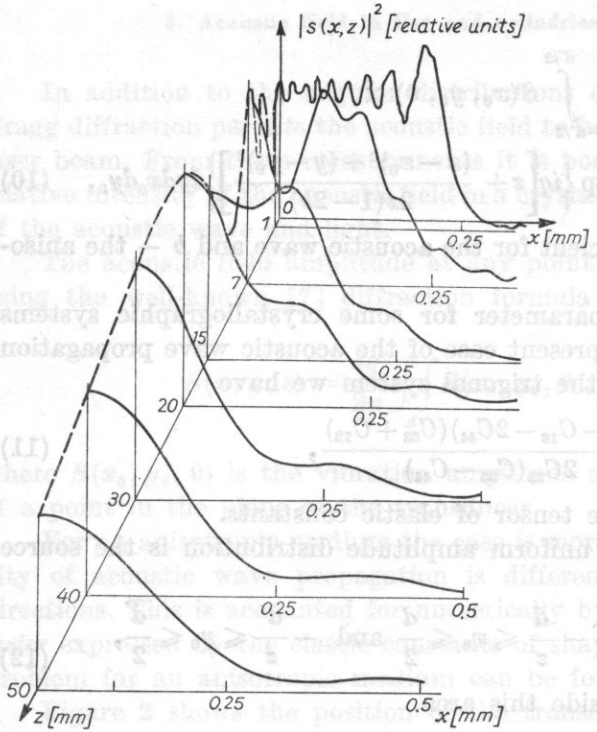

Fig. 3. Theoretical distribution of the acoustic field intensity produced by a flat transducer
$f = 216$ Hz, $d' = 5$ mm, $d = 1$ mm, $b = -0.232$

The results of measurements of the field intensity distribution at a frequency of 340 MHz are presented in Fig. 4. It has been assumed that $R = 5$ mm, $d = 4$ mm, $d' = 6$ mm, $b = -0.232$. It should be noted that the distance from the acoustic beam focus in anisotropic media is different from R, and is $R' = R/(1-2b)$. In the present case $R' = 3.41$ mm.

4. Measurement system

The measurement system used is shown in Fig. 5. Quartz and $LiIO_3$ transducers working at fundamental frequencies between 200-400 MHz were the sources of longitudinal acoustic waves. The transducers were excited form generators *G*3-20 and *G*4-37A, modulated by rectangular pulses with a duration of 0.1 μs and a repetition frequency of 1 kHz. Crystals, in which the distributions of acoustic fields were investigated, had lengths from 40 to 60 mm and transverse dimensions 10×10 mm. In the investigation of the distribution of acoustic fields, created by flat transducers, the back wall of the crystal was ground at an angle of several degrees to the acoustic wave front. This prevented diffraction of light by the reflected wave or the occurrence of a stationary wave. In the investigation of the acoustic field distribution of the focussed diffracted wave, however, the back wall of the crystal had

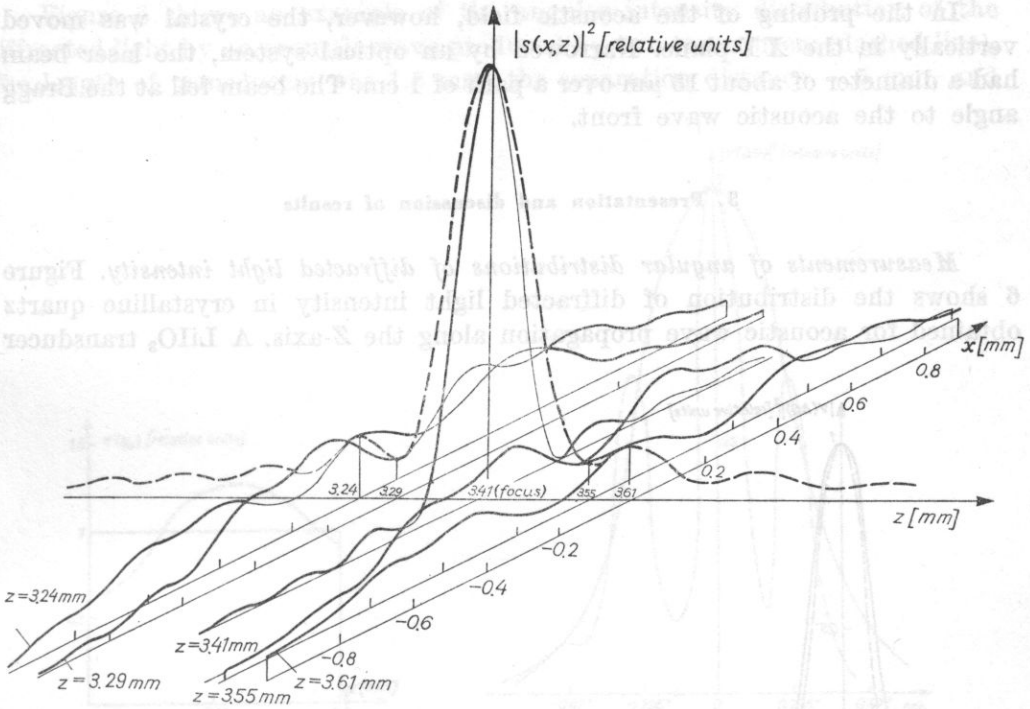

Fig. 4. Theoretical distribution of the acoustic field produced by a cylindrical transducer $f = 340$ MHz, $d' = 6$ mm, $d = 4$ mm, $R = 5$ mm, $b = -0.232$, $R' = R/(1-2b) = 3.41$ mm

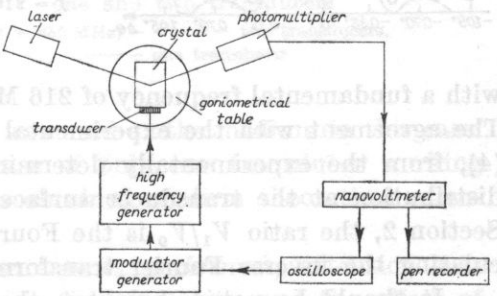

Fig. 5. Block diagram of the experimental apparatus

a cylindrical surface, the passage time of the acoustic wave was considerably longer than the duration of the acoustic pulse but at the same time considerably shorter than the pulse repetition time. The crystals were placed on a goniometrical table, which ensured precise turning and moving of the sample.

A 5-mW He-Ne laser was the light source. Diffracted light was registered by a photomultiplier from which a signal was shown on nanovoltmeter and a pen recorder.

Angular distributions of the diffracted light intensity were measured with the crystal being rotated in the diffraction plane. The angle $\Delta\theta$ was measured with an accuracy of 1′.

In the probing of the acoustic field, however, the crystal was moved vertically in the XY-plane. Narrowed by an optical system, the laser beam had a diameter of about 15 μm over a path of 1 cm. The beam fell at the Bragg angle to the acoustic wave front.

5. Presentation and discussion of results

Measurements of angular distributions of diffracted light intensity. Figure 6 shows the distribution of diffracted light intensity in crystalline quartz obtained for acoustic wave propagation along the Z-axis. A $LiIO_3$ transducer

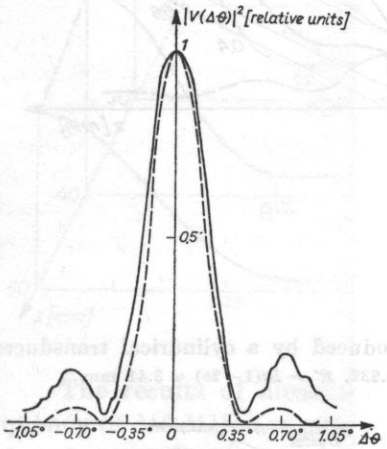

Fig. 6. Angular distribution of the diffracted light intensity in crystalline quartz
f = 216 MHz, ——— experimental curve, – – – – – theoretical curve

with a fundamental frequency of 216 MHz was the source of the acoustic wave. The agreement with the experimental curve is not very good. Using relation (4), from the experimentally determined behaviour of $I(\Delta\theta)$, the amplitude distribution at the transducer surface was estimated. As was mentioned in Section 2, the ratio V_1/V_0 is the Fourier transform of the function $a(y)$. Calculating the inverse Fourier transform, we obtain $a(y)$ if we know $|V_1/V_0|$.

It should be noted, however, that we obtain only V_1/V_0 measurements and we do not know the analytical form of the relation $V_1\Delta\theta/V_0$. Therefore, to calculate the inverse transform we used the trapezoidal method of approximation. The results of the calculation are shown in Fig. 7 (for one half of the transducer). The dashed line shows the vibration amplitude distribution at the transducer, obtained by the method discussed, while the full line represents the vibration amplitude distribution on an ideal transducer. The experimentally obtained distribution differs from the uniform distribution assumed.

It appears that the above method, although it is approximate and slightly troublesome in calculation, can be successfully used for determination of the vibration amplitude in piezoelectric transducers.

Figure 8 shows an example of the angular intensity distribution of the diffracted light by an acoustic wave produced by two transducers (dashed line). The length of transducers was 1.5 mm, the separation distance — 5 mm, and

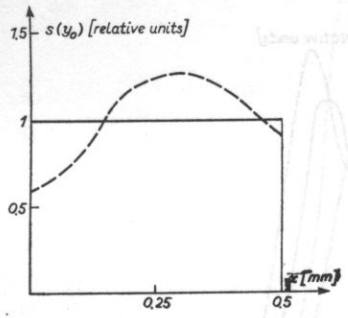

Fig. 7. Vibration amplitude on the transducer surface studied

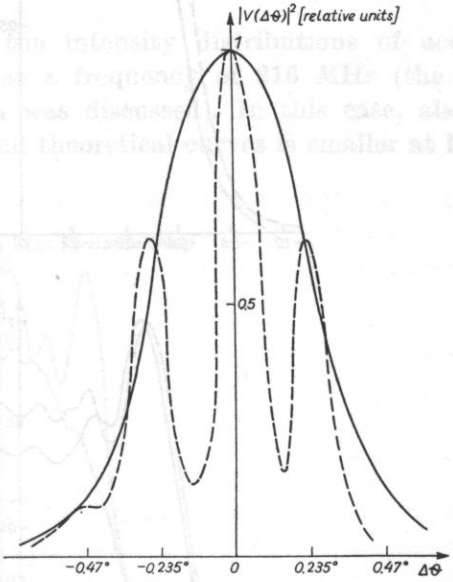

Fig. 8. Angular distribution of the acoustic field intensity produced by one and two transducers
f = 285 MHz, – – – – – two transducers, ——— one transducer

the frequency — 285 MHz. Fused quartz was used as the medium in this case. For comparison, the behaviour in the case of only one transducer working (full line) is also presented. The relations obtained confirm theoretical calculations performed in point two.

Acoustic field probing. In the measurements performed, attention was paid to direct measurement of the acoustic field intensity and the effect of focussing on the field distribution. The measurements were made by probing the acoustic field with a laser beam. The measurements were restricted to the Fresnel zone which in the present case was several centimetres long.

Figs. 9a, 9b and 9c show the intensity distributions of acoustic fields in the fused quartz obtained at distances of 2, 3 and 7 mm from a $LiIO_3$ transducer whose dimensions were $d' = 8$ mm, $d = 1.5$ mm, and whose frequency was 200 MHz. It follows from a comparison of the experimental and theoretical behaviour that the agreement is not very good close to the transducer, while further away the experimental and theoretical behaviours were practically the same. It seems that the fact that it does not vibrate in a piston mode, which

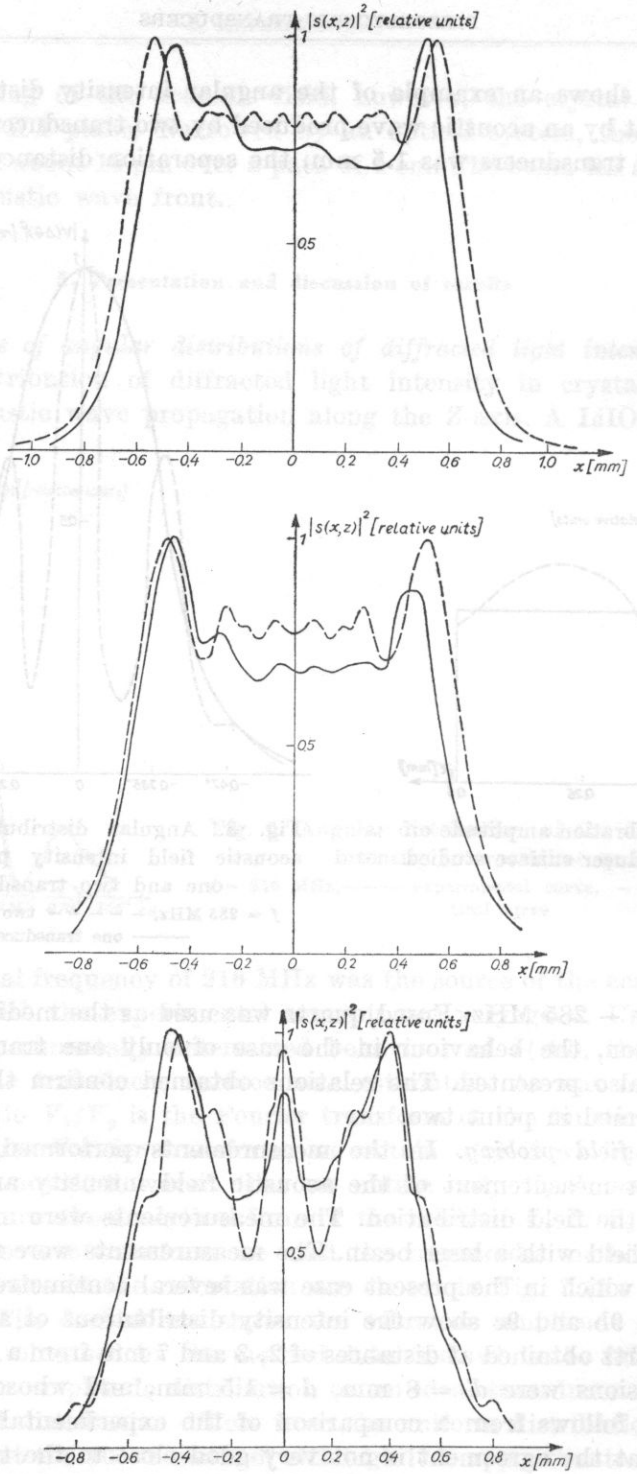

Fig. 9. Distribution of the acoustic field intensity in fused quartz at various distances from the transducer

f = 200 MHz, d' = 8 mm, d = 1.5 mm, (*a*) z = 2 mm, (*b*) z = 3 mm, (*c*) z = 7 mm, ——— experimental curve, – – – – – theoretical curve

was also shown by measurement of angular distributions, is the main reason for this difference close to the transducer. Inadequate narrowing of the laser beam had a great effect on the results obtained.

It is difficult, however, to obtain a narrowing to several μm over a path of 1 cm.

Figures 10a and 10b represent the intensity distributions of acoustic fields in crystalline quartz obtained at a frequency of 216 MHz (the same transducer whose angular distribution was discussed). In this case, also the difference between the experimental and theoretical curves is smaller at longer distances from the transducer.

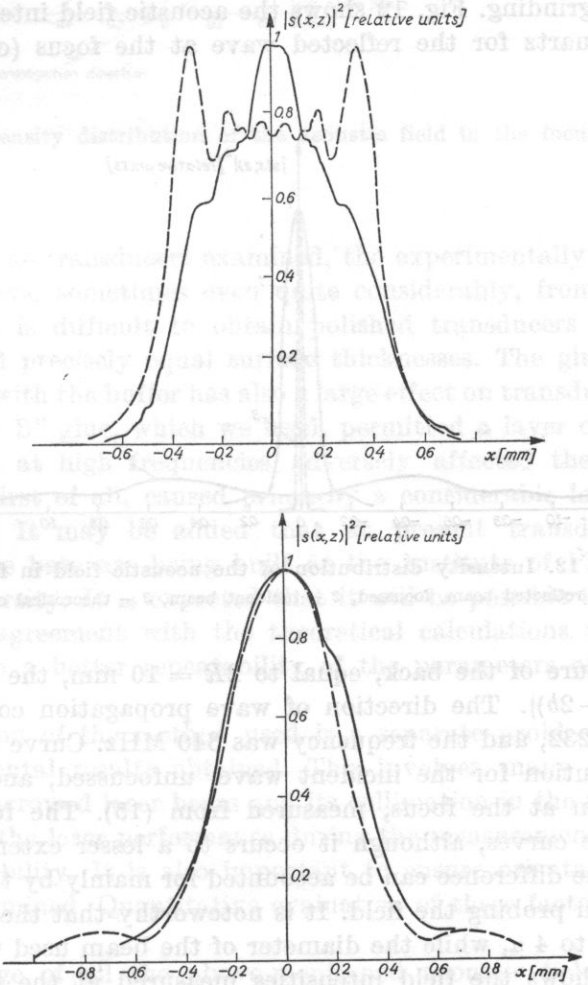

Fig. 10. Intensity distribution of the acoustic field in crystalline quartz at various distances from the transducer

f = 216 MHz, d' = 5 mm, d = 1.5 mm, (*a*) z = 2 mm, (*b*) z = 15 mm, ——— experimental curve, – – – – – theoretical curve

The investigation of focussing was performed in the system shown in Fig. 11. The reflection of the acoustic beam from the back, cylindrical wall of the buffer was used here. The use of such an acoustic focussing mirror was

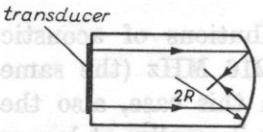

Fig. 11. Focussing acoustic mirror

necessary because it was found impossible to produce cylindrical transducers by the manual grinding. Fig. 12 shows the acoustic field intensity distribution in crystalline quartz for the reflected wave at the focus (curve *1*). For the

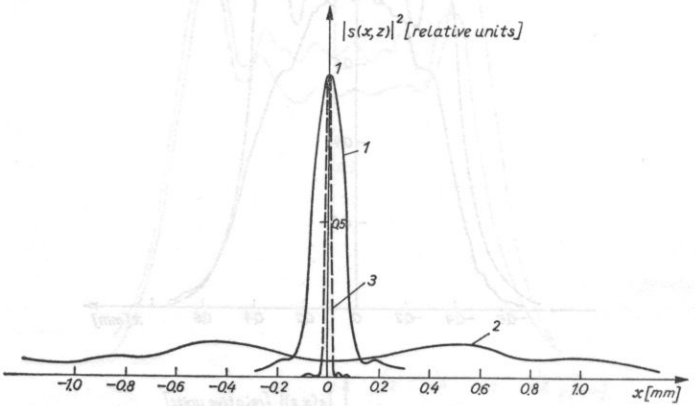

Fig. 12. Intensity distribution of the acoustic field in focus
1 – reflected beam, focussed, *2* – incident beam, *3* – theoretical curve

radius of curvature of the back, equal to $2R = 10$ mm, the focal length was 3.41 mm $(R/(1-2b))$. The direction of wave propagation coincided with the Z-axis, $b = -0.232$, and the frequency was 340 MHz. Curve *2* shows the field intensity distribution for the incident wave, unfocussed, and the theoretical field distribution at the focus, measured from (15). The focussing effect is distinct in these curves, although it occurs to a lesser extent than predicted theoretically. The difference can be accounted for mainly by the large diameter of the laser beam probing the field. It is noteworthy that theoretical focussing should occur up to 4 μ, while the diameter of the beam used was 15 μ.

Figure 13 shows the field intensities measured at the focus and 1 mm before and after the focus.

It follows from the measurements taken that the method can be successfully used for the investigation of acoustic field distributions in crystals.

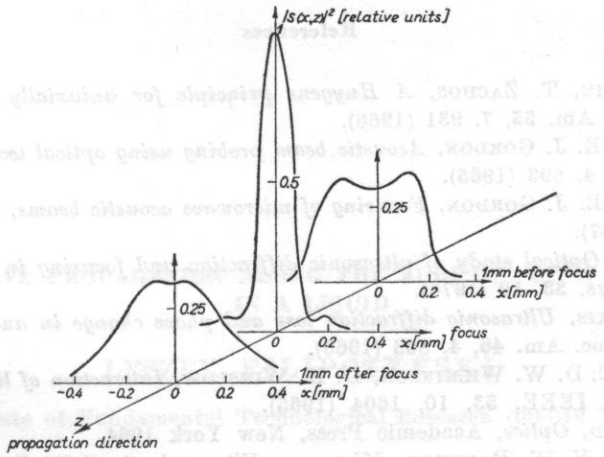

Fig. 13. Intensity distribution of the acoustic field in the focussing system

As regards the transducers examined, the experimentally determined field distribution differs, sometimes even quite considerably, from the theoretical distributions. It is difficult to obtain polished transducers with thicknesses of several μ and precisely equal surface thicknesses. The glue layer coupling the transducers with the buffer has also a large effect on transducer performance. The "Cyjanopan B" glue, which we used, permitted a layer of several μ to be obtained which at high frequencies adversely affected the transducer performance and, first of all, caused primarily a considerable loss in the electric power supplied. It may be added that at present transducers adhesively coupled with the base are being built at the Institute of Physics of Silesian Technical University. It is expected that it will be possible to obtain a considerably better agreement with the theoretical calculations with these transducers, and also a better repeatability of the parameters of the transducers made.

The precision of the method used is a separate problem in the analysis of the experimental results obtained. This involves many factors, e.g. the diameter of a narrowed laser beam and its collimation in the area investigated, the stability of the laser performance during the measurements, and the recording system stability. It is also important to ensure orientation precision for the samples examined. Quantitative evaluation of these factors is a very complicated matter.

A knowledge of all the above-mentioned acoustic field distributions is very important for the calculation of the parameters of many acousto-optical devices and it is this point of view that has stimulated the measurements described in this paper.

References

[1] L. Bergstein, T. Zachos, *A Huygens principle for uniaxially anisotropic media*, J. Opt. Soc. Am. **55**, 7, 931 (1966).

[2] M. G. Cohen, E. J. Gordon, *Acoustic beam probing using optical techniques*, Bell Syst. Tech. J. **44**, 4, 693 (1965).

[3] M. G. Cohen, E. J. Gordon, *Focusing of microwave acoustic beams*, J. Appl. Phys. **38**, 5, 2340 (1967).

[4] M. G. Cohen, *Optical study of ultrasonic diffraction and focusing in anisotropic media*, J. Appl. Phys. **38**, 10 (1976).

[5] E. P. Papadakis, *Ultrasonic diffraction loss and phase change in anisotropic materials*, J. Acoust. Soc. Am. **40**, 4, 863 (1966).

[6] G. F. Quate, C. D. W. Wilkinson, D. K. Winslow, *Interaction of light and microwave sound*, Proc. IEEE. **53**, 10, 1604 (1965).

[7] A. Sommerfeld, *Optics*, Academic Press, New York 1964.

[8] J. W. Tucker, V. W. Rampton, *Microwave Ultrasonics in Solid State Physics*, North-Holland Publishing Company, Amsterdam 1972.

Received on November 7, 1977;
final version — on January 10, 1979

ARCHIVES OF ACOUSTICS
4, 3 (1979)

ULTRASONIC WAVE PROPAGATION ALONG THE SURFACE OF A ROD IMMERSED IN A LIQUID

LESZEK FILIPCZYŃSKI

The Institute of Fundamental Technological Research (00-049 Warszawa)

This paper describes the wave phenomena occurring in a needle used for puncture of body organs, under the simplifying assumption that this needle is an ideal elastic cylinder immersed in an ideal liquid.

Investigations carried out by the author using an echo method showed that the velocity of the wave propagating in the needle immersed in water is close to the velocity of the wave propagating in water.

The author has analysed the propagation of waves along a cylindrical rod of infinite length immersed in a liquid, solving the wave equations for displacement potentials in the rod surrounding liquid, taking into consideration the boundary conditions on the rod surface. It was found that it is possible for the velocity of the propagating wave to be lower than the velocity of the wave in water, with the wave being guided by the rod and the surrounding liquid layer. The characteristic equation obtained was solved numerically for a 1.5 mm diameter steel rod immersed in water at wave frequencies of 3 and 5 MHz. Stress distributions, acoustic pressure and the propagating wave displacements were determined. It can be concluded from the character of the wave that it is a surface wave.

The results obtained can be used as the first approximation to the problem of wave propagation along a needle in the case where the needle wall thickness and the frequency are adequately large.

Notation

a — rod radius

A, B, C — constants

c_0, c_g — phase velocity and group velocity of wave along the rod, respectively

C_L, C_T — velocities of longitudinal and transverse waves, respectively, in a solid medium

C_W — wave velocity in liquid

f — frequency

$H_n^{(2)}$ — Hankel function of the second kind of order n

J_n — Bessel function of the n-th order
I_n — modified Bessel function of the first kind of order n
k_0 — wave number, see formula (15a)
k_L, k_T, k_W — see formulae (22)-(24)
K_n — modified Bessel function of the second kind of order n
L, T, W — see formulae (39), (40) and (41)
p — acoustic pressure
r, θ, z — cylindrical coordinates
t — time
$\boldsymbol{u}$ — vector of displacement in the rod
u_r, u_z — components of vector $\boldsymbol{u}$
$\boldsymbol{U}_W$ — vector of displacement in liquid
u_{Wr}, u_{Wz} — components of vector $\boldsymbol{U}_W$
$\boldsymbol{W}$ — vector potential of displacement
W_θ — component of vector $\boldsymbol{W}$
λ, μ — Lamé constants
ϱ, ϱ_W — densities of rod and liquid, respectively
σ_{zz}, σ_{rr} — normal components of stress
τ_{rz} — tangential component of stress
φ, χ — scalar potentials of displacement in rod and liquid, respectively
ψ — see formula (9)
ω — angular frequency.

1. Introduction

The puncture of various body organs with a needle was recently introduced into ultrasonic medical diagnostics, with the direction and also sometimes the depth of puncture being ultrasonically controlled. The above method has been used in obstetrics in amniocentosis to investigate genetically conditioned foetus deformations, in phthisiology in punctures to remove fluids from pleura, in oncology in histopathological investigations of tissues suspected of cancer development, and for localization and puncture of blood vessels [1, 7, 6, 13]. In these cases ultrasonic waves of frequencies usually between 2 and 8 MHz are introduced along a steel needle of 2 mm diameter into the interior of the patient's body which from the viewpoint of its elastic properties is comparable to a liquid.

The puncture of the body is achieved with a needle whose hole is filled with a metal rod which is removed after the puncture has been made. The needle itself is in turn placed in a hole concentrically made in the centre of a disc-shaped piezoelectric transducer (Fig. 1). By means of the ultrasonic

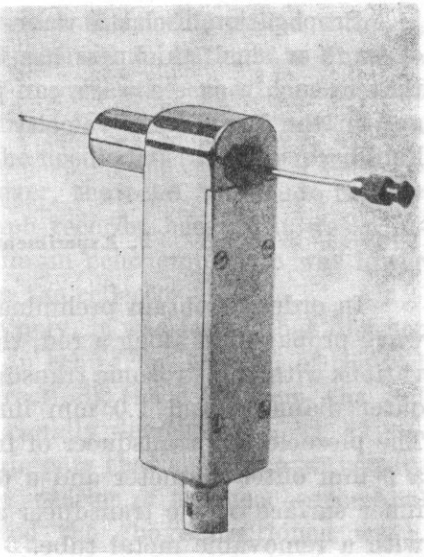

Fig. 1. An ultrasonic transducer for ultrasonically guided punctures [6]

beam radiated by the echoscope or ultrasonograph head the biological structure to be investigated is localized and the needle is subsequently entered along the ultrasonic beam into the patient's body, the needle being inserted through the hole in the piezoelectric transducer (Fig. 2).

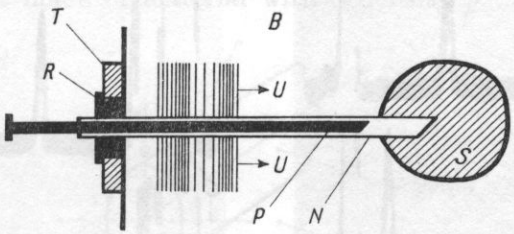

Fig. 2. The principle of a needle guided by an ultrasonic beam
B – a patient's body, S – the biological structure investigated, T – the piezoelectric transducer, R – tube, N – the needle, U – the ultrasonic wave, P – the rod filling the needle

The objective of this investigation is an explanation of the wave phenomena occurring in the needle used for puncture of the body organs, under the simplifying assumption that this needle is an ideal elastic cylinder immersed in an ideal liquid.

The problem of ultrasonic wave propagation along a rod immersed in a liquid was first examined by BJÖRNO and KUMAR [3]. In the present investigation the author uses a similar analysis, the different approach to the problem resulting from the particular conditions imposed by the puncture, which was the primary object of the author's consideration.

Propagation of elastic waves in a liquid along a flat layer of a solid medium of large or small thickness has been investigated by GRABOWSKA [5] showing that in such a case a wave can propagate simultaneously in the solid medium and in the liquid at a velocity slightly lower than the wave velocity in the liquid.

2. Experiments carried out using a needle

In order to obtain preliminary knowledge of the phenomena of ultrasonic wave propagation along a rod, the author made a series of experimental observations with an ultrasonic transducer as shown in Fig. 1, and a needle of 1.5 mm outer diameter and 1.0 mm inner diameter, using an ultrasonic echoscope. The piezoelectric transducer of frequency 3 MHz had the shape of a ring with a 9 mm outer diameter and a 6 mm inner diameter. The space between the inner surface of the transducer and the outer surface of the needle was filled with a removable metal tube.

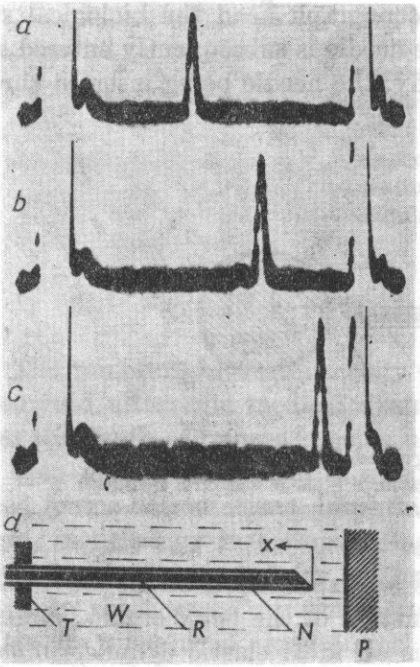

Fig. 3. Oscillographic records of ultrasonic pulses (*a*, *b*, *c*) and the measuring system (*d*)

T – a piezoelectric transducer, *W* – water, *N* – the needle, *R* – the rod filling the needle, *P* – a flat reflector of methyl metacrylate, *x* – direction of motion of the needle and the rod, as shown in (*d*)

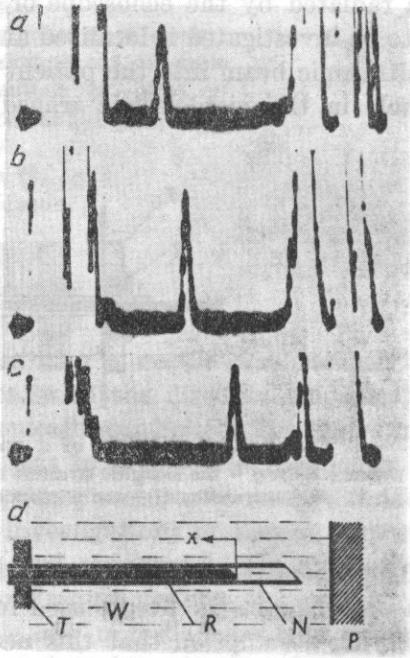

Fig. 4. Oscillographic records of ultrasonic pulses (*a*, *b*, *c*) and the measuring system (*d*)

The record (*c*) corresponds to the position of the needle and the rod, as shown in (*d*). Notation as in Fig. 3

Figure 3d shows the ultrasonic transducer with the needle pulled through, filled with a metal rod, and a flat reflector immersed in water at a distance of 5 cm from the transducer. The transmitted impulse, the echo from the flat reflector (methyl metracrylate) and the echo from the needle end are shown in the oscillograph records above. If we move the needle left (in the x direction), the echo from its end also moves left. However, the echo amplitude rapidly decreases. This is not visible on the oscillograph records, because it was compensated by amplification variation. The maximum echo emplitude was lower by 14 dB than the amplitude of the echo from the reflector.

An interesting fact is shown in Fig. 4. Namely, it was found that distinct from the needle end echo, there also occurs an echo from the end of the rod filling it. If we move the rod left (in the x direction), the echo from the rod end also moves left, and the echo amplitude rapidly decreases.

It can be concluded from the above experiments that there is a wave propagating simultaneously in the water and the interior of the needle; removal of water from the tank completely eliminated the above-mentioned wave. The velocity of the wave is approximately equal to the wave velocity in water, as can be determined from the oscillograph records (with a precision of 5%).

3. Initial equations

Let us consider ultrasonic wave propagation along a rod of circular cross-section, as in the cylindrical coordinate system shown in Fig. 5. The rod with a diameter of $2a$ is made of material with a density ϱ, and the velocities of

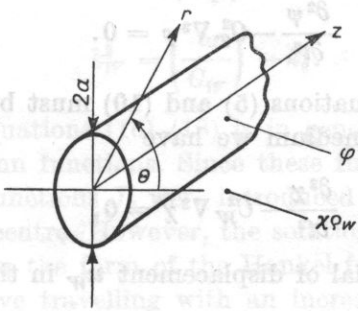

Fig. 5. The cylindrical coordinate system assumed in the analysis

longitudinal and transverse waves in the material are c_L and c_T, respectively. The rod is immersed in a liquid with a density ϱ_W, where the ultrasonic wave velocity is c_W.

The displacement vector in the rod is the sum

$$\boldsymbol{u} = \boldsymbol{u}_L + \boldsymbol{u}_T, \tag{1}$$

where

$$\operatorname{curl} \boldsymbol{u}_L = 0, \tag{2}$$

$$\operatorname{div} \boldsymbol{u}_T = 0 \tag{3}$$

thus

$$\boldsymbol{u} = \operatorname{grad}\varphi + \operatorname{curl}\boldsymbol{W}, \tag{4}$$

potentials φ and $\boldsymbol{W}$ satisfying the scalar and vector wave equations:

$$\frac{\partial^2\varphi}{\partial t^2} - C_L^2\nabla^2\varphi = 0, \tag{5}$$

$$\frac{\partial^2\boldsymbol{W}}{\partial t^2} - C_T^2\nabla^2\boldsymbol{W} = 0. \tag{6}$$

Because of rotational symmetry only the component W_θ of the vector potential is different from zero while $W_r = W_z = 0$. Thus, expanding (4), we can write

$$u_r = \frac{\partial\varphi}{\partial r} - \frac{\partial W_\theta}{\partial z} \tag{7}$$

$$u_z = \frac{\partial\varphi}{\partial z} + \frac{\partial(rW_\theta)}{r\partial r}. \tag{8}$$

Equation (6) can be reduced to a scalar equation, introducing [10] a new scalar quantity ψ from the relation

$$W_\theta = -\frac{\partial\psi}{\partial r}, \tag{9}$$

where the quantity ψ satisfies the wave equation

$$\frac{\partial^2\psi}{\partial t^2} - C_T^2\nabla^2\psi = 0. \tag{10}$$

Thus, finally, scalar equations (5) and (10) must be satisfied for the rod, while for the surrounding medium we have

$$\frac{\partial^2\chi}{\partial t^2} - C_W^2\nabla^2\chi = 0, \tag{11}$$

where χ is the scalar potential of displacement $\boldsymbol{u}_W$ in the liquid in accordance with the relation

$$\boldsymbol{U}_W = \operatorname{grad}\chi. \tag{12}$$

The solutions of equations (5), (10) and (11) can be assumed in the form of waves travelling in the direction z,

$$\varphi = \varphi_0(r)\,e^{j(\omega t - k_0 z)}, \tag{13}$$

$$\psi = \psi_0(r)\,e^{j(\omega t - k_0 z)}, \tag{14}$$

$$\chi = \chi_0(r)\,e^{j(\omega t - k_0 z)}, \tag{15}$$

where $k_0 = \omega/c_0$, $\omega = 2\pi f$, f — frequency, and c_0 — phase velocity of a wave travelling along the z-axis.

Substituting (13), (14) and (15) into the wave equations (5), (10) and (11) we obtain the Bessel equations of the zero order:

$$\frac{\partial^2 \varphi_0(r)}{\partial r^2} + \frac{1}{r}\frac{\partial \varphi_0(r)}{\partial r} + \left[\left(\frac{\omega}{C_L}\right)^2 - k_0^2\right]\varphi_0(r) = 0, \tag{16}$$

$$\frac{\partial^2 \psi_0(r)}{\partial r^2} + \frac{1}{r}\frac{\partial \psi_0(r)}{\partial r} + \left[\left(\frac{\omega}{C_T}\right)^2 - k_0^2\right]\psi_0(r) = 0, \tag{17}$$

$$\frac{\partial^2 \chi_0(r)}{\partial r^2} + \frac{1}{r}\frac{\partial \chi_0(r)}{\partial r} + \left[\left(\frac{\omega}{C_W}\right)^2 - k_0^2\right]\chi_0(r) = 0. \tag{18}$$

The solutions of these equations can be given [11] in the form

$$\varphi = AJ_0(k_L r)e^{j(\omega t - k_0 z)}, \tag{19}$$

$$\psi = CJ_0(k_T r)e^{j(\omega t - k_0 z)} \tag{20}$$

$$\chi = BH_0^{(2)}(k_W r)e^{j(\omega t - k_0 z)}, \tag{21}$$

where J_0 is the Bessel function of zero order, $H_0^{(2)}$ – the Hankel function of the second kind of zero order, and

$$k_L^2 = \left(\frac{\omega}{C_L}\right)^2 - k_0^2, \tag{22}$$

$$k_T^2 = \left(\frac{\omega}{C_T}\right)^2 - k_0^2, \tag{23}$$

$$k_W^2 = \left(\frac{\omega}{C_W}\right)^2 - k_0^2. \tag{24}$$

The solution of equations (16)-(18) is in general a linear combination of the Bessel and Neumann functions. Since these functions tend to infinity for $r \to 0$, only the Bessel functions J_0 were introduced into solutions (19) and (20) which include the rod centre. However, the solution for the liquid surrounding the rod was assumed in the form of the Hankel functions of the second kind which represents a wave travelling with an increasing value of r.

4. Boundary conditions

On the rod surface ($r = a$) boundary conditions in the form of equality of normal stresses in the rod σ_{rr} and of acoustic pressure p (in the liquid) must be satisfied, while tangential stress τ_{rz} on the rod surface must be equal to zero. The first condition takes [9] the form

$$\sigma_{rr} = \lambda\left[\frac{u_r}{r} + \frac{\partial u_r}{\partial r} + \frac{\partial u_z}{\partial z}\right] + 2\mu\frac{\partial u_r}{\partial r} = -p \quad \text{for } r = a \tag{25}$$

where

$$p = -\varrho_W \frac{\partial^2 \chi}{\partial t^2}, \tag{26}$$

and λ and μ are the Lamé constants. The second derivative, instead of the first one, appears in formula (26) because, in accordance with formula (12), the function is the potential of displacement, and not that of velocity, as is usually assumed in acoustics.

The second condition for disappearance of tangent stresses takes [9] the form

$$\tau_{rz} = \mu \left[\frac{\partial u_r}{\partial z} + \frac{\partial u_z}{\partial r} \right] = 0 \quad \text{for } r = a. \tag{27}$$

Subsequently we shall introduce the third boundary condition in the form of equality of the radial displacements in the rod (u_r) and in the liquid (u_{wr}) on the boundaries of the rod and the liquid:

$$u_r = u_{wr} \quad \text{for } r = a. \tag{28}$$

The components of displacements in the rod and displacements in the liquid can be expressed by means of functions of φ, ψ, χ, on the basis of relations (7)-(9) and (12):

$$u_r = \frac{\partial \varphi}{\partial r} + \frac{\partial^2 \psi}{\partial r \partial z}, \tag{29}$$

$$u_z = \frac{\partial \varphi}{\partial z} - \frac{\partial \psi}{r \partial r} - \frac{\partial^2 \psi}{\partial r^2}, \tag{30}$$

$$u_{wr} = \frac{\partial \chi}{\partial r}, \qquad u_{wz} = \frac{\partial \chi}{\partial z}. \tag{31}$$

Substituting formulae (29) and (31) into (25), (27) and (28) we obtain the three ultimate boundary conditions

$$A \left[\frac{1}{2}(k_0^2 - k_T^2) J_0(k_L a) + \frac{k_T}{a} J_1(k_L a) \right] + Cjk_0 k_T \left[k_T J_0(k_T a) - \frac{1}{a} J_1(k_T a) \right] +$$

$$+ B \frac{\omega^2 \varrho_W}{2\varrho C_T^2} H_0^{(2)}(k_W a) = 0, \tag{32}$$

$$A[2jk_L k_0 J_1(k_L a)] + C[(k_0^2 k_T - k_T^3) J_1(k_T a)] = 0, \tag{33}$$

$$-A[k_L J_1(k_L a)] + C[jk_0 k_T J_1(k_T a)] + Bk_W H_1^{(2)}(k_W a) = 0, \tag{34}$$

where J_1 and $H_1^{(2)}$ are the Bessel and Hankel functions of the first order, respectively.

5. The characteristic equation

Eliminating quantities A, B and C from equations (32)-(34), after numerous transformations we obtain the characteristic equation for the problem under consideration:

$$\frac{\varrho_w}{4\varrho}\left(\frac{\omega}{C_T}\right)^4 \frac{1}{k_W}\frac{H_0^{(2)}(k_W a)}{H_1^{(2)}(k_W a)} = k_0^2 k_T \frac{J_0(k_T a)}{J_1(k_T a)} - \frac{1}{2a}\left(\frac{\omega}{C_T}\right)^2 + \left[\frac{1}{2}\left(\frac{\omega}{C_T}\right)^2 - k_0^2\right]^2 \frac{1}{k_L}\frac{J_0(k_L a)}{J_1(k_L a)}. \tag{35}$$

In the case where a vacuum surrounds the rod instead of a liquid we have $\varrho_W = 0$ and the left-hand side of equation (35) disappears. Thus we obtain the characteristic equation for a cylinder, as given by REDWOOD [10] after POCHHAMMER and CHREE.

When solving the characteristic equation, only real constants of propagation k_0 will be considered. In the general case, a finite number of imaginary propagation constants, satisfying the equation, occurs for each given frequency. They are analogous to propagation constants occurring in acoustic waveguides below the cut-off frequency, when the vibration modes investigated do not propagate, being completely attenuated ($Re(k_0 a) = 0$, $Im(k_0 a) \neq 0$). We can also neglect the case of complex propagation constants k_0, since the imaginary component of these constants represents spatial wave attenuation. The waves of this type will in practice decrease their amplitude until totally attenuated [14].

We investigate the case where the ultrasonic wave is guided along the rod and is not attenuated in the rod, nor re-radiated by the rod to the liquid.

The function $H_0^{(2)}$, occurring in the assumed solution (21), corresponds to the radiation of wave by the rod to the liquid along the axis r. This follows from the asymptotic value of this function which for high values of r takes [11] the form

$$H_0^2(x) \cong \sqrt{\frac{2}{\pi x}}\, e^{-j(x-\pi/4)}\left[1 - \frac{1}{j\cdot 8x} + \ldots\right]. \tag{36}$$

However, in the case where the phase velocity c_0 of wave is lower than the velocity c_W, in accordance with (24) the wave number k_W becomes an imaginary quantity and the Hankel function passes into a modified Bessel function of the second kind $K_n(x)$, in accordance [2, 8] with the relation

$$K_n(x) \cong \frac{1}{2}\pi \cdot j^{-n-1} H_n^2(-jx). \tag{37}$$

Of all cylindrical functions only this function decreases monotonically to zero for the argument tending to infinity, and this occurs only when the

Hankel function argument is a negative imaginary quantity [8], because [2] for the modified Bessel function $K_n(x)$ we have

$$K_n(x) \cong \sqrt{\frac{\pi}{2x}}\, e^{-x}\left[1+\frac{\mu-1}{8x}+\ldots\right], \tag{38}$$

where $\mu = 4n^2$ for $x \gg n$.

When $c_0 < c_W$, the wave numbers k_W, k_L, k_T are imaginary:

$$k_W = \pm j\frac{\omega}{C_W}\sqrt{\frac{C_W^2}{c_0^2}-1} = \pm jW, \tag{39}$$

$$k_L = \pm j\frac{\omega}{C_L}\sqrt{\frac{C_L^2}{c_0^2}-1} = \pm jL, \tag{40}$$

$$k_T = \pm j\frac{\omega}{C_T}\sqrt{\frac{C_T^2}{c_0^2}-1} = \pm jT. \tag{41}$$

Assuming, from the above discussion, a negative value of the imaginary wave number k_W (see (39)), we obtain from (37)

$$\frac{H_0^{(2)}(-jWa)}{H_1^{(2)}(-jWa)} = -j\frac{K_0(Wa)}{K_1(Wa)}. \tag{42}$$

Similarly for imaginary arguments: the Bessel functions of the first kind pass into the modified Bessel functions of the first kind, in accordance [12] with the relation

$$I_n(x) = j^{-n}J_n(jx). \tag{43}$$

It should be noted [12] that

$$J_0(jx) = J_0(-jx) \tag{44}$$

and

$$J_1(jx) = -J_1(-jx). \tag{45}$$

Taking into consideration relations (43)-(45) and also (42), we obtain for both positive and negative imaginary wave numbers k_L, k_T (see (40) and (41)) a new form of the characteristic equation (35):

$$\frac{\varrho_W}{4\varrho}\left(\frac{\omega}{C_T}\right)^4\frac{1}{W}\frac{K_0(Wa)}{K_1(Wa)} = k_0^2 T\frac{I_0(Ta)}{I_1(Ta)} - \frac{1}{2a}\left(\frac{\omega}{C_T}\right)^2 - \left[\frac{1}{2}\left(\frac{\omega}{C_T}\right)^2 - k_0^2\right]^2\frac{1}{L}\frac{I_0(La)}{I_1(La)}. \tag{46}$$

Such an involved form of this equation makes its solution very difficult, because the quantities T, L and W depend on k_0 through relations (39)-(41) and (22)-(24). Therefore equation (46) was solved taking into consideration the fact experimentally determined in Section 2 that the velocity of the wave

discussed propagating along the rod is very close to that of wave in water. In such a case only the value of W depends essentially on the value of c_0, while the value of c_0 has little influence on the values of L, T and k_0. Thus, assuming $c_0 = c_W$ in formulae (40), (41) and (15a), we can solve the characteristic equation (46) for the quantity W.

Under such conditions, equation (46) was numerically solved assuming a frequency $f = 3$ MHz, a rod diameter equal to $2a = 1.5$ mm, a rod made of steel in which longitudinal and transverse waves velocities are equal to $c_L = 5.9$ km/s and $c_T = 3.23$ km/s, respectively, and the wave velocity in water equal to 1.48 km/s. Equation (46) is satisfied for wave numbers equal to $k_W = 0.18$ cm^{-1}, $k_T = \pm j \cdot 113$ cm^{-1}, $k_L = \pm j \cdot 123$ cm^{-1}. Having the wave number k_W, the phase velocity of wave travelling along the rod was determined. Being equal to $c_0 = 1.479998$ km/s, it is thus only slightly lower than the wave velocity in water without a rod. Other possible solutions of the characteristic equation were not examined.

The group velocity c_g of the wave propagating along the rod is equal to the phase velocity c_0,

$$c_g = \frac{d\omega}{dk_0} = \frac{d\omega}{d(\omega/c_0)} \cong c_0, \tag{46a}$$

in the range of the considered frequencies of 3-5 MHz, because the phase velocity c_0 is in this case practically constant. This can be concluded from the numerical computations carried out, since in this frequency range its value changes only at the fifth decimal place.

6. Wave distribution inside and outside the rod

The distribution of displacements in the rod and the surrounding liquid occurring for the wave type considered appears to be of interest. Taking into consideration relations (37), (43) and (44), solutions (19)-(21) take the following form:

$$\varphi = AI_0(Lr)e^{j(\omega t - k_0 z)}, \tag{47}$$

$$\psi = CI_0(Tr)e^{j(\omega t - k_0 z)}, \tag{48}$$

$$\chi = B\frac{2}{\pi} jK_0(Wr)e^{j(\omega t - k_0 z)}. \tag{49}$$

From relation (33) we find the ratio A/C,

$$\frac{A}{C} = \frac{k_T(k_T^2 - k_0^2)}{2jk_L k_0} \frac{J_1(k_T a)}{J_1(k_L a)}, \tag{50}$$

which for imaginary values of wave numbers, in accordance with (40), (41) and (43)-(45) takes the following form:

$$\frac{A}{C} = \pm j \frac{T(T^2 + k_0^2)}{2Lk_0} \frac{I_1(Ta)}{I_1(La)}. \tag{51}$$

It can be readily checked that condition (33), from which the ratio A/C was determined, is satisfied only for the positive sign on the right-hand side of formula (51). Therefore positive and negative values should be at the same time assumed for the imaginary wave numbers (40) and (41).

Similarly, from relation (34) we obtain a value for the ratio B/C equal to

$$\frac{B}{C} = -j\frac{k_T(k_T^2-k_0^2)}{2k_0k_W}\frac{J_1(k_Ta)}{H_1^{(2)}(k_Wa)}, \tag{52}$$

which, after taking into consideration (37), (40), (41), (43)-(45), takes the form

$$\frac{B}{C} = \frac{\pi T(k_0^2-T^2)}{4k_0W}\frac{I_1(Ta)}{K_1(Wa)}. \tag{53}$$

The value of (53) does not depend on the sign of the imaginary wave number $k_T = \pm jT$. Earlier we assumed a negative sign for the wave number $k_W = \pm jW$. Substituting the values of the potential (47) and (48) into formulae (29) and (30), and taking into consideration the relation

$$\frac{dI_n(x)}{dx} = I_{n-1}(x) - \frac{n}{x}I_n(x); \quad I_0'(x) = I_1(x), \tag{54}$$

we obtain displacements related to a constant coefficient C:

$$\frac{u_r}{C} = \left[\frac{A}{C}LI_1(Lr) - jk_0TJ_1(Tr)\right]e^{j(\omega t-k_0z)}, \tag{55}$$

$$\frac{u_z}{C} = \left[-jk_0\frac{A}{C}I_0(Lr) - T^2I_0(Tr)\right]e^{j(\omega t-k_0z)}. \tag{56}$$

The stress σ_{rr} in the rod will be determined on the basis of formula (25). Taking into consideration the values obtained for dispacements u_r and u_z, we finally obtain

$$\frac{\sigma_{rr}}{C} = \frac{A\varrho}{C}\left\{\left\{[L^2C_L^2 - k_0^2(C_L^2-2C_T^2)]I_0(Lr) - 2C_T^2L\frac{I_1(Lr)}{r}\right\} + \right.$$
$$\left. + j\cdot 2k_0C_T^2\varrho T\left\{\frac{I_1(Tr)}{r} - TI_0(Tr)\right\}\right\}e^{j(\omega t-k_0z)}. \tag{57}$$

The stresses σ_{zz} in the rod will be determined [9] from formula

$$\sigma_{zz} = \lambda\left[\frac{u_r}{r} - \frac{\partial u_r}{\partial r} - \frac{\partial u_z}{\partial z}\right] + 2\mu\frac{\partial u_z}{\partial z} \tag{58}$$

whence, taking into account (55), (56) and the relations

$$\lambda = \varrho(C_L^2-2C_T^2), \tag{59}$$

$$\mu = \varrho C_T^2, \tag{60}$$

we finally get

$$\frac{\sigma_{zz}}{C} = \frac{A}{C}\varrho\{[L^2(C_L^2 - C_T^2) - k_0^2 C_L^2]I_0(Lr) + jk_0 T^2 \varrho C_T^2 I_0(Tr)\}e^{j(\omega t - k_0 z)}. \tag{61}$$

The tangential stresses τ_{rz} will be determined on the basis of relation (27). Taking into consideration (55), (56) and (60), we obtain

$$\frac{\tau_{rz}}{C} = \varrho C_T^2\left[-2jk_0\frac{A}{C}LI_1(Lr) - T(k_0^2 + T^2)I_1(Tr)\right]e^{j(\omega t - k_0 z)}. \tag{62}$$

The value of the acoustic pressure in the liquid is determined from formulae (26) and (49). Thus we have

$$\frac{p}{C} = j\frac{B}{C}\varrho_W \omega^2 \frac{2}{\pi}K_0(Wr)e^{j(\omega t - k_0 z)}. \tag{63}$$

The values of displacements and stresses in the rod and the acoustic pressure in the liquid, calculated on the basis of the above formulae for the case investigated, are shown in Figs. 6 and 7, while comparable values, calculated for a frequency of 5 MHz, are shown in Figs. 8 and 9.

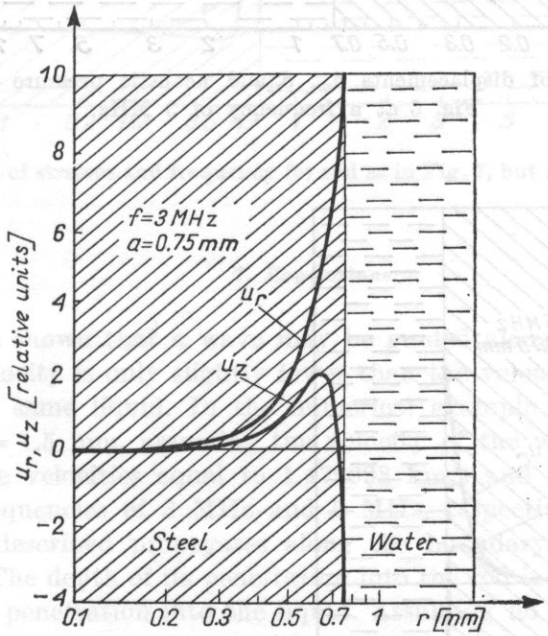

Fig. 6. Distribution of displacements (u_r), (u_z) in the rod with a radius $a = 0.75$ mm at a frequency of 3 MHz

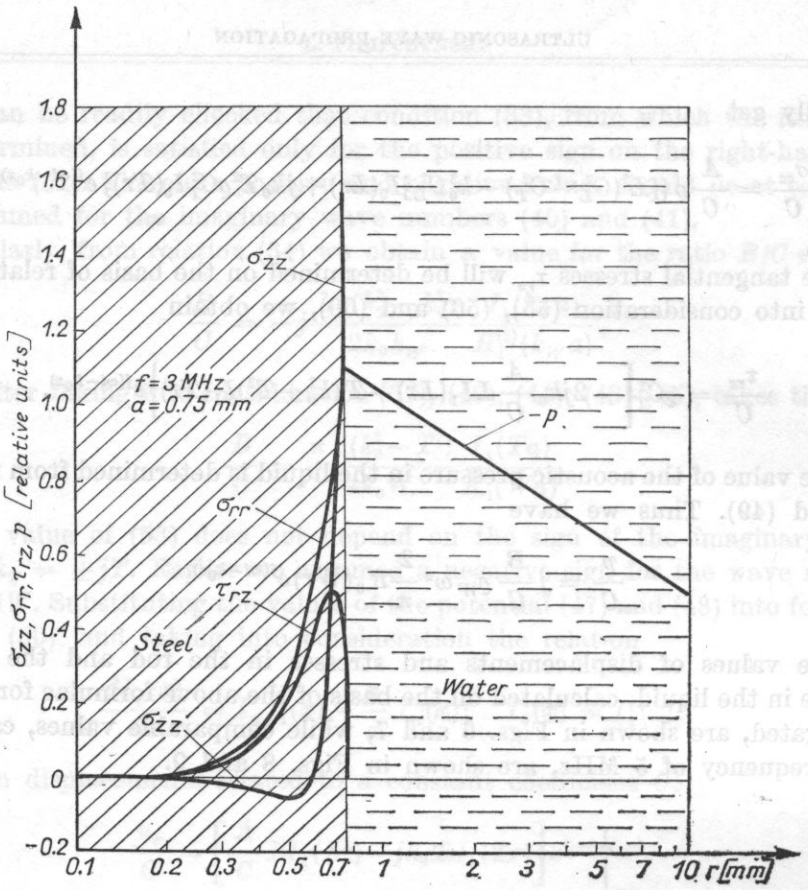

Fig. 7 Distribution of displacements δ_{zz}, δ_{rz} and acoustic pressure p for the rod as in Fig. 6 at a frequency of 3 MHz.

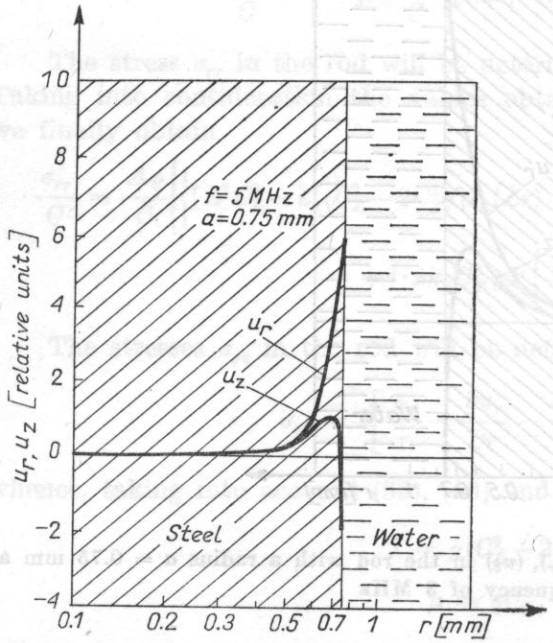

Fig. 8. Distribution of displacement in the rod as in Fig. 6, but at a frequency of 5 MHz

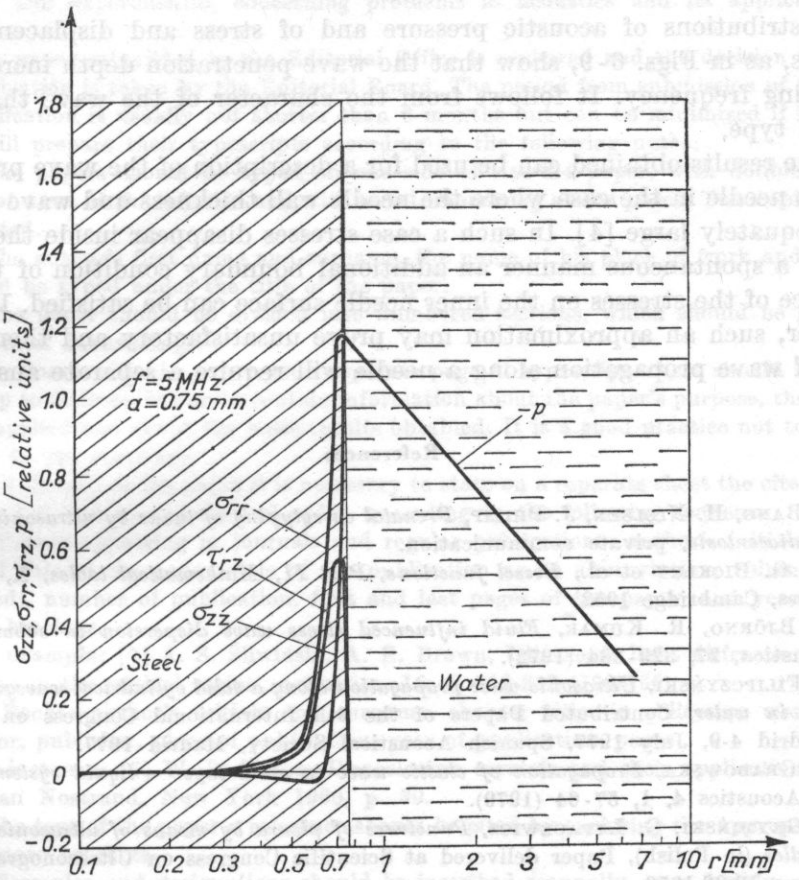

Fig. 9. Distribution of stresses and frequency for rod as in Fig. 7, but at a frequency of 5 MHz

7. Conclusions

It has been shown that a wave may be guided along a rod immersed in liquid whose velocity is only slightly lower than the velocity of the wave propagating in the same liquid. In the numerical example of a steel rod with a diameter $2a = 1.5$ mm, assuming the velocity of the wave in liquid to be 1.48 km/s, wave velocities equal to 1.479998 km/s and 1.479980 km/s were obtained for frequencies of 3 MHz and 5 MHz, respectively.

The wave described propagates along the boundary surface of the rod and the liquid. The depth of its penetration into the rod is considerably smaller than that of its penetration into the liquid. Assuming no propagation loss for both media, the wave propagates without attenuation; the wave number k_0 is real, because this wave is not radiated into the liquid perpendicular the rod axis.

Distributions of acoustic pressure and of stress and displacement components, as in Figs. 6-9, show that the wave penetration depth increases with increasing frequency. It follows from the character of the wave that it is of surface type.

The results obtained can be used for a description of the wave propagation along a needle in the case where the needle wall thickness and wave frequency are adequately large [4]. In such a case stresses disappear inside the rod, and thus in a spontaneous manner an additional boundary condition of the disappearance of the stresses on the inner needle surface can be satisfied. In general, however, such an approximation may prove unsatisfactory and then the problem of wave propagation along a needle will require a separate analysis.

References

[1] J. BANG, H. NIELSEN, J. PHILIP, *Prenatal carrytyping of twins by ultrasonically guided amniocentosis*, private communication.

[2] W. G. BICKLEY et al., *Bessel functions, Part II, Mathematical tables*, **X**, University Press, Cambridge 1952.

[3] L. BJÖRNO, R. KUMAR, *Fluid influenced stress wave dispersion in submerged rods*, Acustica, **27**, 329-334 (1972).

[4] L. FILIPCZYŃSKI, *Ultrasonic wave propagation along a solid cylindrical waveguide immersed in water*, Contributed Papers of the 9th International Congress on Acoustics, Madrid 4-9, July 1977, Spanish Acoustical Society, Madrid 1977.

[5] A. GRABOWSKA, *Propagation of elastic wave in solid layer – liquid system*, Archives of Acoustics **4**, 1, 57-64 (1979).

[6] J. GRYMIŃSKI, G. ŁYPACEWICZ, *Punctures of pleura by means of ultrasonically guided needles* (in Polish), Paper delivered at Scientific Congress on Ultrasonography, Warszawa 19.02.1976.

[7] H. H. HOLM, J. K. KRYSTENSEN, S. N. RASMUSSEN, A. NORTHEVED, H. BARLEBO, *Ultrasound as a guide in percutaneous puncture technique*, Ultrasonics, March, 183-186 (1972).

[8] JANKE-EMDE, *Tables of higher functions*, Teubner, Leipzig 1950.

[9] A. E. H. LOVE, *A treatise on the mathematical theory of elasticity*, Dover Publications, New York 1944.

[10] M. REDWOOD, *Mechanical waveguides*, Pergamon Press, Oxford 1960.

[11] N. W. LACHLAN, *Bessel functions for engineers* (in Polish), PWN, Warszawa 1974.

[12] H. TAUTZ, *Wärmeleitung und Temperaturausgleich*, Akademie Verlag, Leipzig 1971.

[13] J. WESOŁOWSKI et al., *Use of ultrasonic transducer with a hole for a puncture of femural arteries*, Medical Weekly, **49**, 4, 459-461 (1977).

[14] J. ZEMANEK, *An experimental and theoretical investigation of elastic waves propagation in a cylinder*, JASA, **51**, 1 Part 2, 265-283 (1972).

Received on April 18, 1978